Research Paper

GEOSPHERE

GEOSPHERE, v. 21, no. 6

https://doi.org/10.1130/GES02857.1

23 figures; 3 tables; 1 set of supplemental files

CORRESPONDENCE: gold@oce.orst.edu

CITATION: Goldfinger, C., Beeson, J., Black, B., Vizcaino, A., Nelson, C.H., Morey, A., Patton, J.R., Gutiérrez-Pastor, J., Romsos, C., and Walzcak, M.D., 2025, Unravelling the dance of earthquakes: Evidence of partial synchronization of the northern San Andreas fault and Cascadia megathrust: Geosphere, v. 21, no. 6, p. 1132–1180, https://doi.org/10.1130/GES02857.1.

Science Editor: Andrea Hampel and David E. Fastovsky
Associate Editor: Nancy Riggs

Received 25 November 2024
Revision received 26 July 2025
Accepted 21 August 2025

Published online 29 September 2025

Unravelling the dance of earthquakes: Evidence of partial synchronization of the northern San Andreas fault and Cascadia megathrust

C. Goldfinger[1], J. Beeson[2], B. Black[1], A. Vizcaino[3], C.H. Nelson[4], A. Morey[1], J.R. Patton[5], J. Gutiérrez-Pastor[4], C. Romsos[1], and M.D. Walzcak[1,*]

[1]College of Earth, Ocean and Atmospheric Sciences, Oregon State University, Corvallis, Oregon 97331, USA
[2]Hatfield Marine Science Center, National Oceanic and Atmospheric Administration–Oregon State University, 2115 SE OSU Drive, Newport, Oregon 97365, USA
[3]Springer Nature Group, Heidelberger Platz 3, 14197 Berlin, Germany
[4]Instituto Andaluz de Ciencias de la Tierra, Consejo Superior de Investigaciones Científicas (CSIC), 18100 Armilla, Granada, Spain
[5]California Department of Conservation, 2120 Campton Road Suite D, Eureka, California 95503, USA

ABSTRACT

Previous paleoseismic work has suggested a possible stress triggering relationship between the Cascadia subduction zone and the northern San Andreas fault based on similar event timings. Turbidite successions correlated to both systems may support this hypothesis. Historic earthquakes in 1980 and 1992 in the Cascadia subduction zone and the 1906 earthquake on the northern San Andreas fault left turbidite records that are temporally well constrained by bomb-carbon–supported age-depth models. The 1906 event bed clearly appears on both sides of the triple junction, as may the 1992 bed. This demonstrates that northern San Andreas fault events have triggered turbidity currents in the southernmost Cascadia subduction zone, and vice versa. Turbidite successions in the southernmost Cascadia subduction zone and the Northern San Andreas fault prior to 1906 have similarities in timing and stratigraphy. During the past ~3100 yr, 18 likely earthquake-generated turbidite beds have been deposited in the southern Cascadia subduction zone. In Noyo Channel, along the northern San Andreas fault, 19 likely earthquake-generated beds were deposited during the same period. Ten of the Cascadia subduction zone beds have a close temporal association with the likely earthquake-generated beds in Noyo Channel. The radiocarbon age medians differ by an average of 63 yr (standard deviation = 51 yr). Eight of 10 of the beds with substantial temporal overlap with major Cascadia subduction zone events have a distinctive thick, inverted doublet stratigraphy in Noyo Channel along the northern San Andreas fault, while beds without timing similarities, including the 1906 earthquake bed, do not. These unusually thick doublets have a lower silty unit directly overlain by a robust sandy unit, commonly with an intervening erosional unconformity. Doublets are also observed in the southern Cascadia subduction zone, though less commonly. The Cascadia subduction zone doublets have a less robust upper unit, and some have the upper unit embedded in the tail of the lower unit. The doublet stratigraphy in Noyo Channel commonly fades southward along the northern San Andreas fault, while that on the Cascadia subduction zone side fades northward. The recurrence rate of major events near the triple junction is not the additive rate of both faults but is similar to the rate for either fault alone, implying the doublet beds represent pairs of beds from each fault, stacked together. We infer that the stratigraphy is best explained by earthquakes on both systems spaced closely in time, beginning with the Cascadia subduction zone, as opposed to aftershock sequences, hydrodynamic generation, or other causes. The Holocene sequence of closely stacked stratigraphic pairs may represent direct evidence of stress triggering and partial synchronization of these two great faults for the latest Holocene, with the possibility of significant interaction at earlier times.

Chris Goldfinger https://orcid.org/0000-0002-4603-6178
*Now at: University of Washington, School of Oceanography, 1503 NE Boat Street, Box 357940, Seattle, WA 98195-7940, USA

INTRODUCTION AND PREVIOUS WORK

Stress transfer and subsequent triggering of one fault or segment by another is now a well-established principle, having been observed in a variety of settings (Stein, 1999; Parsons et al., 1999; Toda et al., 2011). Observations and model forecasts of this phenomenon come from instrumental records and have become part of seismological research. However, only a single modern forecast of one great earthquake triggering another has been made, in Sumatra (McCloskey et al., 2005), which subsequently occurred. Evidence in the paleoseismic record for triggering of great events is limited to the last few hundred years in Sumatra (Meltzner et al., 2010; Philibosian et al., 2017). The lack of such records may be due to the short length of the instrumental records or the paucity of high-precision paleoseismic records (Sieh et al., 2008). Paleoseismic records can be much longer and offer opportunities to search for other such events, but they commonly lack the precision needed to test for such occurrences. Marine and lacustrine subaqueous paleoseismic data offer very long records and have been in use in a number of locales, including

the Caribbean (Seibert et al., 2024; McHugh et al., 2024), Iberia (Gràcia et al., 2010), New Zealand (Howarth et al., 2021), Sumatra (Patton et al., 2015; Wils et al., 2021), Chile (Moernaut et al., 2017), Japan (Noda et al., 2008; Ikehara et al., 2023; Kanamatsu et al., 2023), Cascadia (Adams, 1990; Kelsey et al., 2005; Goldfinger et al., 2012, 2013a, 2013b, 2017; Enkin et al., 2013; Hamilton et al., 2015; Brothers et al., 2024), and the northern San Andreas fault (Goldfinger et al., 2008). In a few cases, relative timing constraints between events can be deduced and can achieve precision similar to or greater than varves and dendrochronology, though with limited linkage to absolute timing (Adams, 1990; Goldfinger et al., 2012, 2017; Enkin et al., 2013).

In the Pacific Northwest of the United States, long paleoseismic datasets for the Cascadia subduction zone and the northern San Andreas fault using terrestrial, marine, and lacustrine records have been evolving over the past several decades and generally show a good correspondence between onshore and offshore data for major events, with typically large uncertainties (Goldfinger et al., 2012, 2017; Nelson et al., 2021, and references therein). These separate records also show an intriguing correspondence of event timings *between* the two faults. This correspondence was explored by Goldfinger et al. (2008), who proposed that the observed temporal correspondence between the two faults may be the result of triggering of one fault by the other over the past ~2500 yr. That paper used a simple comparison of event-bed timings, estimated from radiocarbon, and included models of several configurations of possible stress interactions between the two faults. The radiocarbon correspondence was good as a series, but with the associated uncertainties, it could not demonstrate a definitive temporal association. Similarly, the modeling showed that the transfer of stress between a shallow-dipping subduction zone and a vertical strike-slip fault was complex and not particularly efficient, though possible. In this paper, we expand and refine the paleoseismic records of both faults using new core data, age models, and subbottom records, and we explore the overlapping stratigraphic relationships from event deposits in both systems that offer relative timing constraints. Stratigraphic constraints are independent of radiocarbon uncertainties and have the potential to test the model of a temporal and stress interaction.

Tectonic and Paleoseismic Setting

The Cascadia subduction zone is formed by the subduction of the oceanic Juan de Fuca and Gorda plates beneath the North American plate off the coast of northern California, Oregon, and Washington, USA, and Vancouver Island, Canada (Fig. 1; DeMets et al., 2010). The convergence rate is ~35–38 mm/yr directed 060° at the latitude of Oregon. The "trench" is filled with sediment that tapers in thickness from 3 km to 4 km in the north to less than 0.5 km in the south, resulting in a smoother plate interface in the north, but it is punctuated by subducting basement features in the south. The Cascadia subduction zone and the northern San Andreas fault meet at the Mendocino triple junction offshore northern California (Fig. 2; Silver, 1971). The paleoseismic records in the Cascadia subduction zone have evolved over several decades following the discoveries of paleoseismic turbidites offshore (Adams, 1990) and of coastal subsidence evidence onshore (Atwater, 1987, 1992). Recent compilations of the onshore and offshore evidence can be found in Nelson et al. (2021) and Goldfinger et al. (2012, 2013b, 2017). Recent work has included the Canadian margin (Enkin et al., 2013; Hamilton et al., 2015), and lacustrine seismo-turbidites as well (Karlin et al., 2004; Morey et al., 2013; Leithold et al., 2019; Goldfinger, 2017, 2021; Gutiérrez, 2020; Brothers et al., 2024; Morey et al., 2024; Morey and Goldfinger, 2024). An integrated model (land and marine data) of along-strike segmentation for the Cascadia subduction zone presented in Goldfinger et al. (2012, 2017) included ruptures that extend much or all of the full length of ~1000 km, and partial lengths as short as 200 km. Onshore evidence appears to include only some of the shorter events, which could be due to either a higher threshold for recording onshore evidence (Nelson et al., 2021, and references therein), incorrect interpretation, or both. A subset of these smaller events appears likely to be represented in both land and marine records (Goldfinger et al., 2012; Nelson et al., 2021; Morey et al., 2013, 2024; Morey, 2020; Morey and Goldfinger, 2024). The causative factors for the proposed segment boundaries are poorly known. McCaffrey and Goldfinger (1995) proposed that transverse strike-slip faults in the lower plate with vertical offset (Goldfinger et al., 1992, 1996, 1997) could bound plate interface ruptures. Deeper seismic work shown in Carbotte et al. (2024) supports this assertion from imaging of the lower-plate offsets, which extend to areas near the coastline.

The San Andreas fault is probably the most intensively studied transform system in the world. Extending along the west coast of North America, from the Gulf of California to Cape Mendocino, the San Andreas fault is the largest component of a complex and wide plate boundary that extends eastward to encompass numerous other strike-slip fault strands and interactions with the Basin and Range extensional province. The Mendocino triple junction lies at the northern termination of the northern San Andreas fault and has migrated northward since ca. 28–25 Ma (Figs. 1 and 2; Dickinson and Snyder, 1979). As the triple junction moves, the former subduction forearc transitions to right-lateral transform motion, and the San Andreas fault continues to lengthen (Lock et al., 2006; Materna et al., 2023). The north coast section of the San Andreas fault is an obvious and significant hazard; however, the history of past events on the San Andreas fault on the peninsula is poorly known. Surprisingly little is known about earthquakes and their timing prior to the great earthquake of 18 April 1906. Several attempts have been made to acquire paleoseismic records for the north coast and peninsula segments of the San Andreas fault, with mixed results. Despite significant efforts (Prentice et al., 1999; Knudsen et al., 2002; Kelson et al., 2006; Zhang et al., 2006; Hall and Niemi, 2008; Fumal, 2012; Schwartz et al., 2014), long records remain elusive, and even the relatively short records available are controversial (Streig et al., 2020). Three longer records exist: the marine record at Noyo Channel and along the offshore area of the northern San Andreas fault (Goldfinger et al., 2007, 2008); a ~2700 yr record at Vedanta Marsh (Zhang et al., 2006); and an ~2200 yr record at Lake Merced, in San Francisco (Goldfinger, 2021; see Fig. 1).

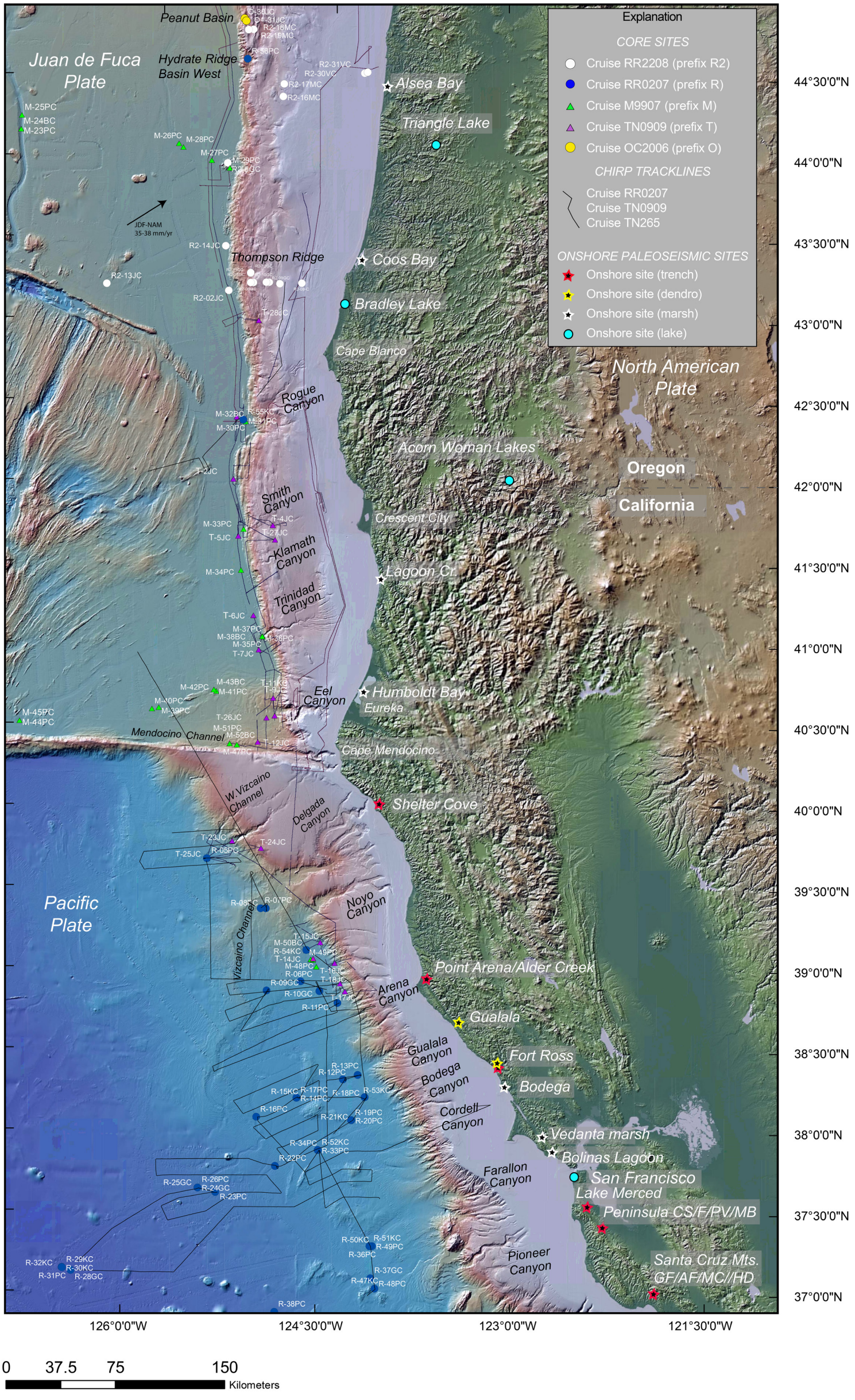

Figure 1. Regional map showing compiled bathymetry, core sites, and subbottom track lines for the southern Cascadia subduction zone and northern California margins. JDF—Juan de Fuca; NAM—North America; CS—Crystal Springs and Crystal Springs South; F—Filoli; PV—Portola Valley; MB—Monte Bello (Seitz, 2018); GF—Grizzly Flat; AF—Arano Flat; MC—Mill Canyon; HD—Hazel Dell.

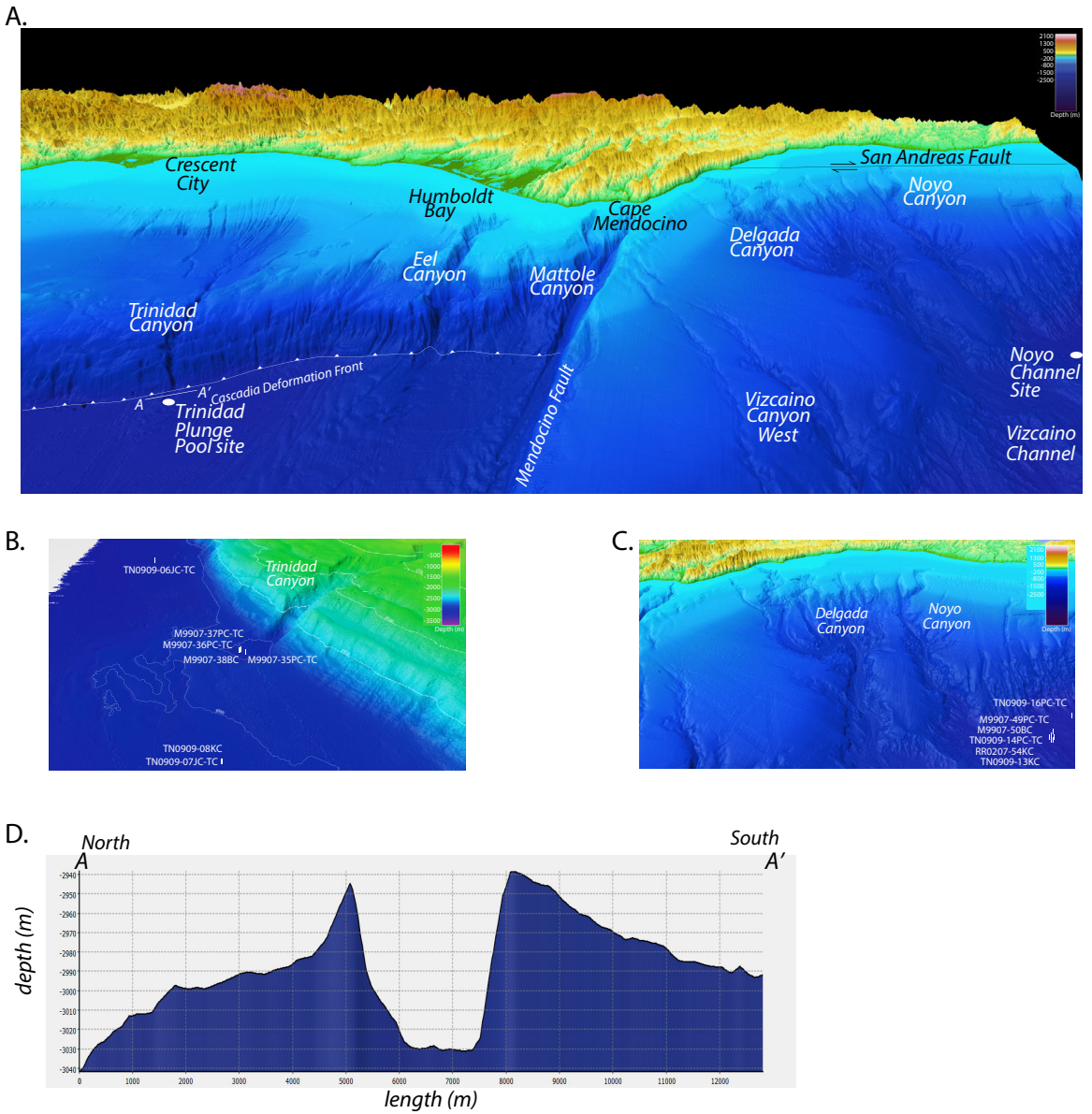

Figure 2. (A) Shaded-relief perspective view of the southern Cascadia subduction zone, the Mendocino triple junction, and northern California margin looking northeast. At left is the Trinidad Canyon system and plunge pool; at center is the Eel Cayon and Mattole Canyon; at right are Delgada/Vizcaino and Noyo Canyons. (B) Perspective view of Trinidad lower canyon, plunge pool, and concentric sediment waves showing core locations. Depths and horizontal ticks are in meters. (C) Perspective view of Noyo and Vizcaino Canyons and upper channels, showing core locations. (D) Depth cross section across Trinidad plunge pool at A-A′.

METHODS

Chirp Subbottom Profiling

We collected ~14,500 km of continuous shallow seismic reflection profiles along the southern Cascadia subduction zone margin acquired in 1999, 2002, 2009, 2015, 2020, and 2022 using Knudsen 320BR and 3260 3.5 kHz chirp echosounder systems (in frequency modulation chirp mode sweeping at 2–6 or 3–10 kHz) at full bandwidth and data rate (Fig. 1). These lines were heave-corrected in real time using the ship's PosMV320 motion sensor and postprocessed with band-pass filtering using Sioseis (Black, 2014; http://sioseis.ucsd.edu/sioseis.html; Henkart, 2003). Data were integrated with bathymetry and interpreted in IHS Kingdom. Synthetic seismograms generated from core data are compared to the chirp traces to aid in testing correlations along strike (see Black, 2014). Further details of processing and resolution are given in Supplemental Text S1.[1]

Core Analysis

We used a core and sample dataset (n = 137) collected on cruises M9907, RR0207, TN0909, OC2006, and RR2208 to explore the Holocene turbidite stratigraphy in the southern Cascadia subduction zone margin and northern San Andreas fault region (Fig. 1). Core locations and metadata are provided in Supplemental Data S1.

Cores were scanned with a Geotek multisensor logger collecting high-resolution visible imagery, gamma density, magnetic susceptibility, P-wave velocity, and resistivity. Both low- and high-resolution point magnetic susceptibility data, X-ray computed tomography (CT), gamma density, P-wave velocity, resistivity, and grain-size data were collected following the methods described in Goldfinger et al. (2012, 2017). Further details are given in Supplemental Text S1.

For selected beds, smear slides supplemented the geophysical, grain-size, and color observations to verify the increased lithic content in interpreted fine-grained beds and the upper contact with hemipelagic sediment (Goldfinger et al., 2013b; Wetzel and Balson, 1992). Further discussion of this proxy and the use of other physical property parameters can be found in Goldfinger et al. (2012). CT scanning was performed at Oregon State University using a 64 slice Toshiba Aquillon system as described in Goldfinger et al. (2012, 2017). Analysis of CT data was done with the software packages OsiriX (Rosset et al., 2004) and Athena Dicom (Haak et al., 2016). The present study used 52 cores from cruises M9907, RR0207, TN0909, and RR2208 that have not been previously published or utilized, enhancing and modifying previous work for the purpose of improving stratigraphic interpretation of the southernmost Cascadia subduction zone.

[1]Supplemental Material. Supplemental Material includes text and figures supporting radiocarbon age models, core correlations, and related details. High-resolutiuon versions of Figures 3, 5, and 8 are also included. Please visit https://doi.org/10.1130/GEOS.S.29996626 to access the supplemental material, and contact editing@geosociety.org with any questions.

Age Control

To date the turbidites, we extracted the calcium carbonate shells of planktic foraminifers preserved in the hemipelagic sediment below each turbidite. Samples were selected below each turbidite because the boundary between the top of the turbidite tail and the hemipelagic sediment can be difficult to identify reliably. Detailed procedures are described in Goldfinger et al. (2012). Radiocarbon data, calibrations, age-model calculations, and error budgets for ages were calculated using an analytical model described in Goldfinger et al. (2012) and with Bayesian age-depth models as described in the following section. The ages used in this study allow estimation of turbidite emplacement ages, accounting for reservoir variation, sediment sample thickness, gaps between the sample and turbidite base, and differential erosion in some cases. All uncertainties were propagated using root mean square (RMS) calculations and estimated basal erosion of the subturbidite hemipelagic sediment using multiple cores as described in Goldfinger et al. (2012). Further details of the analytical model ages are given in Supplemental Text S1. Ages and model results reported here supersede earlier works. Several samples had evidence of post-1950 bomb carbon, and those ages were calibrated with Cali-Bomb (Queen's University Belfast, http://calib.org/CALIBomb/, accessed 15 July 2020; McKay et al., 1986). For convenience, ages for historical events (including 1700 CE) are reported as CE; all other ages are reported as yr B.P. (which is defined as A.D. 1950, per convention).

Age Models

Age-depth models were computed for selected cores using OxCal, a Bayesian Markov chain Monte Carlo calibration and age-model software package (Ramsey, 2001, 2008, 2009). For primary sites at Noyo Channel and Trinidad plunge pool and auxiliary sites at Hydrate Ridge Basin (west) and Rogue, Smith, and Klamath Aprons, OxCal P-sequence age models were computed (Ramsey, 2008), with turbidite stratigraphy removed to develop an "event-free" stratigraphy. See Supplemental Text S1 for details of improvements made to the benthic-planktic differencing calculations, replicate ages, and the time and space variable reservoir model. For this study, the entire dataset was recalibrated with Marine20 (Heaton et al., 2020). The Marine20 database calculation includes significant improvements in ocean circulation modeling and error propagation (see Supplemental Text S1). The uppermost model ages supported by bomb-carbon are reported to the year; all others are rounded to the decade.

Ages for events deemed to be likely correlative were statistically combined using OxCal, with recalibrated ages and other improvements to the dataset used to reexamine the temporal statistical correspondence of the proposed correlations of Goldfinger et al. (2012). See Supplemental Text S1 for discussion of sedimentation rates used. Individual ages were also ranked in a quality assessment scheme, outlined in the Data Quality tab in Supplemental Material Data S2 and described in Supplemental Text S1.

The previously mentioned revisions, and numerous other minor revisions in this work, are included in Supplemental Data S2, which supersede previous versions in Goldfinger et al. (2012, 2017). Age model input parameters and outputs are given in Tables S3–S19.

Lithostratigraphic Correlation

Cascadia subduction zone turbidites are typically composed of multiple stacked and truncated, fining-upward sequences (Bouma A–C) capped by a fine-grained, fining-upward tail associated with waning of the turbidity current (Bouma D). These are termed multipulsed or amalgamated turbidites (Gutiérrez-Pastor et al., 2013; Van Daele et al., 2017). The magnetic susceptibility, density, and grain-size trends within each event are closely correlated, allowing the use of high-resolution density and magnetic data as grain-size proxies in many cases, verified with particle-size analysis (Goldfinger et al., 2012, 2017, and references therein).

Intrasite and intersite correlation was performed by lithostratigraphic correlation, simultaneously integrating physical property parameters with core imagery, age data, CT data, and interactively testing alternate correlations or lack thereof to compare key beds among core sites. Correlations were temporally constrained by the well-dated Mazama ash (7680–7580 cal. yr B.P.; Egan et al., 2015), radiocarbon data, and the Holocene-Pleistocene faunal boundary (Goldfinger et al., 2012, and references therein). Additional ash analyses were performed to expand the ash dataset for this margin.

Potential correlations were tested using a well-logging procedure known as "flattening" (the common industry term "well logging" is also applied to cores). This involves choosing a core that remains at true scale (reference core), while other data (physical property traces, CT, and visible imagery) from other cores are warped to use the bases and tops of all potentially correlative turbidites as tie points on the same temporal (vertical) scale as the reference core (for details, see Goldfinger et al., 2012, and references therein). In this process, the interpreter identifies similar patterns in individual beds and sequences of beds in the age-constrained cores and applies knowledge of the depositional model, core anomalies, site setting, and dynamics to form a stratigraphic model. The combined dataset from the turbidite sequence is shifted iteratively relative to each other, using "ghost traces" to compare alternative detailed matching (or lack thereof) of wiggle traces of physical properties, imagery, and age control from site to site, similar to e-log correlation in the oil industry (McCubbin, 1982; Mitchum and Wagoner, 1991; Løvlie and van Veen, 1995; Rao et al., 2005; Mari and Coppens, 2003) and other academic applications (e.g., Fukuma, 1998; Karlin et al., 2004; Abdeldayem et al., 2004; St-Onge et al., 2004; Patton et al., 2015; Howarth et al., 2021; Seibert et al., 2024). We also tested the correspondence, or lack thereof, of turbidite sequences using the simple metrics of bed thickness and mass per event. Sequences were compared visually and statistically to examine the quality of results from the previously mentioned steps.

To investigate possible doublet stratigraphy expected from a recent hypothesis about the 1700 CE Cascadia subduction zone earthquake, we examined 108 published examples in marine and lacustrine cores interpreted as the 1700 CE event. With nine equivocal examples with core tops missing or deformed, 99 viable examples remained that were utilized (excepting the Trinidad plunge pool; Goldfinger et al., 2012, 2017; Goldfinger, 2017; Gutiérrez, 2020; Morey et al., 2013; Morey and Goldfinger, 2024).

RESULTS

In order to develop the basis for comparison of the southern Cascadia subduction zone with the northern San Andreas fault stratigraphy and event ages, we first describe the age-model results and then the integrated correlation results from both systems in detail. Additional age models used in supporting roles are given in Supplemental Text S1.

Age Models for the Northern San Andreas Fault and Cascadia Subduction Zone

Noyo Channel Age Model

The new age model for Noyo Channel uses cores M9907–49PC/TC and TN0909–14JC/TC, box core M9907–50BC, and Kasten cores RR0207–54KC and TN0909–13KC. Additional cores (TN0909) allowed a more detailed site correlation for the mid–Noyo Channel site (Fig. 3) than that in previous work, with all cores located within ~50 m of each other (Fig. 1). The local stratigraphic variability was significant, most likely due to the proximal position of the cores in the upper part of the abyssal Noyo Channel system. The relatively proximal site was chosen in part to remain above the calcium compensation depth for datable calcareous foraminifera. Coring artifacts and their implications at this site have been further discussed in Goldfinger (2021). For the best overall quality, M9907–49PC/TC served as the age-model basis (Fig. 4), as these cores had better resolution (lower compression) than the 2009 cores, though there was greater suction deformation. The upper part of the model, above event NT3–NT4, is from box core M9907–50BC, which had seven pristine subsamples. The remaining ages came mainly from M9907–49PC, a few meters away. The OxCal quality indices are A_{model} = 93.4 and $A_{overall}$ = 93.1.

Trinidad Plunge Pool Age Model

Trinidad Canyon is a unique system that comprises a large drainage basin with multiple feeder canyons that merge and drop steeply down the lower slope into a plunge pool (Lee et al., 2002). The plunge pool in turn has no well-defined exit and is surrounded by a concentric wavefield that indicates

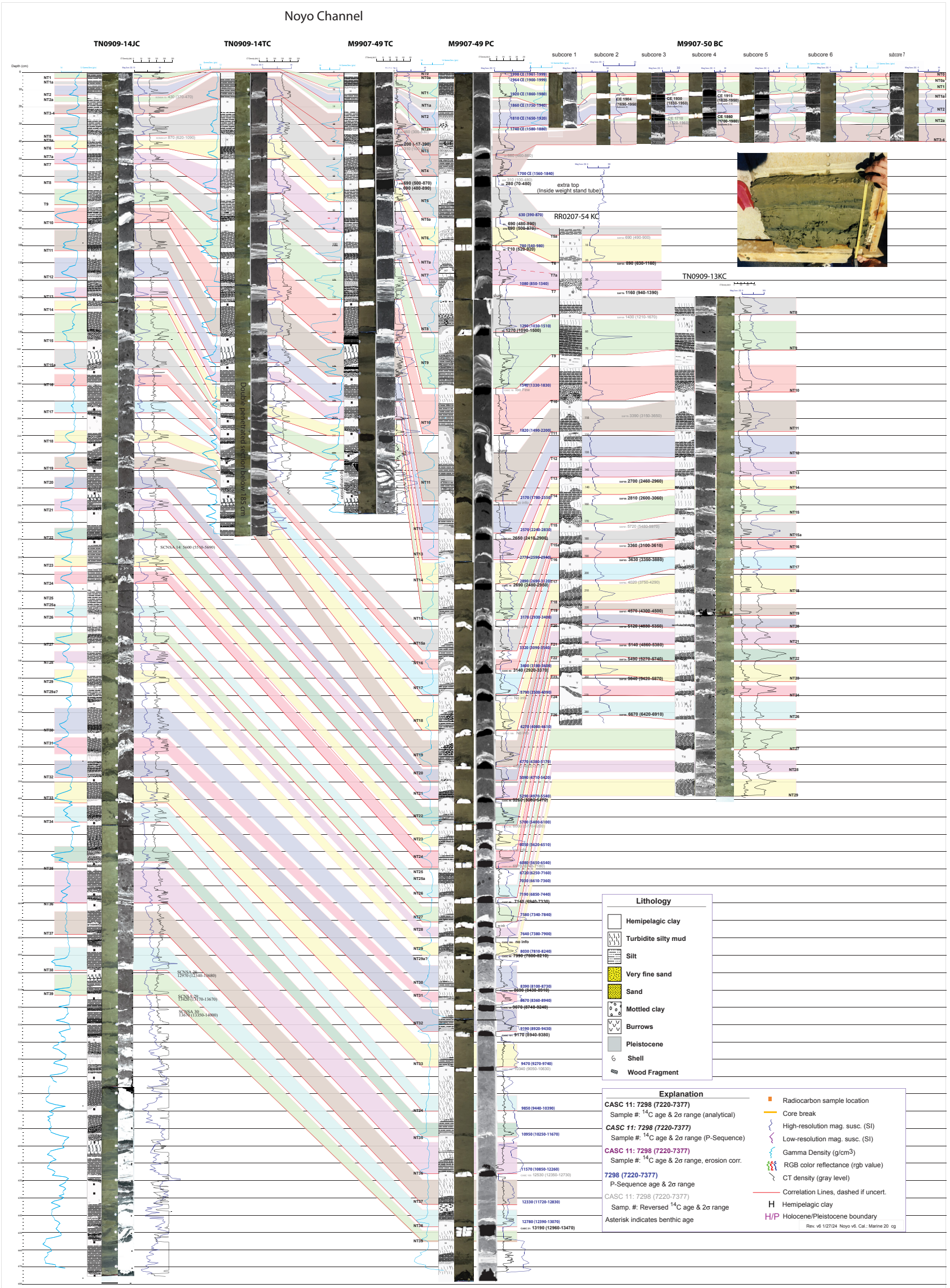

Figure 3. Correlation diagram for Noyo Channel cores, northern San Andreas fault. Computed tomography (CT) imagery, red-green-blue (RGB) imagery, and physical traces are shown with core log details. OxCal P-sequence model ages are shown with calibrated radiocarbon ages where available. Ages from ca. 1700 CE and younger beds are shown as CE for historical convenience; all others are yr B.P. (relative to 1950). Grayed out ages indicate reversed or outlier older ages. Subsample cores for M9907–50BC are shown, with representative photo of the excavated box core. mag. susc.—magnetic susceptibility. A high-resolution version of this figure is available with the supplemental material files (see text footnote 1).

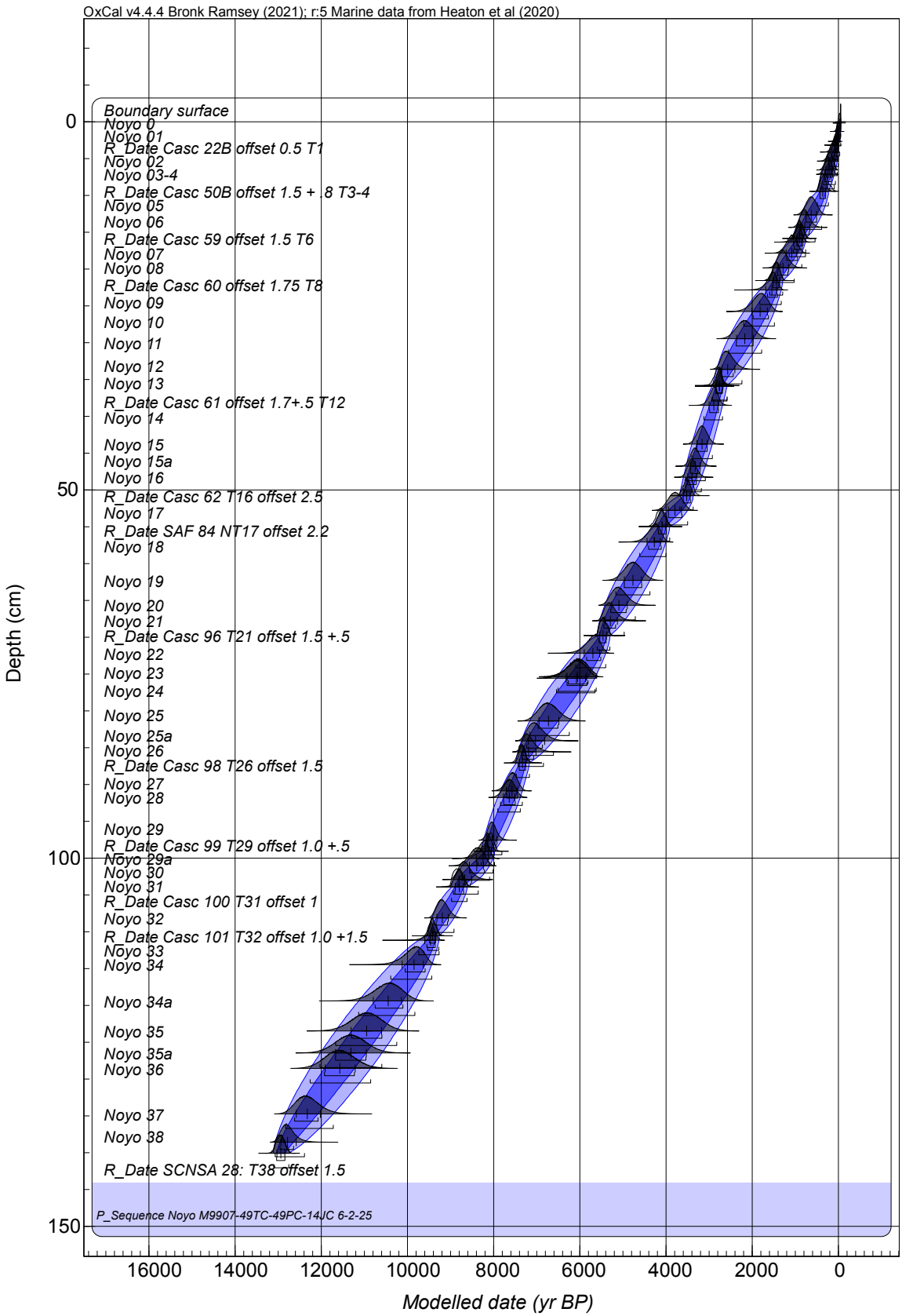

Figure 4. Holocene OxCal P-sequence age model for Noyo Channel. Upper beds utilize box core M9907–50BC, subcores 6 and 7; beds below Noyo event NT3–NT4 use core M9907–49PC. These cores have similar compaction and are suitable for this composite age model. Blue shadings show 1σ and 2σ ranges; medians and individual uncertainty ranges are also shown. See Table S8A for the model code and tabular output (see text footnote 1).

outward flow. Goldfinger et al. (2012) originally sampled the plunge pool and subsequently cored the areas immediately to the north and south to characterize this site in more detail. The seven plunge pool cores included M9907–35 to M9907–37PC-TC and box core M9907–32BC. The record is of excellent quality, without obvious core disturbances (Fig. 5).

The best available intervals from the Trinidad plunge pool core set between the beds from the surface down to the 6 m level were used, anchored with core M9907–36PC (Fig. 5). The OxCal P-Sequence depositional age models are supported by bomb-carbon (post-1950) and Accelerator Mass Spectrometry ^{14}C ages (Figs. 6 and 7). We calculated two models, one with the local radiocarbon age of the T1 bed, and one without that age. The models were virtually identical; however, the model without the interpreted 1700 CE direct age is preferred, as the sample (Casc 210) age is a benthic sample, which has much larger uncertainty. Also critical was the constraint that the upper three beds must all be post-1950, based on the bomb-carbon age in bed T0c, the third bed from the surface. The resulting tables for all age models are given in Tables S3–S19, and the depth figure from OxCal is shown in Figure 6. This simple model has no significant errors, and no sharp kinks in sedimentation rate, suggesting a relatively straightforward result. OxCal agreement indexes are A_{model} = 99.5 and $A_{overall}$ = 85.5.

Revised Offshore Event Stratigraphy in the Southern Cascadia Subduction Zone

In this section, we present results from lithostratigraphic correlation of the southern Cascadia subduction zone, which integrates the new age models and the Chirp subbottom along-strike correlation. We then present evidence of the unusual stratigraphic doublets that are the focus of this investigation.

Southern Cascadia Subduction Zone Lithostratigraphic Correlation

The southern Cascadia subduction zone "mud" turbidites were described in some detail in Goldfinger et al. (2013b). In this work, further details of these beds were examined using additional cores and our new age-model data. A revised correlation plot for the Trinidad plunge pool site is shown in Figure 5. This site is key to understanding southern Cascadia subduction zone event stratigraphy and has a set of high-resolution records, well recovered in the cores with minimal disturbance. The combined radiocarbon and well-log correlation shown in Figure 5 is an evolution of the Trinidad site figure in Goldfinger et al. (2012).

Anchored by the Trinidad pool correlation, an updated stratigraphic correlation for the southern Cascadia subduction zone is given in Figure 8 (full version given in Fig. S1). The improved correlation builds on Goldfinger et al. (2013b) using additional CT data, additional cores not previously used, additional radiocarbon ages, and the P-sequence age models. This plot also takes advantage of the synthetic seismogram correlation as described in the Methods section, and supporting age models shown in Figures S2A–S2F, with input and output given in Tables S3–S19. We note, as did Goldfinger et al. (2012), that the stratigraphy thickens southward, making the highest-resolution records recoverable with our piston-coring methods ~3–4000 yr in length south of Klamath Canyon, as opposed to the >10,000 yr recoverable elsewhere in the Cascadia subduction zone. A representative pair of these cores flattened on bed tops and bases to assist in visualizing the correlation is shown in Figure 9. A flattened diagram showing the uppermost stratigraphy in this area is shown in Figure 10.

Post–1700 CE Stratigraphy

The post–1700 CE stratigraphy at Trinidad Canyon shows three significant and several minor beds. The uppermost significant bed (T0a) is effectively a surface sand, and negligible hemipelagic material is observed above it (Fig. 7). The uppermost beds are consistent between the 1999 and 2009 cores just outside the plunge pool, suggesting no event beds were deposited in that decade. The lack of hemipelagic material observed, even in the box core with nearly perfect preservation of the seafloor, indicates that little time had elapsed since that event bed was deposited, prior to the date of collection in 1999 (Fig. 7). The second bed from the top, a faint one, returned a post-bomb radiocarbon age at two nearby correlated sites, indicating the three uppermost beds are post-1950 (Reimer et al., 2004, and references therein; see Fig. 8). Post–1700 CE beds can be correlated northward variable distances on the basis of stratigraphic consistency and compatible age models. The upper bed, T0a, is significant and can be tentatively traced 140 km to the north (Figs. 8–10). The second and third beds, T0b and T0c, are faint and can likely be traced 75 km northward from Trinidad to Smith Apron (Figs. 8–10). Post-1700 age models (Fig. 7) suggest the ages of the beds younger than 1950 are: T0a ~1993 (1968–1999); T0b ~1988 (1962–1999); and T0c ~1959 (1950–1988; see Figs. 5 and 8). The fourth significant bed from the surface, T0f, is dated at 1920 CE (1830–1960).

Key Correlation Linkages

Several key tie points in the sedimentary section help to link sites in the southern Cascadia subduction zone. Use of the full Holocene section when possible is critical, as these tie points are scattered throughout the Holocene. A strong tie is T11, a thick coarse-grained event bed with a distinctive two-pulse stratigraphy. This bed has been a key tie point throughout the Cascadia subduction zone, including interpretation of it at all offshore sites, in Triangle Lake (Fig. 1), and in several other lakes and inlets (Goldfinger et al., 2012, 2013b, 2017; Morey et al., 2013; Enkin et al., 2013). This bed, however, cannot be recovered south of Klamath Apron (Figs. 1 and 8) due to limitation of the coring systems in use. Three other prominent beds, T1/T2, T3, and T8, are thick and coarse grained and clearly stand out in the physical property data

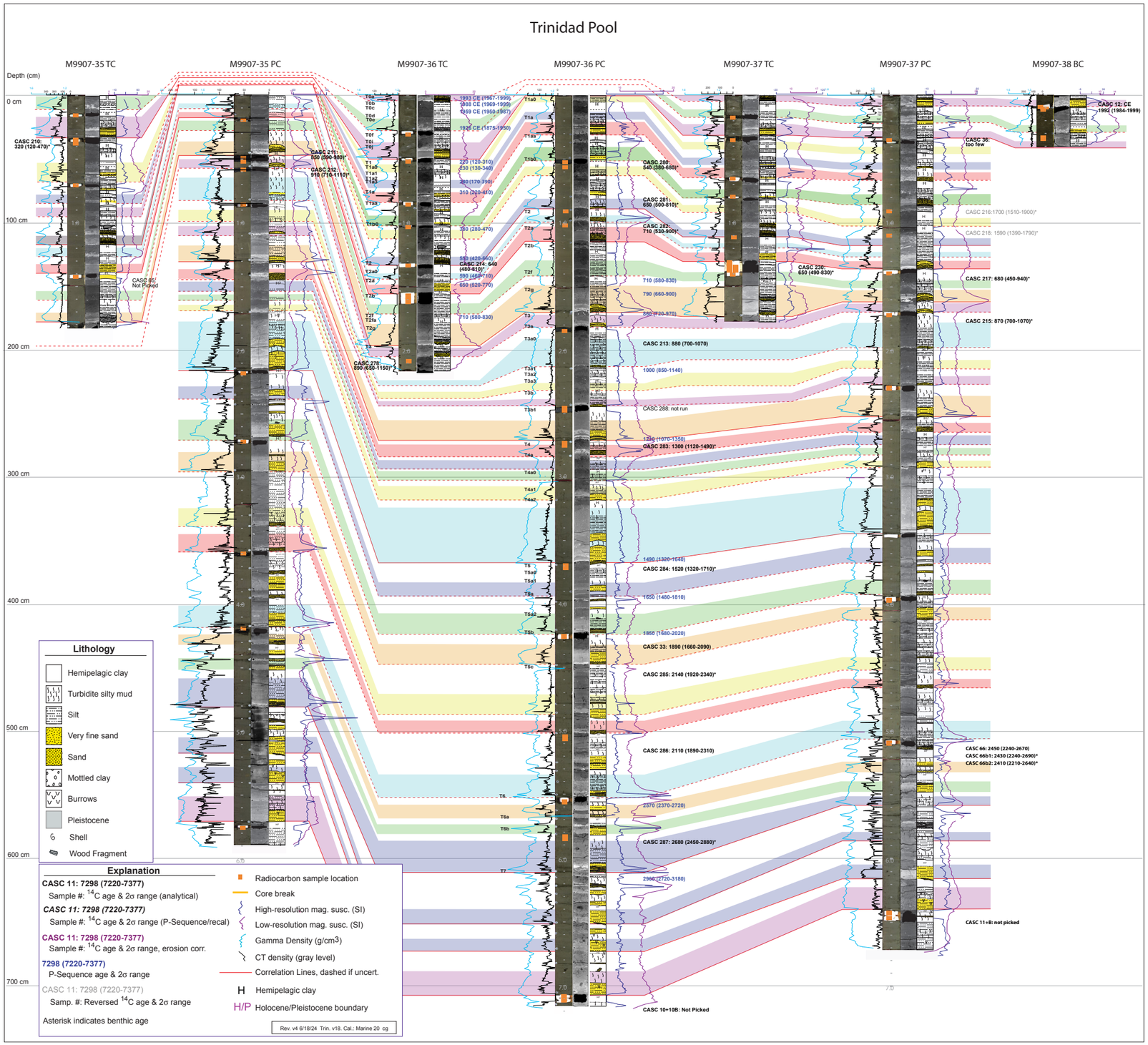

Figure 5. Correlation diagram for Trinidad plunge pool, modified with additional core, petrophysical, and computed tomography (CT) data after Goldfinger et al. (2012, 2013b). Ages for M9907–36PC are shown with original analytical ages in black; recalibrated OxCal P-sequence model ages are shown in blue for comparison. mag. susc.—magnetic susceptibility. A high-resolution version of this figure is available with the supplemental material files (see text footnote 1).

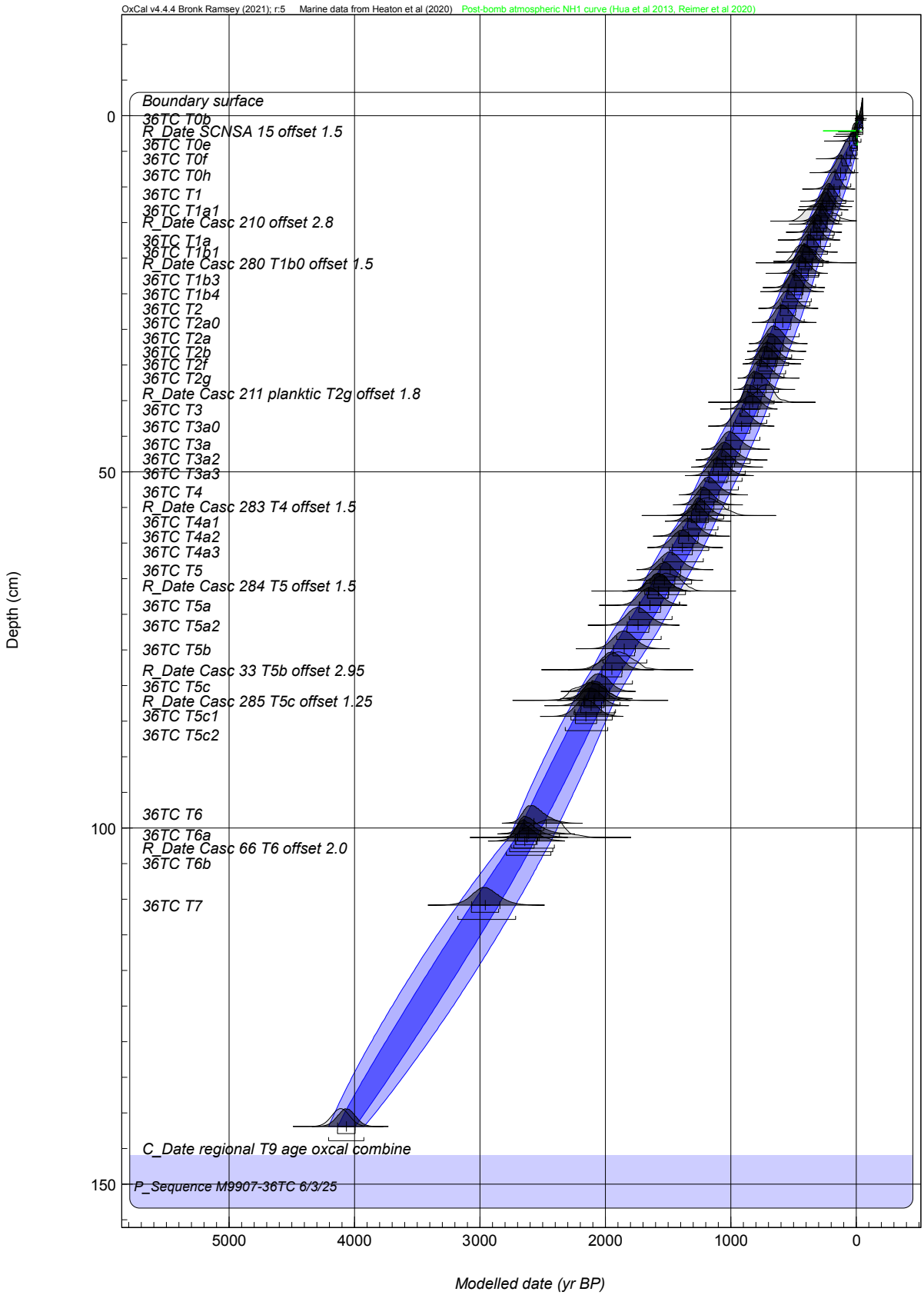

Figure 6. OxCal P-Sequence age model for post–4100 yr B.P. time in Trinidad Canyon, from cores M9907–36 PC and TC. Upper 250 yr of model are shown in more detail in Figure 7. Numerous small events included in the model are omitted here for clarity. The 1σ and 2σ envelopes are shown with blue shadings; medians and individual uncertainty ranges are shown.

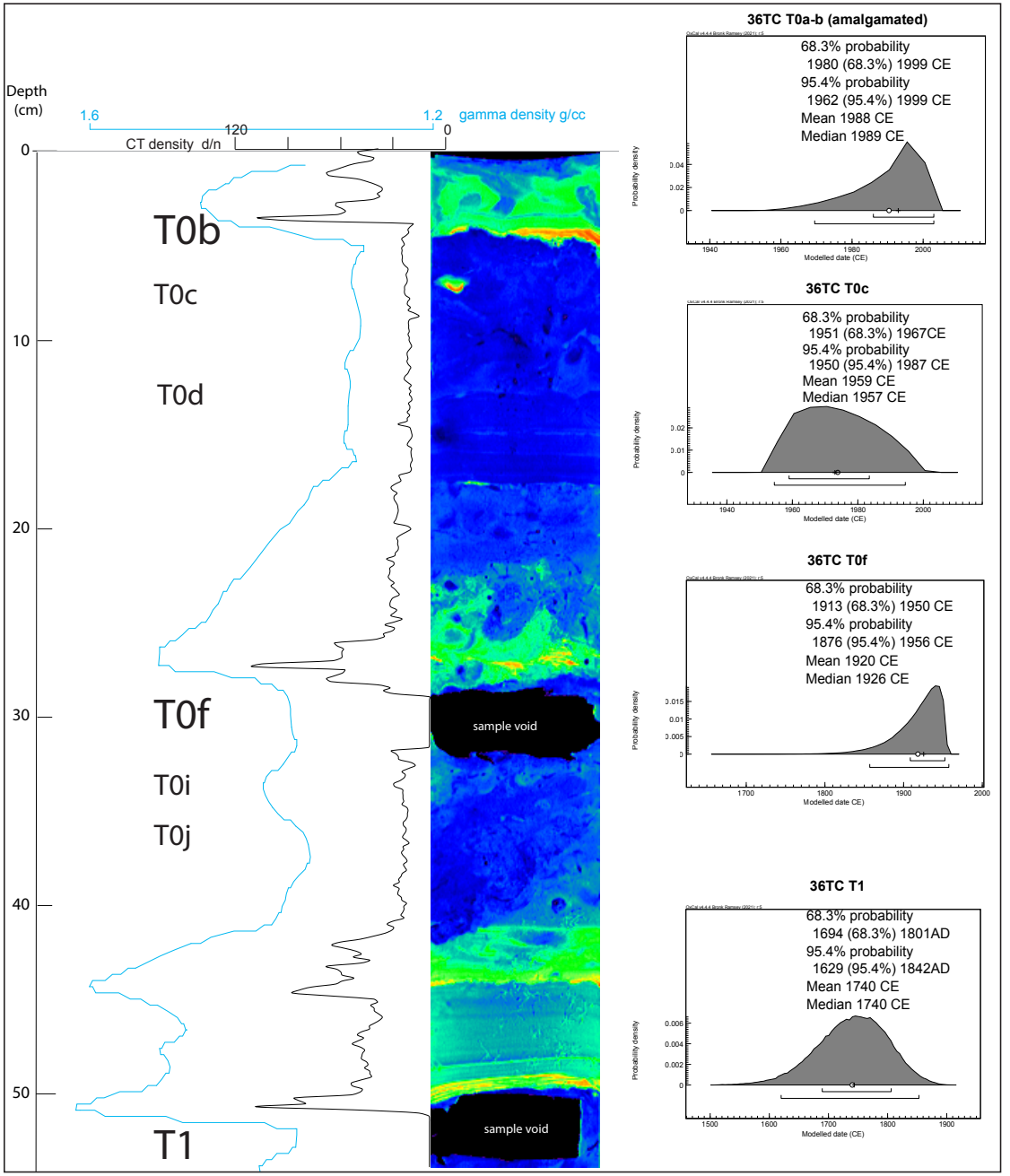

Figure 7. Computed tomography (CT) imagery of uppermost 53 cm of core M9907–36-TC. Detailed CT imagery shows the inferred 1700 CE Cascadia subduction zone T1 event and subsequent event beds. Model probability distribution functions for the ages of these events are shown at right based on the OxCal P-Sequence age model for post–1700 CE time in Trinidad plunge pool, using cores M9907–36PC/TC and M9907–38BC.

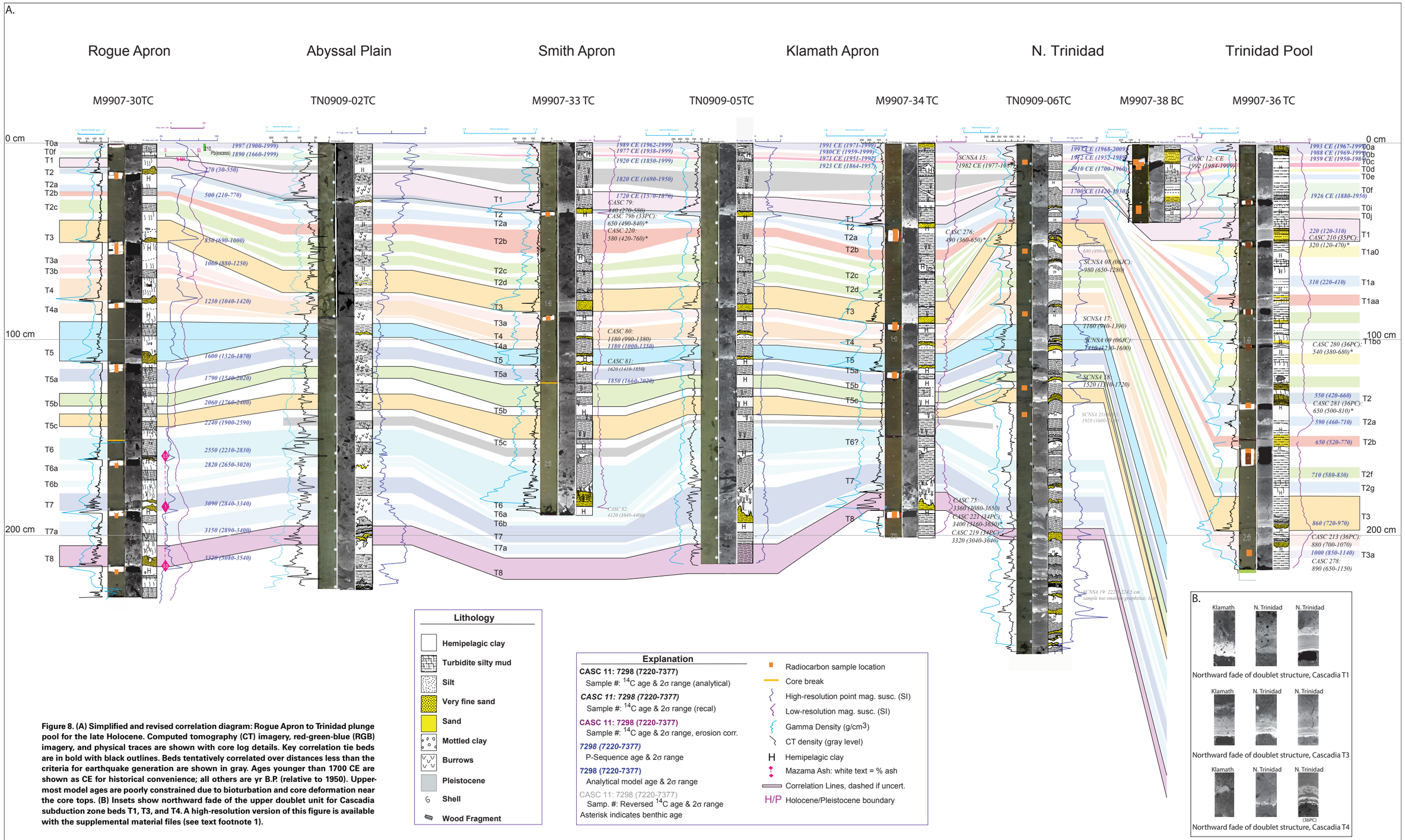

Figure 8. (A) Simplified and revised correlation diagram: Rogue Apron to Trinidad plunge pool for the late Holocene. Computed tomography (CT) imagery, red-green-blue (RGB) imagery, and physical traces are shown with core log details. Key correlation tie beds are in bold with black outlines. Beds tentatively correlated over distances less than the criteria for earthquake generation are shown in gray. Ages younger than 1700 CE are shown as CE for historical convenience; all others are yr B.P. (relative to 1950). Uppermost model ages are poorly constrained due to bioturbation and core deformation near the core tops. (B) Insets show northward fade of the upper doublet unit for Cascadia subduction zone beds T1, T3, and T4. A high-resolution version of this figure is available with the supplemental material files (see text footnote 1).

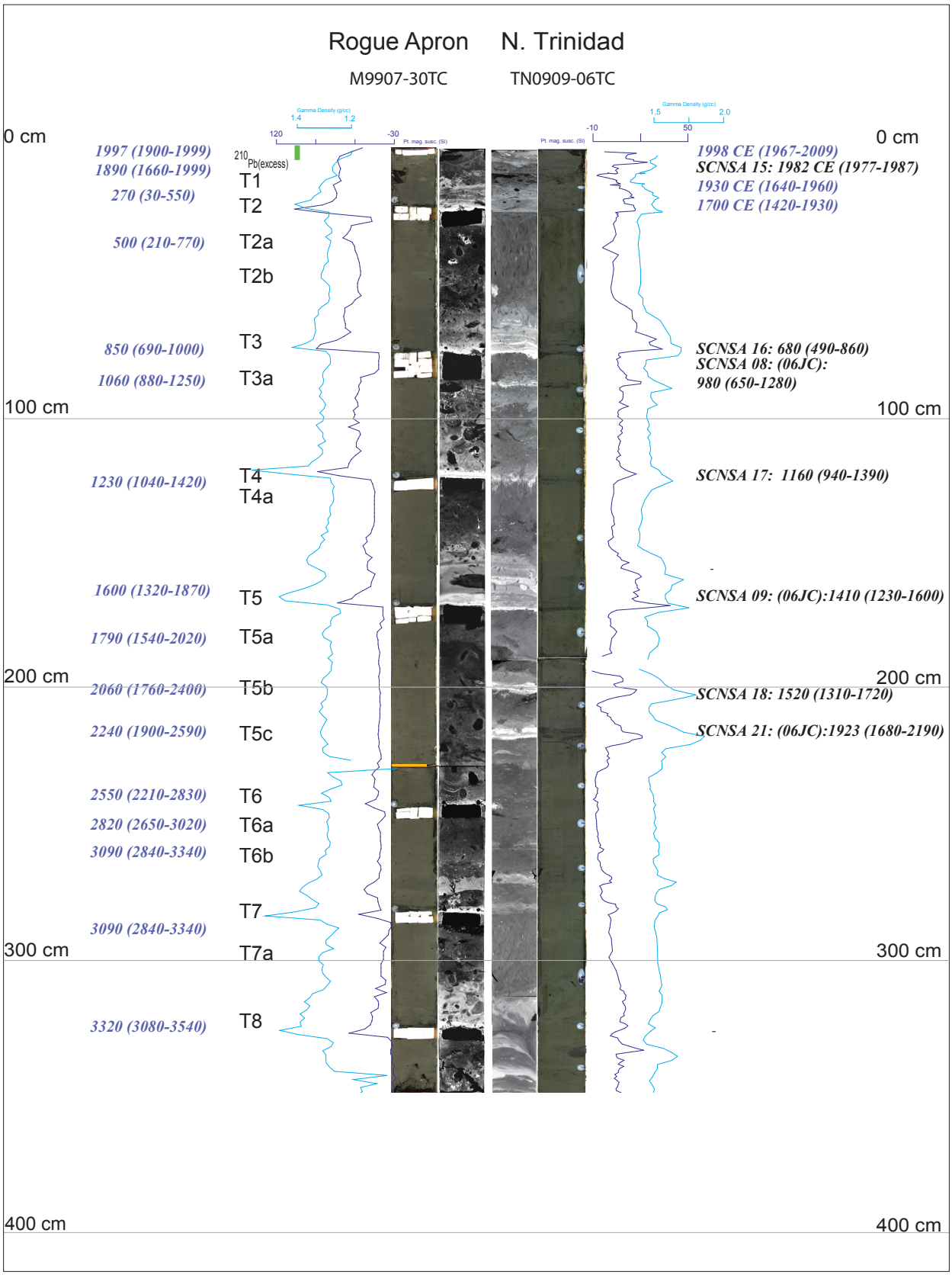

Figure 9. Flattened core diagram comparing Rogue apron core M9907–30TC to core TN0909–06TC, just north of the Trinidad plunge pool. The major event beds and their proposed correlations are apparent in this figure. Other southern Cascadia subduction zone event beds vary along strike, with most weakening northward in thickness, density, and grain size. Compare the robust T5B and T5c in the right core (TN0909–06TC) to the weak diffuse correlatives at left (M9907–30TC).

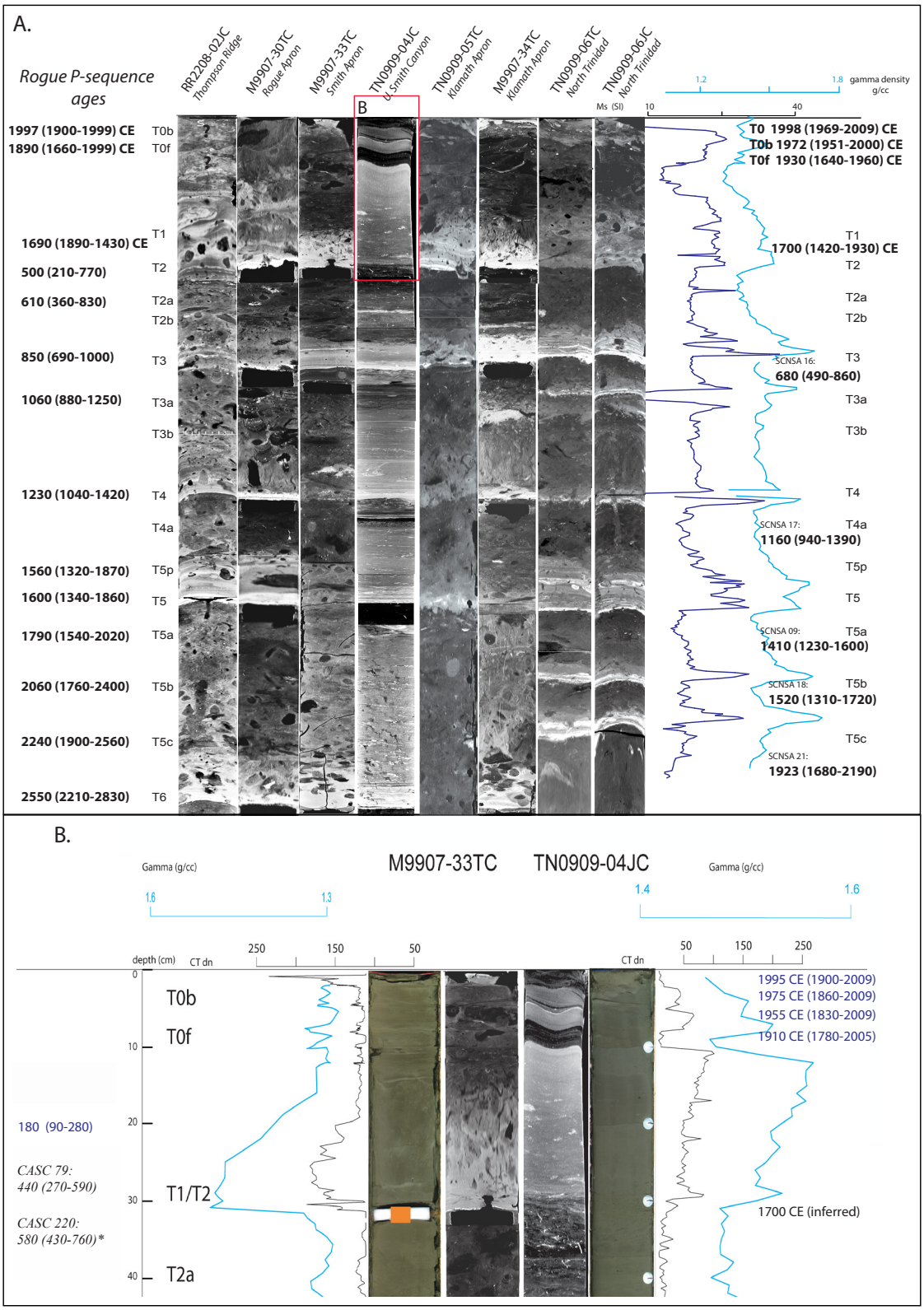

Figure 10. (A) Plot of computed tomography (CT) data for representative cores between Thompson Ridge and Trinidad Canyons, showing the upper meter of section in detail, and extending downward to Cascadia subduction zone regional event T6. At right, core TN0909–06JC is shown with magnetic susceptibility (right) and gamma density (left), and model (postbomb) and analytical event ages (all others). At left, equivalent sections are shown for other cores as noted; OxCal P-sequence model ages are shown for the Rogue Apron site. These cores have been flattened to match event bed tops and bases to TN0909–06TC at true scale (except for TN0909–04 JC, which had a much higher overall sedimentation rate and was reduced ~50% vertically). (Note: Upper two events at Thompson Ridge are unlikely to be correlative to other sites.) Red box is the area of B. (B) Inset showing upper part of TN0909–04JC (slope basin site), showing interpreted events T0a (1992?) and T0f (1906?). P-sequence model ages for upper events are shown, based on the likely T1-T2 pair at base, correlated to nearby core M9907–33PC/TC.

(Goldfinger et al., 2013b). These beds link across the Smith-Klamath reach of the abyssal system, where many events have weak definition. Another key linkage is the sequence T5, T5a, T5b, and T5c. T5 is a distinctive and prominent doublet bed that is present regionally in much of the Cascadia subduction zone (Goldfinger et al., 2012, 2013b, 2017; see also Figs. 8 and 11). There may be time separation between the doublet beds, with intervening sediment observed at Rogue Apron and observed for a likely correlative at Bradley Lake (Kelsey et al. 2005; Goldfinger et al., 2012). The mean age is ca. 1550 yr B.P., and the next oldest major event, regionally correlated T6, has a mean age of ca. 2540 yr B.P. (Goldfinger et al., 2012, 2017). This ~1000 yr gap is represented at all Cascadia subduction zone marine sites, and virtually all land paleoseismic sites as well (Kelsey et al., 2005; Goldfinger et al., 2012, 2017; Nelson et al., 2021; Brothers et al., 2024), adding a strong interdisciplinary tie between methods and site types in Cascadia subduction zone paleoseismology. Goldfinger et al. (2012) found that three fine-grained mud turbidites, all faint, but the lower two bolder (Figs. 5, 8, and 11), lie in this ~1000 yr span. These beds were named T5a, T5b, and T5c after they were tentatively correlated over along-strike distances exceeding 200 km. This pattern has been observed in numerous locales and is used as an additional tie point throughout the Oregon and northern California margins. The ages of these beds are less precise due to the ubiquitous bioturbation of fine-grained beds, but the stratigraphic pattern remains (Fig. 5). In the southern Cascadia subduction zone at Trinidad plunge pool, these beds are correlated to equivalent beds to the north outside the plunge pool, enabling ties across the plunge pool levees. They are coarser grained and conspicuous, and their ages are more reliable due to the lower bioturbation of the more robust beds at that site. Similarly, the ~1100 yr span between regional events T10 and T11 is filled with four event beds south of Hydrate Ridge, T10a, T10b, T10c, and T10f. These have a characteristic pattern, with T10b and T10f being robust thick, coarse beds, and the others relatively faint. Similar to the previous sequence, these beds are observed at all sites in this temporal range and form another unique sequence that is part of the correlation framework (Figs. 8 and 11).

Cascadia Subduction Zone Subbottom Chirp Profile Correlation

Subbottom profiles were correlated 140 km from Rogue Apron southward to Trinidad plunge pool and linked directly to the cores lying along the profiles in Goldfinger et al. (2013b) using synthetic seismogram matching to the chirp records (Black, 2014). Correlation plots from the southern edge of the Astoria Fan southward to the Trinidad plunge pool (Figs. 12–13), a distance of ~240 km, build on the previous work. Processed and flattened subbottom data extending from the intersection of the profile with the relict Astoria Channel allow correlation southward to the Trinidad area (Fig. 12). The section is coherent and can be correlated ~100 km to the north of Rogue Apron, to the site of core RR2208–02JC. The base of the Holocene section is clearly bounded by two to four thick basal reflectors sampled in this core at 10 m depth, providing a reliable baseline for the Holocene. Above these marker beds, 22 beds can be traced between Rogue Apron and the site of RR2208–02JC at Thompson Ridge (Fig. 1). As noted in Goldfinger et al. (2013b), the subbottom profiles cannot resolve the thinner beds, but they can resolve the major turbidite beds. Along the northern San Andreas fault, an observed increase in the ruggedness of terrain and the decreased data density and gaps in the northern San Andreas fault data compared to the Cascadia subduction zone prohibit a robust correlation of reflectors between core sites in the northern San Andreas fault region.

Revised Northern San Andreas Event Stratigraphy

Noyo Channel Stratigraphy

A revised stratigraphy for the Noyo Channel cores is shown in Figure 3. TN0909–14TC double-penetrated the seafloor, with its upper stratigraphy repeated in the lower part of the core (Fig. 3). With that exception, correlation of the new channel cores and previous cores was relatively straightforward and provided additional constraints on the local variability of the beds. While the correlation is clear, local variability is significant at this relatively proximal site. The newer cores are more compressed than the original 1999 cores, which may be due to a shift in the coring gear configuration (see Supplemental Text S1). The correlated site diagram extending into the late deglacial period (Fig. 3) includes 37 event beds, yielding a mean repeat time of ~370 yr. Figure 3 used the OxCal model ages (Fig. 4) for all events in our primary core, M9907–49PC, and single recalibrated ages are also shown. One of the main features of these cores, particularly for times younger than ~4100 yr B.P., is an unusual doublet stratigraphy, which is the focus of the remainder of the paper, discussed in the Doublet Stratigraphy in the Noyo and Trinidad Systems section.

North Coast Northern San Andreas Fault Stratigraphy

We additionally reexamined the turbidite record along the north coast segment of the northern San Andreas fault between San Francisco and Noyo Channel. Preliminary assessments of this record were published in Goldfinger et al. (2003, 2007, 2008). At that time, they had significant difficulties in several respects. Some of the issues are resolved in this work; however, the results remain incomplete and are used only sparingly in this paper. The results of the new correlation show that, as in previous work, many event beds are likely to be correlated over much or all of the 280 km between Noyo and Pioneer Canyons offshore San Francisco (Fig. S3). Of the 19 correlated beds extending southward from Noyo Channel, 11 of them are interpreted to extend to Pioneer Canyon, with one terminating just short. Four beds are interpreted to extend between Noyo and Bodega Canyons, spanning ~160 km, and one bed terminates at Gualala Canyon, a distance of ~130 km. Three beds correlate much of the full length, terminating at Noyo Channel, and several other beds are limited

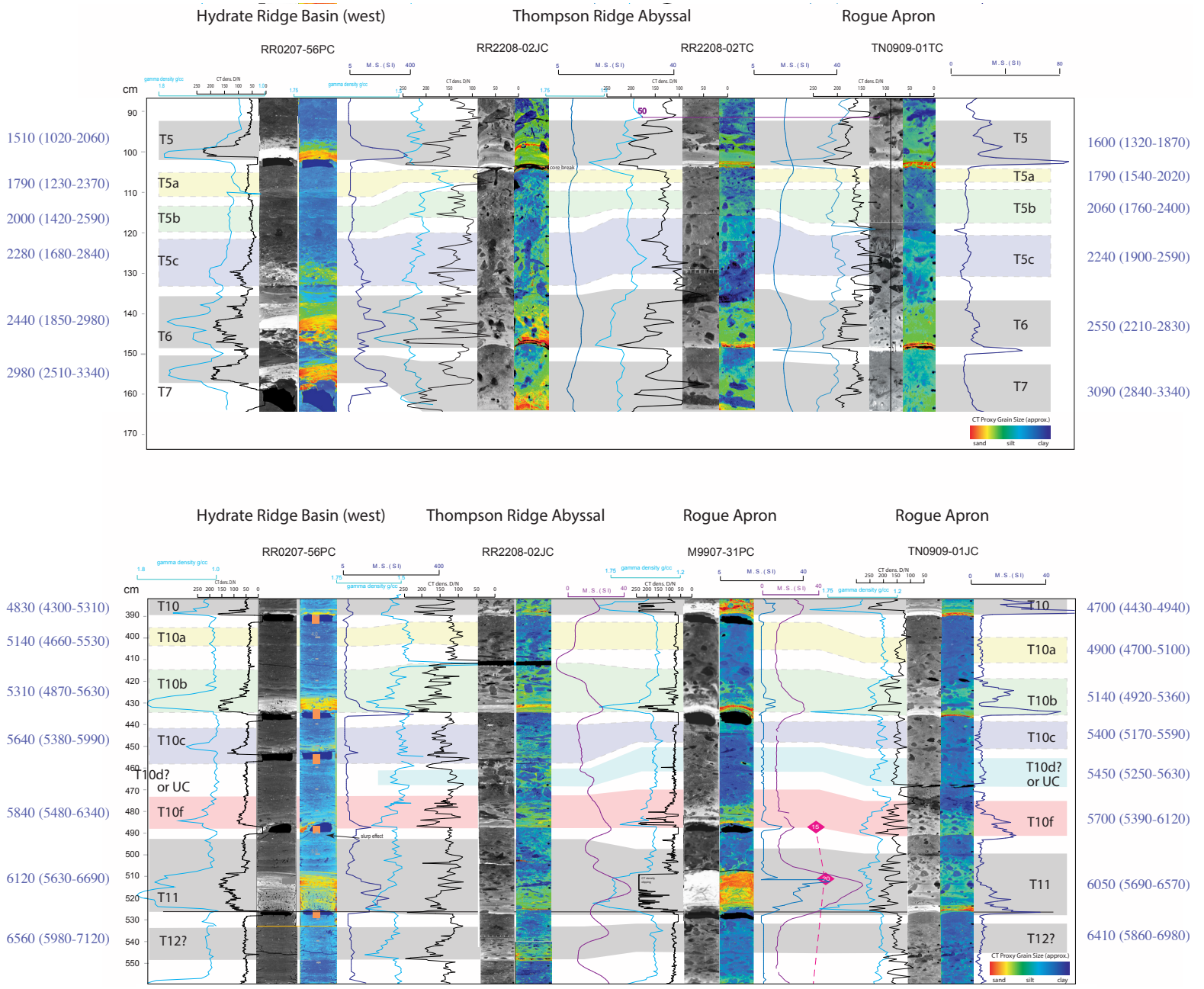

Figure 11. (A) Comparison of events T5–T7 between Rogue Apron and Hydrate Ridge. Gray level and false color computed tomography (CT) images are shown. The spatial and temporal gap between major events T5 and T6 is ~1000 yr based on Goldfinger et al. (2017), Nelson et al. (2021), and Kelsey et al. (2005). This time gap is a key element in linking the land and marine records unequivocally. Between these two events, fine-grained beds T5a, T5b, and T5c are observed. Grain size and smear slide lithic descriptions may be found in Goldfinger et al. (2013b). Physical property traces are as in Figure 5. OxCal model ages for Hydrate Ridge and Rogue Apron are shown at left and right respectively. Approximate CT proxy grain size is shown in color CT imagery. Overall vertical scales were adjusted slightly for clarity (<5%); RR2208–02TC is at true scale. M.S.—magnetic susceptibility. (B) Comparison of events T10–T12 between Rogue Apron and Hydrate Ridge. The ~1100 yr span between full-length events T10 and T11 is filled with four thinner event beds south of Hydrate Ridge, T10a, T10b, T10c, and T10f. These have a characteristic pattern, with T10B and T10f being robust beds and T10a and T10c being relatively faint. See Figure 8 for rest of legend.

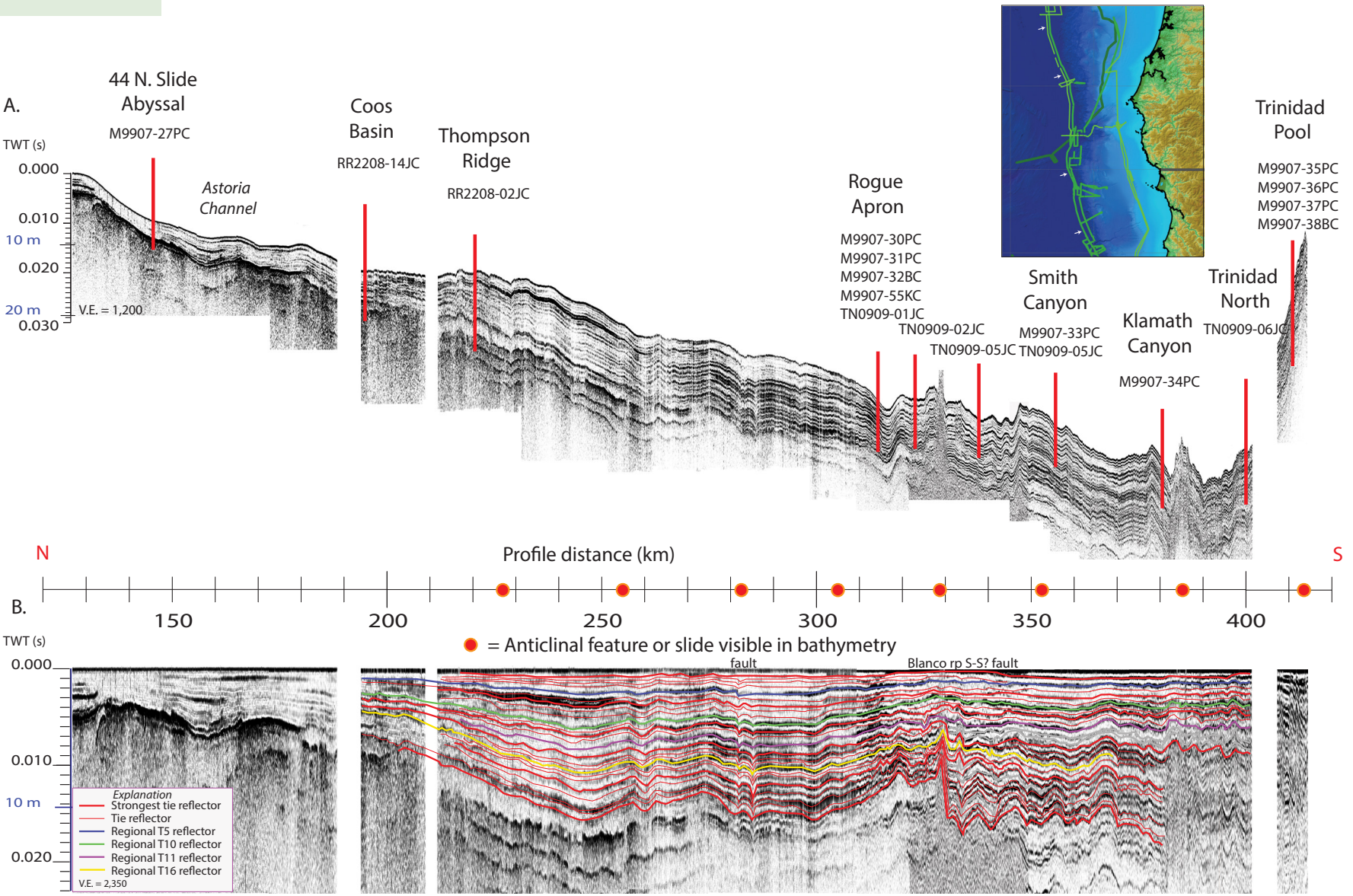

Figure 12. Seaward subbottom profile paralleling the southern Cascadia deformation front. In total, ~280 km of subbottom data from the southern edge of the Astoria Fan off northern Oregon to Trinidad plunge pool in northern California are displayed; white arrows indicate profile track in location map. (A) Subbottom profile with individual turbidite reflectors shown. Approximate core locations and depths of penetration are shown, projected onto the profile. (B) Profile data flattened to the seafloor. Correlated regional reflectors tied to core data in Goldfinger et al. (2013b) are shown. Uncorrelated early Holocene reflectors south of Rogue Apron in the downthrown block of the Blanco rift propagator (rp) fault (where S-S? indicates strike-slip?) are shown in gray. Along-strike range is shown in km. Two-way time (TWT) and approximate depth conversion (V.E.—vertical exaggeration) is shown for each image. The bathymetry is extremely flat—note extreme vertical exaggeration required to make the profiles viewable.

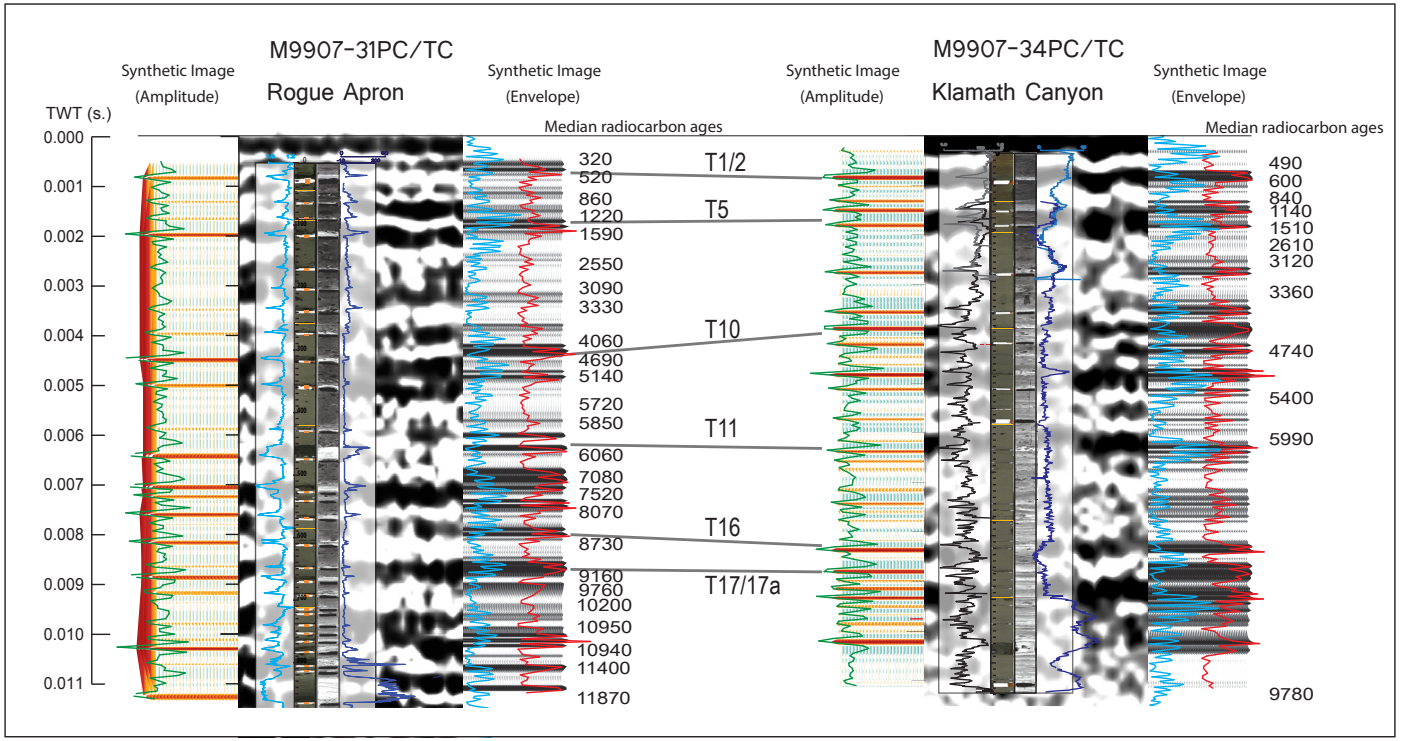

Figure 13. Representative core and subbottom comparison for two Cascadia subduction zone core sites. Stacked image to left of subbottom profile: synthetic seismogram. Stacked image to right of subbottom profile: envelope of synthetic seismogram. Green traces—synthetic seismograms; orange traces—representative core site traces; blue traces—envelope of representative core site traces; red traces—envelope of synthetic seismogram. Core, image, and computed tomography data with density and magnetic traces are shown at center. Median radiocarbon ages and representative tie lines between sites are labeled with interpreted event bed names, after Goldfinger et al. (2013b). Slight mismatches are observed, likely due to the sampling scale of the subbottom profile, and location of the profile traces that are within 1.6 km of the core sites but not exactly intersecting with them. TWT—two-way time.

to smaller sections of the middle part of the north coast transect. The quality of the correlations is highly variable, from very strong to weak. Typically, the thick doublet beds observed in Noyo Channel correlate robustly along much or all of the full transect length. Further discussion of the north coast regional stratigraphy is included in the Supplemental Material.

Doublet Stratigraphy in the Noyo and Trinidad Systems

Noyo Channel Doublets

In Noyo Channel, many of the Holocene turbidites have an unusual, inverted doublet appearance. The petrophysical traces suggest a coarsening-upward unit, but the CT images and close examination revealed two subunits: a coarse, sandy bed deposited on top of a silty fining-upward bed. Most examples are composed of similar pairs of fining-upward sequences, closely stacked, with the upper unit typically denser, thicker, and coarser than the lower unit. Commonly, the upper units have a sharp upper contact between the $T_{A–C}$ and T_E units (Fig. 14). (The magnetic and CT density data were collected after the 1999 core was sampled and are disrupted by the sample voids, but the gamma density was collected from the core onboard before splitting and is unaffected.) The majority of the late Holocene Noyo beds show similar structure and have no evidence of hemipelagic sediment between the two coarse pulses (Fig. 15). The doublet stratigraphy commonly fades southward from Noyo Channel, with the lower unit fading from the sequence (Fig. S3, inset).

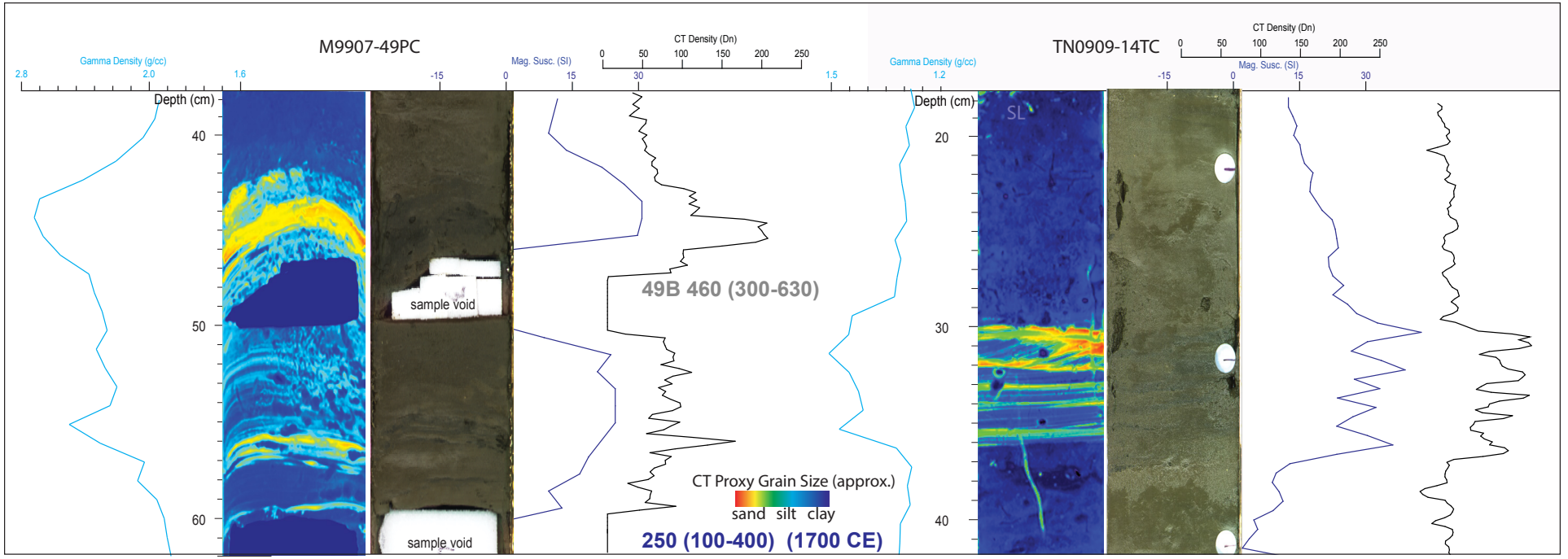

Figure 14. Two examples of the doublet stratigraphy commonly observed in Noyo Channel event beds in detail. This unit (NT3–NT4) was thought to be two separate turbidites, and both units were sampled and ^{14}C dated, yielding the upper grayed out, reversed age and the lower valid age. The stacking of a dense, sand-rich unit above a finer-grained unit is evident. The age obtained from below the doublet is similar to the ages for this event to the south along the northern San Andreas fault, and to the 1700 CE event in the Cascadia subduction zone. Right example is from TN0909–14TC, a trigger core, and is more vertically compressed than the piston core at left. Approximate grain size in false-color computed tomography (CT) imagery is shown by color scale. mag. susc.—magnetic susceptibility.

Cascadia Subduction Zone Doublets

Doublet stratigraphy is also observed in the southern Cascadia subduction zone. The Cascadia subduction zone doublets are less pronounced and, where present, are comprised of an upward-fining lower unit and a second upward-fining unit of coarser material embedded in the event bed tail, or, in some cases, a separate event with some hemipelagic sediment between the two. The likely 1700 CE bed has a typical coarse base and rapid upward-fining sequence, and it has a second upward-fining coarse bed with loading structures embedded in the tail of the primary bed (Fig. 16). Within the interpretable time range of the Trinidad plunge pool (<2500 yr B.P.), there are three other doublets that have similarities with the upper doublet (Figs. 5 and 17), suggesting close timing between the two elements, and several others with some hemipelagic material between the two units. This doublet stratigraphy fades northward from Trinidad plunge pool (Fig. 8, inset). This northward change consists of the upper unit fading from the sequence.

DISCUSSION

We now discuss the potential interaction of the Cascadia subduction zone and the northern San Andreas fault. The two adjacent major fault systems both have long paleoseismic records with which we evaluated hypotheses that might explain the data, and finally we discuss implications of our preferred hypothesis.

Refinement of the Event Correlation for the Southern Cascadia Subduction Zone and Northern San Andreas Fault

Age Control

The differences between the analytical and Bayesian age models are, for the most part, negligible (see Fig. S4; Table S1). Some of the variation likely

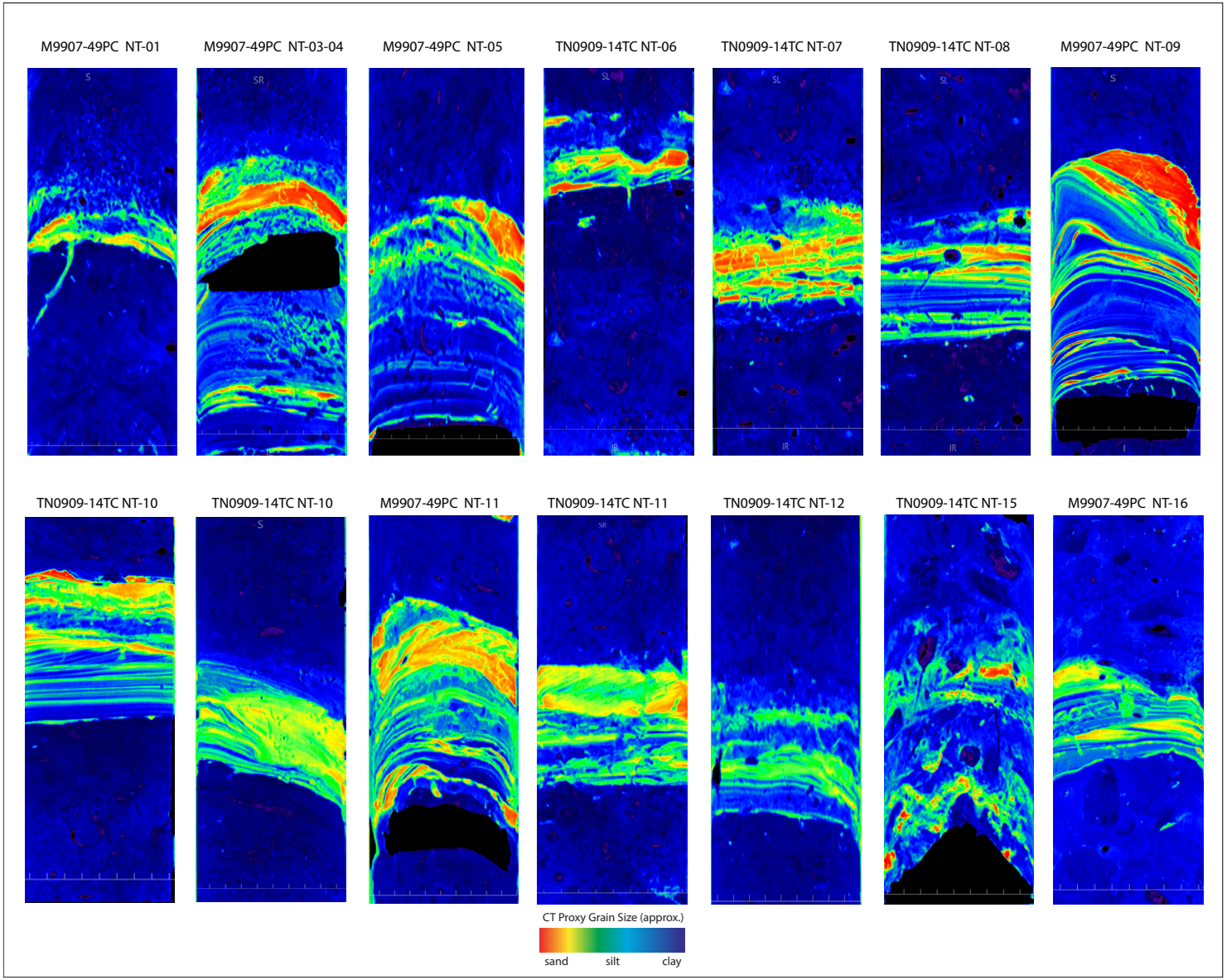

Figure 15. Examples of the Noyo Canyon/Channel inverted doublet stratigraphy (several showing multiple examples). The local core numbers and bed designations are shown. Warmer colors indicate elevated density and grain size; dark areas are radiocarbon sample voids. The interpreted 1906 CE bed (NT-01, upper left) is one of the few in the past ~4000 yr that does not have the inverted doublet sequence, although it does have a thinner poorly developed doublet. Another example, NT-06, also does not have the inverted doublet structure. See Figure 3 for the variability across the core set for each event, and other examples of doublet and non-doublet stratigraphy. Scales are 1 cm ticks. CT—computed tomography.

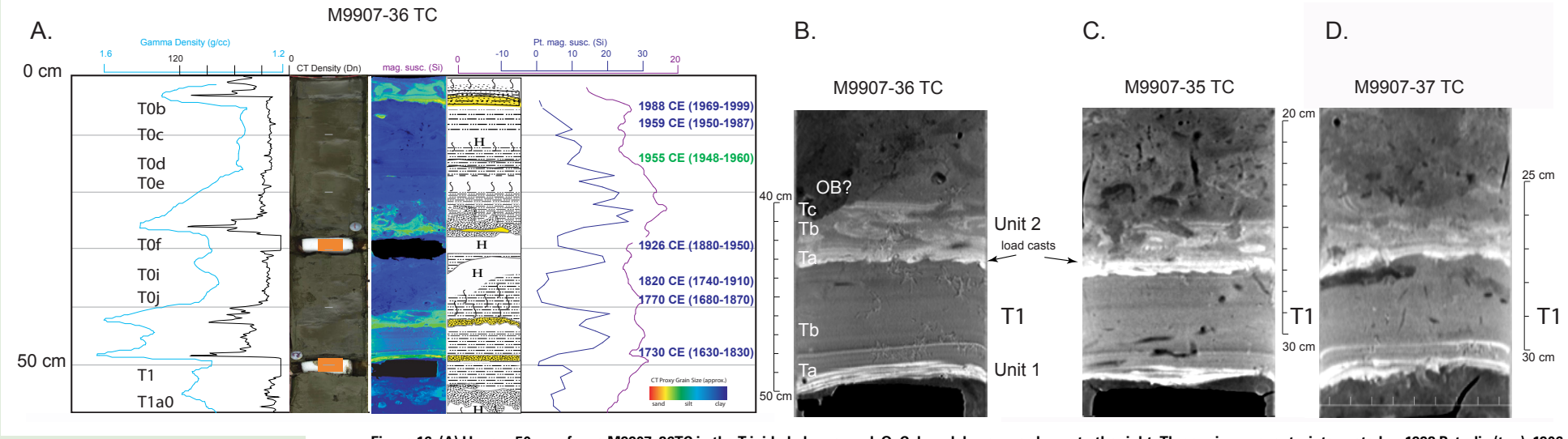

Figure 16. (A) Upper ~50 cm of core M9907–36TC in the Trinidad plunge pool. OxCal model ages are shown to the right. Three primary events, interpreted as 1992 Petrolia (top), 1906 CE northern San Andreas fault (middle), and 1700 CE Cascadia subduction zone (bottom), are shown, and several smaller events are named at left. Bomb-carbon age are shown in green from nearby core TN0909–06TC. CT—computed tomography. See Figure 8 for rest of legend. (B) Unit T1 from the same core as in A, showing depositional details, and interpreted load casts below upper subunit of this bed. Possible octopus burrow (OB) is indicated. (C) Bed T1 in nearby core M9907–35TC with similar structure to the bed in B (note scale change). (D) Bed T1 in nearby core M9907–37TC with similar structure to the beds in B and C (note scale change). Ages are shown in CE for historical convenience. mag. susc.—magnetic susceptibility; pt. mag. susc.—point magnetic susceptibility.

comes from the different strategies used for the two models, as well as better observations for the new models, undetected erosion or core deformation, incorrect thickness observations, or differential compaction. The two age and sedimentation-rate realizations represent end-member treatments of the same data, yet they yield similar values well within the 1σ uncertainty, lending confidence to the results. In the analytical model, sedimentation rate is an input, whereas it is an output in the Bayesian models. Regional provenance and sedimentation rate variability is driven mainly by river discharge along a given coast (e.g., Aksu et al., 1995), as shown in Cascadia (Griggs and Kulm, 1970; Nelson, 1976; Underwood and Hoke, 2000). As the overall regional rates for the entire Holocene are quite stable (Fig. S5), we infer that real sedimentation rate variability over short time frames was not likely and is not observed or expected for deep-water hemipelagic sedimentation (e.g., Stow and Tabrez, 1998; Pickering and Hiscott, 2016; Kemnitz et al., 2020; Stow and Smillie, 2020). In most cases, the revised ages from the Bayesian models improved the alignment of event ages within sites and regionally; this is expected if the event ages are synchronous, and unlikely otherwise. Finally, we recomputed statistics for OxCal combinations (OxCal Combine function) of the radiocarbon data from events interpreted to be correlative in the Cascadia subduction zone (Goldfinger et al., 2012, 2017). This comparison shows that for all events with enough data to perform this test (n = 30), all pass the χ^2 and OxCal A_Comb statistics for coevality (Figs. S6 and S7; Tables S2 and S2a).

Revised Cascadia Subduction Zone Stratigraphy

The Trinidad plunge pool site captures a high-resolution record in the late Holocene and includes the historic beds discussed in the following section. Figure 5 shows an anomalously large number of uncorrelated beds located between Cascadia subduction zone (CSZ) event beds T1 and T3. In most of the Cascadia subduction zone, nothing significant is in this interval except T2, while in the southern Cascadia subduction zone, T2a and T2b are present as faint beds that are interpreted based on the continuity of stratigraphy and compatible age models. In the Trinidad plunge pool, however, there are ~8–10 beds, four significant, in that time interval. These beds are not observed outside the plunge pool or represented in onshore or lacustrine paleoseismic records. This sequence has a normal radiocarbon age progression during that time range, so seiches within the pool are unlikely explanations. Otherwise, we are unable to interpret the origin of these events at present. Much of the Trinidad section between ~800 yr B.P. and ~2500 yr B.P. is a good match for the regional Cascadia subduction zone sequence (Goldfinger et al., 2012, 2013b),

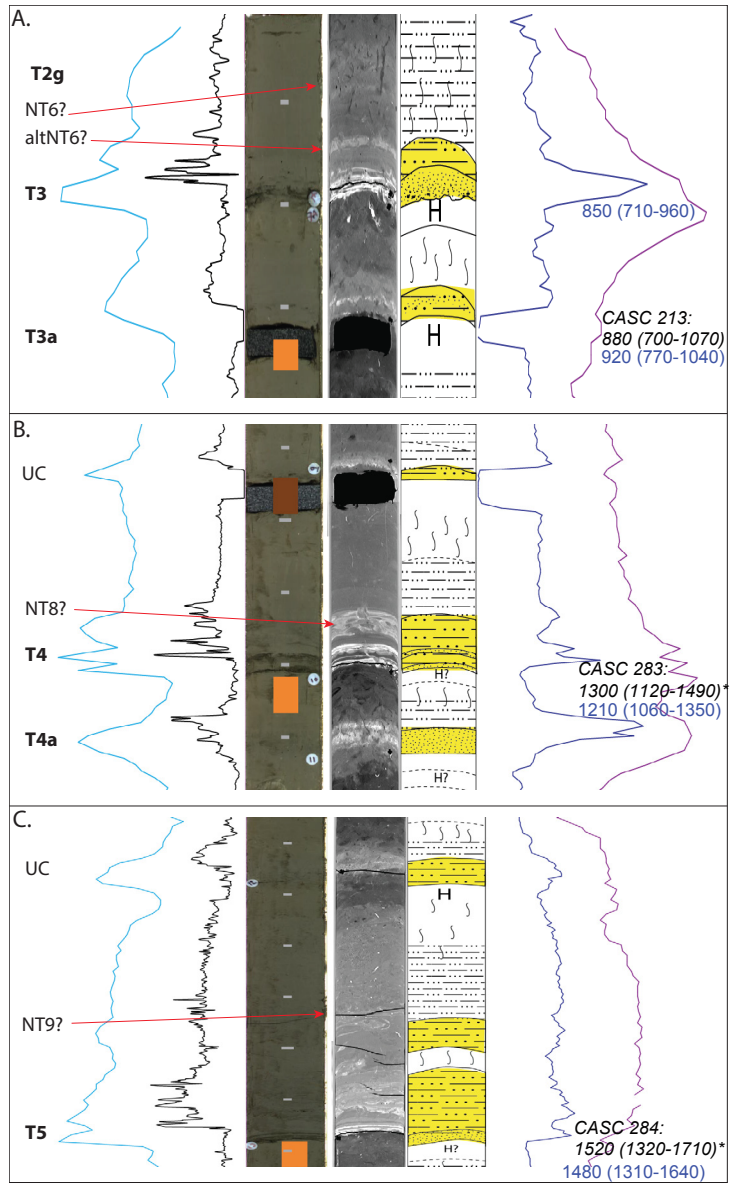

Figure 17. Three complex late Holocene turbidites from Trinidad plunge pool. (A) Cascadia subduction zone (CSZ) T3 is overlain by a bed labeled T2g, with a thin interval of hemipelagic material and a median age slightly younger than T3. It has a secondary coarse unit between the main body and tail. (B) CSZ T4 is a complex triplet, the middle interval of which shows load casts into the basal unit, and a finer-grained upper pulse prior to the tail. (C) CSZ T5 is a complex multipulse bed, with two primary coarse units overlain by a third pulse deposited before the tail, which is directly overlain by a second uncorrelated event labeled UC. Radiocarbon median ages with 2σ ranges are shown. Gray ticks are 10-cm depth markers. See Figure 8 for rest of legend. UC—uncorrelated event.

with a modest number of minor additional beds. Below that age, the bed frequency increases dramatically and becomes uninterpretable (Goldfinger et al., 2012). The origins of this frequency shift were discussed in Goldfinger et al. (2012), and they are beyond the scope of this work. The Trinidad site is fed by Trinidad Canyon almost exclusively. We infer that sediment sources were most likely the Klamath River, feeding the system from the northeast, dominated by sediment plumes from the Eel River during winter storm conditions (Wheatcroft et al., 1997; Burger et al., 2002; Puig et al., 2003), similar to the recharge of the SW Washington canyons from the Columbia River (Sternberg, 1986).

More regionally, thickness and grain-size trends increase southward from Rogue Apron to the southern limit of the Cascadia subduction zone (Fig. 8), but not in all cases (cf. Goldfinger et al., 2013b). The bed thickness and grain-size characteristics are modulated by canyon proximity, described previously and in Goldfinger et al. (2013b). This is supported by several cores collected between canyon systems that show a fainter, finer-grained turbidite stratigraphy (TN0909–02 and 05 JC/TC in Fig. 8). Given the weaker constraints available with which to correlate beds, we relied more on the frequency, timing, and similarity of the sequences to interpret their linkages.

The southernmost Cascadia subduction zone systems, Eel and Mendocino Channels, have been sampled extensively and found to have very high turbidite frequency. Paull et al. (2014) found the turbidite frequency on Eel Fan is approximately one event per ~36 yr for the middle to late Holocene. We found a nearly identical value of 39 yr recurrence in the post–1500 yr B.P. section of our TN0909 Eel cores (Fig. S1). Analysis of the complex high-frequency turbidite record contained in the Eel cores, while potentially useful, is beyond the scope of this study.

Some modest revisions to the stratigraphy reported in Goldfinger et al. (2013b) are briefly discussed here. As the thinner beds are observed to wax and wane with proximity to canyon sources, these regions can be "flattened" to help visualize the effect and the correlation (Figs. 9–11). Two cores spanning that area without the more difficult intervening sites show very similar stratigraphy found at the end-member sites (Fig. 9), supporting the correlation despite the problematic intervening sites.

An important observation relates to CSZ T1 and T2. Goldfinger et al. (2012) observed that across seven cores at the Rogue Apron site, only one core reliably revealed time separation between these two events. The rest of the cores showed these two events amalgamated, with the thin hemipelagic interval

obscured or eroded. Many of the southern Cascadia subduction zone cores have a similar relationship (Fig. 8). At the best sites, such as Trinidad plunge pool, these events are clearly separated by the high sedimentation rate. At other sites between Rogue Apron and Trinidad pool, many do not show this clear relation, and in fact appear to be missing one of the two events (Fig. 8). For example, the event originally labeled T2 in Goldfinger et al. (2012) was interpreted as such by the radiocarbon ages at Klamath and Smith Canyons, which were compatible with the mean age of T2 (~480 ± 95 cal yr B.P.) regionally (Goldfinger et al., 2012). However, this meant that T1 would have to have been the faint event above that. The 1700 CE event is of average thickness throughout Cascadia subduction zone marine records, while observations of subsidence and tsunami deposits in the southern Cascadia subduction zone mostly do not support a very weak 1700 CE event at those latitudes (Garrison-Laney 1998; Valentine et al., 2012). However, the likely 1700 CE event at Bradley Lake in fact is relatively thin (Kelsey et al., 2005). This ambiguity could be due to low tide occurring at the time of the event in the southern Cascadia subduction zone (Mofjeld et al., 1997) or other external factors, so we favor reinterpreting the large event with the T2-like age as an amalgamated T1 and T2 bed with a basal radiocarbon age similar to that of regional T2, similar to Rogue Apron. Age models for the uppermost section are also consistent with this interpretation (Figs. 8 and 9).

Some of the more robust thin beds, such as T3a, T3b, T5a, T5b, and T5c, become as coarse and thick locally in the southern Cascadia subduction zone as the interpreted regional events. The latter three events do not have coastal correlatives (Nelson et al., 2021) but may appear in higher-sensitivity lake records (Morey, 2020; Morey and Goldfinger, 2024).

As a final addition to the topic of along-strike correlation, an observation tool for examining the intersite Holocene sections not previously used is given in Supplemental Text S1 and Figure S8. The Holocene series of primary beds, previously reported at primary sites, is represented only by bed thickness in this figure. The stratigraphic sequences, represented by thickness variability alone, are similar across varied sites, a result not expected from random processes, but compatible with regional earthquake energy-release sequences (see Supplemental Text S1).

Along-strike sediment transport could play a role in correlation; however, the abyssal plain between the Rogue Apron and Trinidad pool has a slope angle of 0.015°. Given the flat bottom, little sediment transport in either direction would be expected. The slight right-turning tendency from the Coriolis force (e.g., Wells, 2007) would counter this slight slope. Thus, along-strike bed correlation is unlikely to be the result of trench-parallel transport. This is supported by the lack of Mazama ash in cores to the south of the abundant source at Rogue Canyon (Goldfinger et al., 2012, 2013b).

Most Recent Stratigraphy

The post–1700 CE stratigraphy has not been previously described, and it is a key element to this study. The uppermost bed (T0a) has no detectable postevent deposition, and the median model ages of 1989–1998 (avg. 1993, $n = 5$; Tables S3–S19) are consistent with the 1992 Petrolia Mw 7.2 earthquake (Oppenheimer et al., 1993), one of the four largest regional events of the twentieth century (with the 1994 Mw 7.0 event on the Mendocino Ridge being a possible alternative at much greater range). The second event from the top, T0b (1988, 1961–1999 CE), is sometimes amalgamated with the uppermost bed, and it is similarly a reasonable match for the 1980 Mw 7.2 Eureka earthquake, which was in the lower plate close to Trinidad Canyon (Dengler et al., 1992), although smaller earthquakes at greater range also exist. The weak third event, T0c, is interpreted to persist over ~75 km along strike between the Trinidad and Smith systems. The model age of this event at Trinidad pool is 1959 (1950–1990 CE), which could be a fit for an earthquake of Mw 6.2 at a distance 17 km west of the plunge pool in 1959. There was also a large flooding event in 1964; however, these possibilities cannot be effectively discriminated at present. Three beds are observed below T0c; the next significant event down, T0f, is traceable 155 km to the north among multiple systems (Fig. 8). This event has a mean age of 1926 CE (1830–1956) and is a reasonable match for the age of the 1906 earthquake on the northern San Andreas fault (Fig. 7). Age models for the upper sections of Klamath, Smith, and Rogue Aprons are consistent with this interpretation (Fig. 8). A time-equivalent event bed interpreted as the 1906 event (1920, 1870–1970 CE) has also been observed in Acorn Woman Lake (Fig. 1; Morey, 2020; Morey et al., 2024). The next event down, T0i, is faint, and it has a model age of ca. 1830 (1740–1910); it is not a good match for either the 1861–1862 major storm or the Mw ~6.8 1873 slab earthquake (Brocher, 2019). It might, however, correspond to a possible Cascadia subduction zone event suggested at about that time (Carver and Plafker, 1999; Carver, 2000). We are unable to discriminate between these (or other) possibilities with present data. One additional faint bed with an age of ca. 1770 CE (1670–1860) lies above T1 at 1700 CE and is not known in other records.

Subbottom Profiles

The subbottom profile correlation shown in Figure 12 shows 22 significant beds that can be traced between Rogue Apron and Thompson Ridge. The Holocene reflector count is consistent with the cores at Rogue Apron, assuming T1 and T2 are imaged as one bed, that beds T10b and T10f are imaged, and that very thin bed T12 is not. The Holocene base is clearly underlain by four thick reflectors that may be the latest Missoula flood beds, indicated by common wood and quartzite fragments in core RR2208 02JC, components consistent with the late Pleistocene outburst floods (e.g., Bjornstad, 2014) and not observed in the overlying Holocene sequence.

The imaged beds can be matched to the cores and individually verified over this 100 km distance, as well as southward to Trinidad plunge pool (Goldfinger et al., 2013b; Black, 2014), a total span of ~240 km. North of the Thompson Ridge site, the profiles begin to climb the southernmost constructional Astoria Fan, and the Holocene section thins, becoming unresolvable. The reflectivity

of these beds fades with distance from the major canyon source at Rogue Canyon both north and south, consistent with density and grain-size decreases away from this source, as previously noted (Fig. 12; Goldfinger et al., 2013b).

Noyo Channel and North Coast Northern San Andreas Fault Stratigraphy

Noyo Channel. The Noyo Channel site is key to interpretation of northern San Andreas fault earthquakes because it has a very short hypocentral distance, as the fault cuts and offsets the canyon head (Fig. 1), making Noyo Channel a very sensitive recorder. Noyo Channel also has several beds with historic-era ages (Figs. 3 and 4). The upper event, NT0, has a range of 1960–1999 (trimmed by the date of collection), and a median of 1995 CE. This event may be the 1992 Petrolia Mw 7.2 earthquake, the largest event in that time period, recorded at a planimetric range of ~100 km. The second very faint event, NT0a, has a mean and median of 1965 (1900–1999) and could be related to the 1964 floods. The mode for this age is younger, ca. 1985; therefore, it is equally likely that this bed is a result of the 1980 Mw 7.2 Eureka earthquake, although it is at a range of 165 km to the head of Noyo Canyon. The model age for NT1, the third event down, is 1923 (mean), with 1919 median (1850–1950, trimmed by absence of bomb carbon; Figs. 18 and 19). Three other ages for this bed from BC50 have direct ages of 1900 (1690–1950), 1930 (1830–1950), and

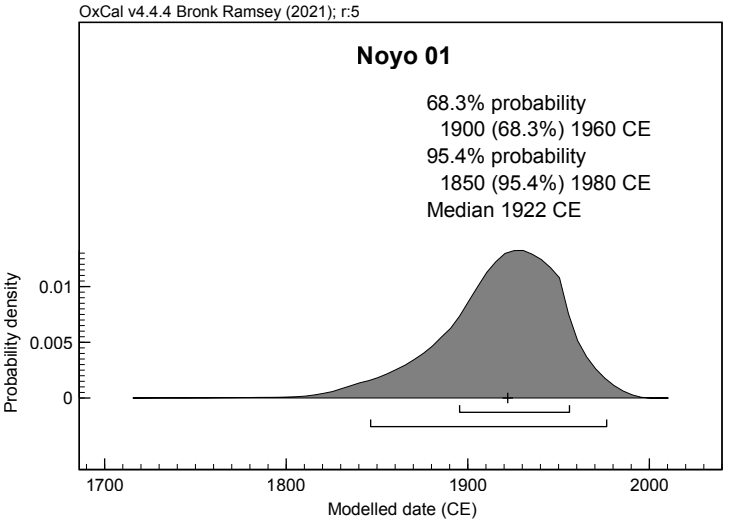

Figure 18. Single plot from the Noyo P-sequence age model. The event, locally called NT1, is the likely event bed from the northern San Andreas fault 1906 earthquake. The 99.7% probability range extends slightly outside the 1950 limit for non-bomb-carbon ^{14}C dating and is noted as "out of range" in the table output, but nevertheless it yielded a valid age for this event.

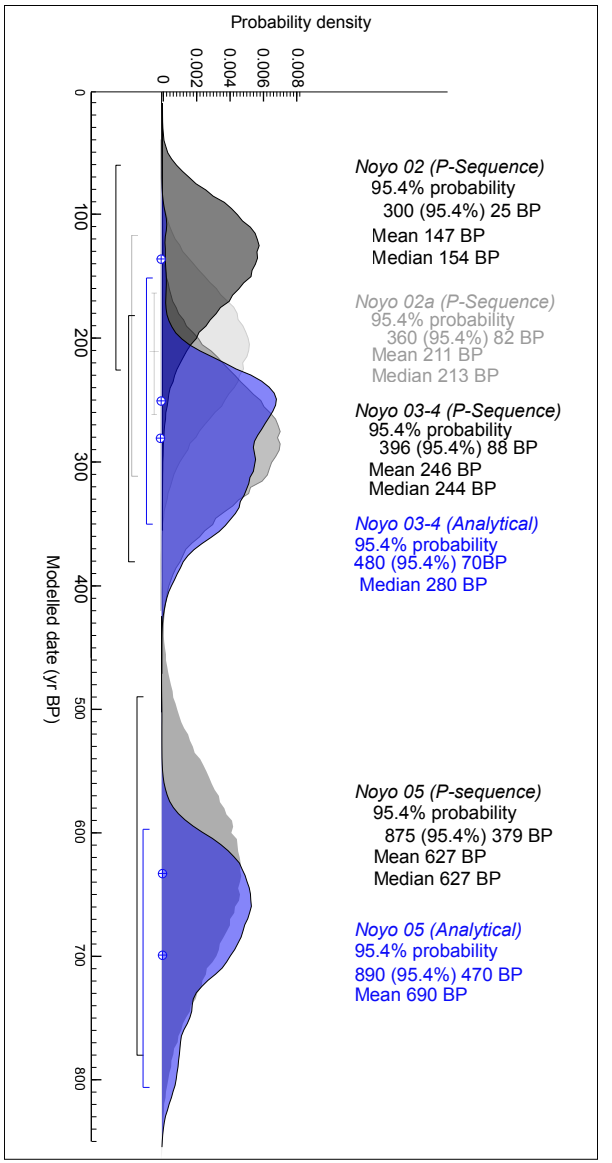

Figure 19. Age model detail of the ca. 1700 CE doublet NT3–NT4, and its immediate neighbors. The ca. 1700 CE event is shown with a P-sequence model age and an analytical age (in blue) for that event, which was directly dated. Similarly, the Noyo NT5 event is also shown with a P-sequence model distribution and the analytical age (in blue). The 2σ ranges are shown. Minor event NT2a is shown in gray due to the low probability that this small event would be confused with the major events above or below.

1920 (1820–1950) CE (Fig. 3). An OxCal combined age for these events yields 1920 (1880–1950) CE. These ages compare favorably to the 1906 northern San Andreas fault earthquake (cf. Goldfinger et al., 2007, 2008). Below the likely 1906 bed, another faint bed, NT1a, is found to have a mean age of ca. 1870 CE (Fig. 3). This faint event could be the result of the 1861–1862 ARkStorm flood event (Null and Hulbert, 2007). One robust bed, NT2, is found between the 1906 and the ca. 1700 CE beds, with a model age of ca. 1800 (1650–1930). A weak event is also observed at about this time on the Cascadia subduction zone side in Trinidad plunge pool. One additional faint event, NT2a, with an age of ca. 1740 (1580–1890) CE overlies the ca. 1700 CE bed. No northern San Andreas fault earthquakes are observed at lake or onshore paleoseismic sites at these times; however, the bed overlying the 1700 CE bed in the southern Cascadia subduction zone is similar in age.

A major event, NT3–NT4, at 1710 (1550–1860) CE is well separated in time from events above and below. The probability distribution function shows the limited radiocarbon overlap for the overlying bed, and none at all for the underlying bed, both of which were dated directly (Fig. 19).

Northern San Andreas fault stratigraphy. While the correlation of the closely spaced Noyo Channel cores was straightforward, regional correlation southward was much more difficult than the equivalent process for the Cascadia subduction zone as previously discussed (see Supplemental Material). Overall, the correlation is similar to the previous publications (Fig. S3), but the ages of the event beds south of Noyo Channel are now much more uncertain due to the contamination issue (Supplemental Text S1), and their use is very limited in this work.

Relation of Correlated North Coast Beds and Onshore and Lacustrine Paleoseismic Sites

Despite problematic age control along the north coast segment, we can make several observations regarding these beds and their possible connections or lack thereof to other paleoseismic sites in the late Holocene. A space-time compilation diagram for relevant onshore and offshore paleoseismic data shows relevant regional relationships (Fig. 21). The uppermost of these beds is the likely 1906 bed. While this bed is thin, it appears consistently along the north coast segment (Fig. S3). Noyo bed NT3–NT4 (1710, 1550–1860 CE) can also be correlated along-strike and has temporal correlatives at numerous land sites, including Alder Creek, Fort Ross, Bodega, Vedanta, Dogtown, Bolinas, and Lake Merced (Fig. 21; Table 1). Beds NT5 through NT11 can similarly be correlated southward to Pioneer Canyon (Fig. S3). There is permissive correlation of these beds and others younger than ~2200 yr B.P. at the north coast land sites as shown in Table 1. Beds NT12 to NT14 do not appear to correlate south of Albion Canyon. Beds NT12, NT13, and NT14 do have radiocarbon overlap with the oldest events at Vedanta but are older than all other land sites. Where they overlap, the offshore north coast record is very similar to that of the onshore sites, suggesting that these records may be evidence of the same series of northern San Andreas fault earthquakes, but closely spaced ruptures cannot be ruled out. At Lake Merced, bed 4, the event below the large probable 1906 bed (bed 3), has a 2σ age of 1730 (1580–1890) CE, indistinguishable from the north coast segment ages at Noyo Channel for turbidite NT3–NT4 of 1710 (1550–1860) CE. The penultimate event age for Vedanta Marsh is similar at 1710 (1670–1740) CE, and similar to preliminary work at Montebello on the San Francisco Peninsula (Seitz, 2018). Merced bed 5 has a model age of 1670 (1510–1830) CE. This also is a plausible match for Noyo Channel, but nothing is observed at Vedanta Marsh in that time range. The Merced bed age is also similar to the peninsula segment penultimate event with a median age of ca. 1620 reported in Schwartz et al. (2014). Other age correlations are suggested in Figure 21 and Table 1. Given the likely recording of both the 1989 Loma Prieta and the 1957 Daly City earthquakes in Lake Merced (Goldfinger, 2021), it is not surprising that the lake has more event beds than can be found on the peninsula or north coast segments of the northern San Andreas fault alone, as it is a likely recorder of both (if they are separable).

Comparing Noyo Channel with Lake Merced, including 1906 and the 14 prior event beds in Lake Merced, 10 of the event beds have significant radiocarbon overlap with Noyo Channel beds, and all but one of these has a potential correlative at Vedanta Marsh (Fig. 21; Table 1). Four beds at Lake Merced do not have temporal equivalents at Noyo Channel or Vedanta Marsh; and one other bed not observed at Noyo Channel does have a correlative observed at Vedanta Marsh. Of these 10, nine are statistically indistinguishable between the two sites, and the remaining bed has significant temporal overlap. No major beds are observed at Noyo Channel that lack potential temporal correlatives at Lake Merced within the ~2300 yr record length at Lake Merced.

Lake Merced may well have captured most or all northern San Andreas fault earthquakes occurring along the north coast segment over the past ~2300 yr, and it also captures local events such as the 1957 event, and Santa Cruz Mountains events such as the 1989 Loma Prieta earthquake, and likely peninsula segment events if they exist as a separate segment. At this stage, it is not clear what the recurrence intervals are for such events, nor the recording fidelity of them at Lake Merced (Goldfinger, 2021).

The good correspondence between Lake Merced and Noyo Channel suggests that 1957 and Loma Prieta–type events could be relatively rare, if Lake Merced is indeed capable of recording all four event types, but the stratigraphy is primarily north coast segment events. One simple scenario of event linkage that is consistent with the data is shown in Table 1. One of these events, Merced bed 7, also has a temporal correlative at Vedanta, but not at Noyo Channel. Four of these five do not have good correlatives at other land sites on the north coast nor at Noyo Channel. Alternatively, these beds could represent local or Loma Prieta–type events.

Doublet Stratigraphy

The presence of unusual doublet stratigraphy in event beds linked to earthquakes in cores near the triple junction is central to evaluating stratigraphy

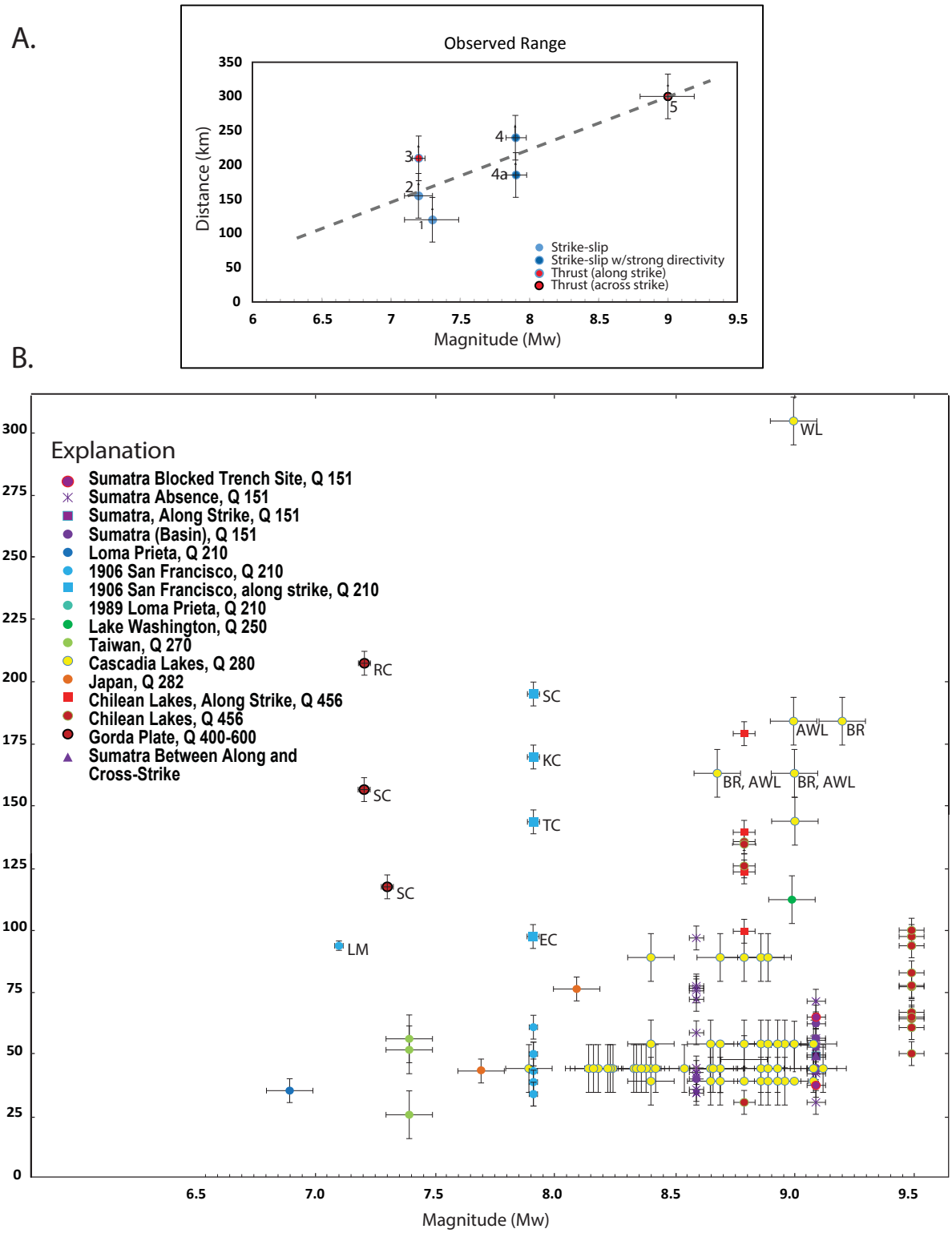

Figure 20. (A) Maximum observed turbidity current triggering range for five Cascadia subduction zone earthquakes for which data can be inferred: 1—1922 Gorda plate Mw 7.3; 2—1980 Eureka Mw 7.2; 3—1992 Petrolia Mw 7.1; 4—northern San Andreas fault Mw 7.9 offshore; 4a—northern San Andreas fault Mw 7.9 Acorn Woman Lake (renamed in 2022); Morey, 2020; Morey and Goldfinger, 2024); and 5—1700 CE (and others) Mw 9.0. All observations were constrained by Rogue Canyon core sites, except 5, which was observed at Wapato Lake, Eastern Washington. Up arrows indicate distances are data limited and could be somewhat larger, though interpreted to be near their maxima. (B) Global observed triggering ranges for turbidity currents from source earthquakes vs. Mw. Markers denote site locales, and cool to warm colors indicate Q value increase (also indicated in the Explanation). Square markers denote along-strike measurement; round markers denote across-strike measurement; triangles denote along- and across-strike measurement. Estimated uncertainties in range and magnitude are shown from the original literature where available (see Black, 2014). Individual controlling maximum range distance sites are: LM—Lake Merced; EC—Eel Canyon; TC—Trinidad canyon; KC—Klamath Canyon; SC—Smith Canyon; RC—Rogue Canyon; WL—Wapato Lake; BR—Bull Run Lake; AWL—Acorn Woman Lake. Figure is modified after Black (2014).

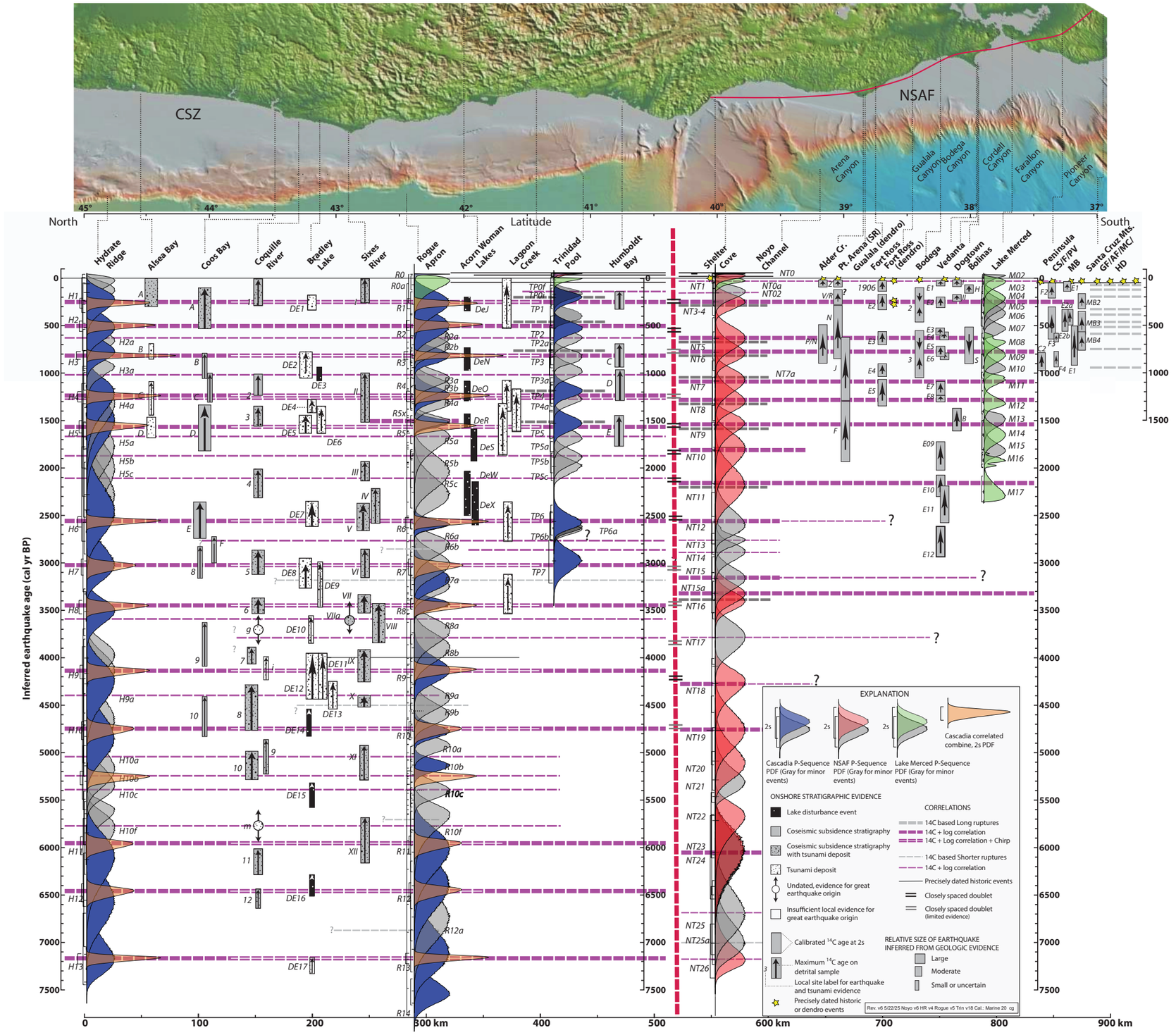

Figure 21. Space-time diagram for the southern Cascadia subduction zone (CSZ) and the northern segment of the northern San Andreas fault (NSAF). Onshore and offshore age data are shown for both fault systems, with the triple junction represented by a red vertical dashed line. Stratigraphic correlations of Cascadia subduction zone turbidites from Goldfinger et al. (2012) are shown to reflect long (>500 km) fault ruptures (bold dashes) of most of the megathrust, as distinguished from shorter (<500 km) fault segments (thin dashes). Correlations supported by well-log methods and/or subbottom profiling are symbolized as shown in the explanation, with heavier lines indicating thicker beds. Best-fitting tie lines are based primarily on OxCal regional Combine functions; thus, some local mismatches can be seen. Northern San Andreas fault correlations based on this work and shown onshore data were extended tentatively to Lake Merced where good temporal correspondence exists. For onshore data, up arrows denote maximum age estimates on detrital samples. Symbol width represents relative size of earthquake inferred from deposit thickness or amount of subsidence evident in change in microfossil assemblages. Rectangles represent inferred earthquake age ranges in calendar years before 1950 CE, calibrated from radiocarbon dates as discussed in the Methods section. The land age ranges presented here in the Cascadia subduction zone have been recalibrated from the original laboratory reported age and are compiled in Supplemental Data S1 of Goldfinger et al. (2012), Nelson et al. (2021), and references therein. Doublet stratigraphy is shown with double lines at the triple junction. Onshore Cascadia subduction zone data are modified after Witter et al. (2013). Northern San Andreas fault peninsula and Santa Cruz Mountains data are from Weldon et al. (2013); Baldwin et al. (2008); Prentice et al. (1999, 2013, 2016); and Streig et al. (2020) and references therein, particularly their figure 8. CS—Crystal Springs and Crystal Springs South; F—Filoli; PV—Portola Valley; MB—Monte Bello (Seitz, 2018); GF—Grizzly Flat; AF—Arano Flat; MC—Mill Canyon; HD—Hazel Dell. North coast land sites: Shelter Cove (Prentice et al., 1999); Alder Creek (Baldwin, 1996; Prentice et al., 1999); Point Arena (SR) (Prentice, 1989; SR—Scaramella ranch); Gualala (Carroll et al., 2025); Fort Ross (Kelson et al., 2006); Bodega lagoon (Knudsen et al., 2002); Vedanta (Zhang, 2005; Zhang et al., 2006); Dogtown (Hall and Niemi, 2008); Bolinas Lagoon (Knudsen et al., 2002). Lake Merced ages were recalibrated using IntCal 20 from Goldfinger et al. (2021, their table S10a). Bathymetry and topography were reprojected on a coastal meridian. Age scale zero mark is radiocarbon zero = 1950 CE. PDF—probability density function.

TABLE 1. ^{14}C AGES FROM THE CASCADIA SUBDUCTION ZONE (CSZ), NOYO CHANNEL, VEDANTA MARSH, AND LAKE MERCED

CSZ	CSZ	Noyo Channel	Noyo Channel	Noyo Channel	Vedanta marsh	Vedanta marsh	Lake Merced (cal. yr B.P.)	Lake Merced (CE)	Lake Merced
Trinidad Bed		Noyo bed	OxCal model (this study)	Analytical (this study)	Zhang et al. (2006)	Zhang (2005)	Goldfinger et al. (2021), recal	Goldfinger et al. (2021), recal	Merced bed
T0a	1993 (1969–1999) CE	NT0	1998 (1961–1999) CE	Not observed	Not observed	Not observed	–36 (–26 to –46)	1986 (1976–1996)	Bed 1
T0b	1988 (1963–1999) CE	NT0a	1964 (1900–1999) CE	Not observed	Not observed	Not observed	–7	1957	Bed 2
T0f	1926 (1880–1956) CE	NT1	1920 (1840–1980) CE	1915 (1810–1950)* CE	E1 44	E1 44	50 (–30–170)	1900 (1780–1980)	Bed 3
T1	220 (120–320)	NT3–4	250 (100–400)	260 (50–450)*	E2 260 (210–280)	E2 265 (230–300)	220 (70–380)	1730 (1570–1880)	Bed 4
	Not observed	Not observed	Not observed	Not observed	Not observed	Not observed	280 (120–440)	1670 (1510–1830)	Bed 5
	Not observed	Not observed	Not observed	Not observed	Not observed	Not observed	370 (200–520)	1580 (1430–1750)	Bed 6
	Not observed	Not observed	Not observed	Not observed	E3 560 (510–600)	E3 560 (520–600)	530 (400–640)	1420 (1310–1550)	Bed 7
T2	550 (420–660)	NT5	630 (390–870)	690 (480–890)	E4 620 (570–660)	E4a 620 (570–660)	690 (570–810)	1260 (1140–1380)	Bed 8
T3	850 (710–960)	NT6	780 (560–970)	710 (520–920)	E5 770 (720–810)	E4b 770 (720–810)	810 (660–970)	1140 (980–1290)	Bed 9
T3a	920 (770–1040)	NT7a	940 (770–1140)		E6 820 (790–850)	E5 820 (790–850)	940 (790–1060)	1020 (890–1170)	Bed 10
T3b	1100 (940–1240)	NT7	1080 (850–1340)		E7 1100 (1070–1130)	E6 1100 (1070–1130)	1070 (990–1190)	880 (760–960)	Bed 11
T4	1210 (1060–1350)	NT8	1290 (1030–1510)	1270 (1090–1500)	E8 1270 (1240–1300)	E7 1270 (1240–1300)	1310 (1180–1440)	640 (520–770)	Bed 12
T5	1480 (1310–1640)	NT9	1540 (1330–1830)		Not observed	Not observed	1510 (1390–1650)	450 (300–560)	Bed 13
T5a	1650 (1470–1810)		Not observed	Not observed	Not observed	Not observed	1660 (1490–1830)	290 (130–470)	Bed 14
T5b	1850 (1670–2020)	NT10	1820 (1490–2190)		E9 1880 (1730–2020)	E8 1880 (1740–2025)	1810 (1640–1940)	140 (10–310)	Bed 15
			Not observed	Not observed	Not observed	Not observed	1930 (1840–2020)	20 (–74–110)	Bed 16
T5c	2050 (1880–2210)	NT11	2170 (1780–2550)		E10 2190 (2070–2300)	E9 2190 (2080–2310)	2250 (2080–2360)	–300 (–130 to –410)	Bed 17
	Not observed	Not observed	Not observed	Not observed	E11 2390 (2190–2580)	E10 2390 (2200–2590)	No data	No data	
T6	2570 (2370–2720)	NT12	2570 (2240–2830)	2650 (2410–2900)	Not observed	Not observed	No data	No data	
	Not observed?	NT13	2760 (2580–2920)		E12 2780 (2610–2940)	E11 2780 (2620–2950)	No data	No data	

Note: Marine ages were calibrated with Marine 20; Lake Merced data were calibrated with IntCal 20. Vedanta ages are listed as originally published. Other ages are revised (5 June 2025) from Goldfinger et al. (2008). All ages are in yr B.P 1950 unless otherwise noted. Color key: green—significant ^{14}C overlap north coast section; yellow—limited ^{14}C overlap north coast section; blue—possible peninsula section events. CSZ—Cascadia Subduction Zona; recal—recalibrated.

*Average of multiple ages.

with similar timing on both faults for evidence of a temporal relationship between the Cascadia subduction zone and the northern San Andreas fault. In the following sections, we discuss the nature and possible origins of these events in detail.

Noyo Channel doublets. The uppermost doublet (NT3–NT4) has a P-sequence model age of ca. 1710 (1550–1860) CE (Figs. 3, 14, and 15). Similar direct analytical ages are shown in Figure 3. An interval between the two coarse units was previously sampled and dated. These dates were reversed: 460 (300–630) yr B.P. and 660 (460–860) yr B.P., showing that the foraminifera collected from the layer between the coarse units were reworked. Eleven examples of this particular doublet are available, seven from subsamples of box core M9907–50BC, and two each from M9907–49PC/TC and TN0909–14JC/TC. Other similar examples are common (Figs. 3 and 15). Several Late Holocene beds do not have the doublet structure, while several are equivocal or intermediate types. A notable post–4000 yr B.P. example is the likely 1906 bed (Goldfinger et al., 2008; this study), a relatively thin single bed.

Cascadia subduction zone doublets. Multiple-pulse turbidites are common in the Cascadia subduction zone (Gutiérrez-Pastor et al., 2013) and form the basis in many cases for intersite correlation (Goldfinger et al., 2012, 2017). Several southern Cascadia subduction zone beds differ from the common multipulse Cascadia subduction zone turbidites in that the second pulse does not appear to be cogenetic with the first. There is not a high-energy signature of laminar and cross-beds commonly observed in typical multipulse beds, but rather a clear second base (Bouma A) embedded in the fining tail of the first

event with load casts (Fig. 16). The load casts imply rapid deposition into a soft, low-energy substrate rather than a dynamic high-energy surging flow event. There are several such beds in Trinidad plunge pool. The uppermost of these beds has a model age of 1730 (1630–1830) CE, an analytical age of 1650 (1490–1850) CE, and a regional OxCal combined age of 1720 (1640–1790) CE, and it is interpreted as the likely 1700 CE event via correlation (Fig. 5).

In all Trinidad cores, CSZ event T3, which is another well-correlated event, is robust in all cores. The model age of T3 at Trinidad, 850 (710–970) cal. yr B.P., is similar to the regional individual ages and the combined age of 800 (730–860) cal. yr B.P. in the Cascadia subduction zone (Fig. 5). Within the upper part of this event, there is a second coarse pulse similar to that observed for T1 (Fig. 8). Directly above T3, there is a second event (T2g) that does not correspond with any known Cascadia subduction zone event nor correlate northward. This bed also has a secondary coarse pulse separating the basal components from the tail. The next significant event down, regional T4, has a model age of 1210 (1060–1350) cal yr B.P. and analytical ages similar to the regional Cascadia subduction zone combined age of 1210 (1150–1270) cal yr B.P., and it also has a doublet upper unit that does not correlate northward (Fig. 8). The T4 bed is actually a triplet and has three coarse elements. The middle element has load casts similar to those observed for the T1 doublet. The third pulse is a weaker silty pulse showing some flow structure (Fig. 5). Like T1, the load casts in the second element of this bed suggest low-energy tail deposition following deposition of the basal bed, with loading of the second pulse into the tail of the first. Another example is CSZ T5, also a well-correlated regional bed, which has a Trinidad model age of 1480 (1320–1640) cal. yr B.P., similar to the regional combined age of 1550 (1470–1620) cal. yr B.P. This bed has multiple internal pulses, with a closely spaced doublet at the base, similar to other Cascadia subduction zone sites, and a second thicker but finer pulse separating the lower components from the tail (Fig. 17).

Sources of the Historical Turbidites in Northern California

A key observation about the post-1700 Cascadia subduction zone turbidites is that they are more extensive than initially recognized, and that historic earthquakes are likely included in the record. With additional data, it became possible to correlate some of them for significant distances of 50–170 km with reasonable confidence (Fig. 8). For long-distance correlations, such as the main series of Cascadia subduction zone earthquakes, local crustal earthquakes are very unlikely sources. However, shorter correlation distances considered here can be explained by smaller plate-boundary earthquakes, slab earthquakes, and crustal earthquakes. Also, very large storms could be candidates as well, given that the criteria used for major plate-boundary earthquakes are not applicable to this more spatially limited setting, though unlikely as discussed in Goldfinger et al. (2012).

From the historic-era results, we constructed an approximate turbidity current triggering range versus Mw plot for events large enough to leave observable beds in multiple systems specific to the southern Cascadia subduction zone (Fig. 20). The plot includes four historic events: the 1922 Gorda Mw 7.3: 120 km; the 1980 Eureka Mw 7.2: ~150 km; the 1992 Petrolia Mw 7.2: 210 km; and the 1906 northern San Andreas fault Mw 7.9: ~240 km. The plot also includes a possible record of several events in Wapato Lake (Washington) reported in Gutiérrez (2020), tentatively correlated to the Cascadia subduction zone series of likely full-margin ruptures. These events are found east of the Cascade arc at a range of ~300 km from the downdip edge of the locked zone. For comparison, Figure 20B shows a compilation of global observations of triggering distances, modified from Black (2014) with the addition of the Cascadia subduction zone data from this investigation. Observed ranges amalgamate the poorly known thresholds for slope failure under seismic loading, transport, deposition, and observation as well as the slant range to the hypocenter. Actual maxima for failure alone should therefore be greater.

Implications of the Historical Event Stratigraphy

The Petrolia and Eureka earthquakes of 1992 and 1980. The Mw 7.2 Eureka and Mw 7.2 Petrolia earthquakes are the two largest earthquakes in northern California in the post-1950 era. The Petrolia earthquake is a shallow east-dipping thrust event that is either on the plate boundary or just above it on a splay thrust (Oppenheimer et al., 1993). Its age and strike-length correlation are consistent with our event T0a. The 1980 event is thought to be a Gorda plate earthquake with a left-lateral motion on a northeast-striking fault plane (Lay et al., 1982), which is compatible with the rapidly deforming Gorda plate structure (Chaytor et al., 2004). Its age and strike-length correlation are consistent with our event T0b. Shake maps for these two events are shown in Figure S9. The 1980 event generated moderate intensities up to modified Mercalli intensity (MMI) VI at Brookings, Oregon, and the 1992 event generated somewhat lower intensities to the north, with MMI III felt at Brookings, although the ground motions were higher locally in the epicentral area.

The 1906 northern San Andreas fault earthquake. The Mw 7.9 northern San Andreas fault earthquake of 1906 is of particular interest for this study, and the presence of paleoseismic evidence of the 1906 event north of the triple junction has not previously been reported. The shake map for this event shows that shaking of MMI intensity VI extended north to about the latitude of Trinidad, California, ~100 km north of the triple junction (Figs. 1 and S9). Felt reports suggest intensity IV extended to about Brookings, Oregon, with I–III felt even farther north (Stover and Coffman, 1993). The age and correlation length of bed T0f are consistent with this event.

The 1964 flood event. The 1964 "Christmas flood" was the largest in recorded history in northern California (Waananen et al., 1970). The discharge of the Eel, Klamath, Trinity, and Smith Rivers set records for years recorded continuously later than ca. 1922–1931. The faint bed T0c could be consistent with this event.

The 1861–1862 flood event. Detailed discharge data do not exist for this event; however, the 46 day storm of the winter of 1861–1862 likely ranks as one of the largest of the past several hundred years (Ralph and Dettinger, 2011). This event must be considered as a viable sediment source for offshore northern California as it inundated most of the west coast. Bed NT 1a in Noyo Channel could be consistent with this event, as could bed T0h in Trinidad plunge pool.

Implications for the Cascadia Subduction Zone Paleoseismic Record

The proposed linkage of the southern Cascadia subduction zone records to several historic crustal and slab earthquakes has several implications that are important for the Cascadia subduction zone–northern San Andreas fault comparison. Triggering distances of 150–230 km can now be expected in the southern Cascadia subduction zone from Mw 7.1–7.9 earthquakes, greater than previously thought. In the case of the Petrolia event, directivity effects would have been approximately normal to the margin, while for the 1906 and 1980 events, they would have been parallel to the margin and would have enhanced ground motions to the north and north-northeast, respectively.

The implication of this increase in triggering range and observation of historic events is that northern San Andreas fault events clearly can be recorded in the Cascadia subduction zone, and if evidence of the 1906 event is present, then evidence of at least some of the previous northern San Andreas fault events is likely present as well. Given that, Cascadia subduction zone events should also be recorded at similar ranges south of the Cascadia subduction zone, for example, in Noyo Channel at 90 km range.

Riedel and Conway (2015) reported only partial recording of presumed Cascadia subduction zone turbidites off Vancouver Island at short ranges, suggesting generalizations of triggering distance should be used with abundant caution.

Magnitude estimates. The historical event bed stratigraphy represents one of the first submarine records of known historical earthquakes in the Cascadia subduction zone. The only other published record is the 1946 Vancouver Island event in Effingham Inlet cores (Enkin et al., 2013). In addition to corroborating the earthquake interpretation, turbidite records of known earthquakes offer the possibility of improving estimates of Cascadia subduction zone earthquake magnitudes. Previously, the only ground truth was the 1700 CE event of Mw 9.0, which was based on a transoceanic tsunami record (Satake et al., 2003). Very rough estimates were made from rupture area and interevent time by Goldfinger et al. (2012); Rong et al. (2014) improved on these estimates using turbidite mass per event and developing a relationship to make this estimate. However, these very crude estimates may now be tested against the historical record.

The historical crustal and probable slab events just described are apparently correlated over distances greater than previously estimated. As a result, some of the events attributed to the southernmost Cascadia subduction zone could have been sourced from crustal or slab earthquakes as well as plate-boundary events. Additionally, previous rough magnitude estimates (Mw 7.5–8.4) for the smallest events that do not extend north of Rogue Canyon and are not found in the tsunami record at Bradley Lake (Kelsey et al., 2005; Priest et al., 2014) may have been overestimated. Some of these events are similar in extent, thickness, mass, and grain size to the event beds associated with the probable 1906, 1922, 1980, and 1992 (Mw 7.2–7.9) earthquakes. Therefore, at least some of these events are very likely not Cascadia subduction zone–sourced events; however, they likely remain evidence of significant earthquakes. The long triggering distance for the 1906 event suggested by our correlation could have been influenced by the northern San Andreas fault (and 1906 rupture) extending to the north of the triple junction, in addition to northward directivity (Song et al., 2008). This extension of dextral strain into the southern Cascadia subduction zone has now been observed geodetically (Materna et al., 2023), though the geologic details and northern rupture terminations of the 1906 event or other northern San Andreas fault events are unknown.

Alternative Models

Sediment Sourcing

Several recent papers have discussed the broad-scale geomorphology and mapped slope failures of the southern Cascadia subduction zone margin in relation to sources and sinks of turbidity currents. Hill et al. (2020) described the long-term processes of canyon aggradation and infilling in southern Cascadia subduction zone canyons, which are some of the conduits for abyssal deposits used here. They suggested that previous models, citing Adams (1990) and Goldfinger et al. (2003, 2012, 2013b), assumed that turbidity currents were sourced solely from canyon-head sources. However, these studies primarily used sites that were known sources of good turbidite records, but they were not based on assumptions about the specific sources. Subsequently, Goldfinger et al. (2017) discussed evidence that an amalgamated set of sources was required to explain the timing and distribution of Cascadia subduction zone turbidites, and this more accurately describes the model used in previous work.

Recent work in several settings has shown that while mapped submarine canyons and slope failures clearly are major contributors (e.g., Mountjoy et al., 2018), they are not the only sediment sources, and they may not be required as the source of typical seismically triggered turbidity currents, as thin failures of surficial material are all that is required to supply sufficient material (Moernaut et al., 2017; Okutsu et al., 2019). Indeed, mappable slide failures are insufficient in number and volume to supply the observed volume of material recorded in seismoturbidites from canyons offshore Washington (Goldfinger et al., 2017). Those authors also inferred that broad, thin failures of surficial materials likely occur, in addition to canyon-wall failures, to account for estimated sediment volume.

The evidence presented in Goldfinger et al. (2013b) and this paper shows the weakening of the turbidite record between canyon sources, establishing that these sources are important contributors, but by no means the only

sources. Goldfinger et al. (2012) also showed a complete record at Hydrate Ridge Basin West, offshore Oregon (Fig. 1), the source of which was an open-faced, failed anticlinal forelimb, clearly another source type, as is the similar setting detailed in Hamilton et al. (2015) at the Slipstream slide. Sediment failures, whether landslides of any size or surface remobilization, are promoted in areas of steeper slopes and/or sediment accumulation. Canyons have an abundance of both, as well as an order of magnitude more surface area per unit of margin length as compared to the frontal thrust. For example, the Rogue Canyon planimetric area is ~1150 km^2, while an equivalent area for the frontal ridge would be ~60 km^2. This difference is higher if the actual surface area is considered. Submarine canyons therefore function as the principal conduits for sediment transport onto the filled trench/abyssal environment. During the Holocene highstands, canyons trapped mostly fine-grained sediments and helped concentrate major and minor sedimentation events and promote downslope transport (Underwood and Hoke, 2000). The overall sediment supply, as indicated by the thickness and grain size of event beds, is moderate near the major Rogue Canyon, low adjacent to the minor Smith and Klamath Canyons, and rises sharply at the major Trinidad and Eel Canyons (Fig. 1). This evidence is consistent with modern river discharge of these systems, suggesting that while most of these systems have been effectively relict during the Holocene, the long-term sediment supply, which is tapped by earthquakes, retains a linkage to the nearby river systems in that sediments delivered during the Holocene and Pleistocene are still available for failure (Goldfinger et al., 2017). Goldfinger et al. (2012, 2017) have shown that the consistency of the Cascadia subduction zone turbidite record across multiple site environments, both with and without sediment recharge, is a robust feature of the stratigraphy, and in fact it can be used directly as a test of seismic origin. Additional details for this topic are included in Supplemental Text S1.

Was 1700 CE Multiple Events?

Melgar (2021) proposed that the Cascadia subduction zone 1700 CE earthquake could have been a doublet or multiple ruptures based on weakly permissive stochastic tsunami modeling of the Japanese arrival of the tsunami. As the generation of doublet turbidites is germane to this work, this hypothesis is addressed here. As noted earlier, the stratigraphic record can resolve time differences between earthquakes of months, hours, and minutes, respectively (Patton et al., 2015; Wils et al., 2021; Howarth et al., 2021). Therefore, the marine and lacustrine records in the Cascadia subduction zone should be capable of similar fidelity. Of the 99 viable examples interpreted as the 1700 CE deposit (see Goldfinger et al., 2012, 2017a), three can be interpreted as doublets, in the sense of two-pulse single events, but not as temporally separable events. Thus, the lack of doublet stratigraphy argues against the hypothesis of Melgar (2021). Recent modeling of multiple tsunami inundation sites along the Cascadia subduction zone coast also supports a single ~Mw 9.1 rupture versus multiple ruptures (Small et al., 2025).

Data Quality

The Data Quality tab in Supplemental Data S2 details the criteria applied to compute an overall relative ranking of the quality of each age. In a web data release, Staisch et al. (2024) included a superficially similar data-quality ranking and attempted to compare the rankings of the marine ages to onshore paleoseismic data. In comparison, that ranking scheme is incomplete, biased toward land methods, and includes conceptual and numeric errors and omissions, so we prefer the more comprehensive quality assessment presented in Supplemental Data S2. We also do not consider it possible to directly compare the land and marine ages as the methods and tools used are too disparate. For example, the beds dated with marine ages have numerous avenues for correlation, whereas the land ages have only the ages themselves. Additionally, bracketing ages are typically not possible to ascertain due to sample-volume constraints for the marine ages, but this can be done with land ages.

Possible Explanations for the Noyo and Trinidad Plunge Pool Doublet Event Beds

Previous work along the Cascadia subduction zone and northern California margins (Goldfinger et al., 2003, 2012, 2007, 2008, 2017; Enkin et al., 2013; Hamilton et al., 2015) shows that the doublet stratigraphy as described here for Noyo Channel and Trinidad Canyons is not common elsewhere along either margin, although there are a few examples. "Inverted" doublets such as those of Noyo Channel are very uncommon. The origins or precise timing of the two units of such doublets are also not clear. Van Daele et al. (2017) separated amalgamated or multipulse turbidites coming from a synchronous source from stacked turbidites coming from sources separated in time. This aspect is explored in the next sections.

Hydrodynamics

Hydrodynamics are commonly cited as the source of bed structures in turbidite deposits (Walker, 1965; Komar, 1985; Kneller and McCaffrey, 2003) and are the most commonly cited explanation for the Bouma or Lowe sequences observed in waning flows. Additional hydrodynamic complexities could come in the form of bathymetric pathway complexities, longitudinal-flow variability (surging flows) due to a complex source, flow-density dynamics, or multiply-sourced turbidity currents that merge along their travel paths (Lowe, 1982; Goldfinger et al., 2012, 2017; Gutiérrez-Pastor et al., 2013; Ho et al., 2018; Howarth et al., 2021). Upper Trinidad Canyon has numerous potential tributaries, ~26 in total, that merge on the midslope terrace to form a simple lower-canyon pathway to the abyssal plunge pool (Fig. 2). If these numerous pathways are influencing the event-bed structure, one might expect to see as many as 26 or more coarse pulses in the beds, but this is not the case, with typically 1–3

fining-upward sequences within a single bed, similar to that observed at other Cascadia subduction zone sites with variable numbers of tributaries (0–7; Goldfinger et al., 2017). Additionally, the numerous features that appear superficially as canyon tributaries (Fig. 2) have been characterized as overlapping lowstand ravinement surfaces (Burger et al., 2002), so it is not clear what role they play, if any, as contributors to amalgamated flow during disturbance events. The northernmost potential tributary, however, is clearly connected to the outflow of the Klamath River system (Goldfinger et al., 2023).

Noyo Canyon has a pathway that only has two short (10 km and 22 km) tributaries on the uppermost slope/outer shelf and is otherwise a simple single pathway (Fig. 2). This two-headed canyon configuration might provide a relatively simple explanation for the Noyo Channel doublets. Previous work has noted that such complexities seem not to generate matching stratigraphies at the scale of a single canyon under earthquake loading and failures (Gutiérrez-Pastor et al., 2013; Goldfinger et al., 2012, 2017). The same appears to be true of canyon systems where numerous failures likely occur along the full length of the system, and yet the turbidite structure does not reflect these individually, though they do commonly thicken downstream, reflecting longitudinal volume additions (Goldfinger et al., 2017). Instead, the primary deposits linked to great earthquakes remain remarkably uniform, to a first order, above and below such proximal confluences and begin to show evidence of stacking only in distal confluences in the northern San Andreas fault system, where traveltime differences likely play a role (Gutiérrez-Pastor et al., 2013). The Noyo Channel turbidite doublets do not include the 1906 event bed, so the only event that is well known is inconsistent with this mechanism. If the doublets in Noyo Channel were created by the double canyon head, one would expect that the 1906 event would have that structure, as do the previous events. The presence of doublets also seems to be associated with the Mendocino triple junction region, fading rapidly to the north and south, and this association is not linked to any specific hydrodynamic condition in that area of which we are aware; therefore, hydrodynamics seems to be a relatively poor candidate for explaining either the Noyo or Trinidad doublets.

Aftershock Sequences

Aftershock sequences could potentially contribute to the paired stratigraphy observed in both canyon systems. Late pulses of coarse material, even within the tail of a settling turbidite bed, would not be a surprising result, and this scenario has been suggested for the 2011 Tohoku earthquake (Oguri et al., 2013; Kioka et al., 2019). In Trinidad plunge pool, several of the event-bed doublets could be consistent with this scenario. Even so, the log-correlation of the Cascadia subduction zone basin turbidites shows that the structural variability of correlated beds from site to site is relatively low, which is inconsistent with significant input from local aftershocks following each major event. The event sequences, which include a variety of site types, from isolated basins to abyssal to canyon systems, show only minor evidence of uncorrelated events or events correlated over short distances; however, aftershock evidence could well be present within what is presently interpreted as single beds. Current information about the lower threshold for triggering and recording events, as discussed in the section "Sources of the Historical Turbidites in Northern California," suggests that in Cascadia basin, aftershocks below Mw 7.0 might not be reliably recorded, although this threshold remains poorly known and is likely subject to wide variability. Supplemental Text S1 suggests one possible aftershock example. In Noyo Channel, however, the upper parts of the doublets are mostly coarser and thicker, not faint. The observation that nearly all of the event beds have this configuration makes alternative explanations unlikely. Overall, aftershocks, while they are likely represented sporadically in the stratigraphic record, are not a likely explanation for the consistency of the Trinidad plunge pool and Noyo Channel doublets.

Directivity of Multipulse Events

One potential source for Noyo Channel doublets could be the directivity of a linear northern San Andreas fault source with two characteristic rupture patches. This could produce a sequence with the more robust part of the doublet on top, in the case where a rupture started far from Noyo Canyon and concluded near the north end of the northern San Andreas fault with stronger ground motion. This explanation has appeal in that the 1906 event was such a doublet seismologically (Song et al., 2008). However, of the 13 examples of the 1906 earthquake, while some are faint doublets (Fig. 3), none resemble the thick inverted doublets deposited earlier in time. Directivity, while it may well be preserved in the beds at some level, is not a robust explanation of the observations.

Retrogressive Failures

A possible scenario for the characteristic doublet stratigraphy could be a retrogressive failure mode akin to that described for the 1929 Grand Banks earthquake (Piper et al., 1988; Henry et al., 2021). Such a failure mode could last many hours or even weeks. This failure mode would have to be something unique to Noyo Canyon in terms of canyon configuration, sediment supply, or other factors. The long retrogressive mechanism for the Grand Banks event was likely related to a long recurrence interval, leaving large masses of unfailed late-glacial and postglacial sediment available. The northern San Andreas fault contrasts with that scenario in that it has relatively low sediment supply and short recurrence times for the northern San Andreas fault of several hundred years. The ubiquitous presence of inverted doublets strongly suggests a less random and more systematic causation. Given the very different scenario and the lack of support for this mechanism by other means, retrogressive failure appears to be a poor match for the observed stratigraphy.

Nonseismic Sources

The primary nonseismic sources would be very large storms, distal tsunamis, or random slope failures. Inverted structures are sometimes invoked for storm-related turbidites, which may show a coarsening-upward and then fining-upward sequence that corresponds to the waxing and waning of the event over a period of days (Mulder et al., 2001; see discussion in Goldfinger et al., 2012). The Noyo doublet beds, however, are not similar to hyperpycnal beds because they are formed of two fining-upward stacked sequences, with the coarser unit uppermost. Additionally, Noyo Canyon is not closely connected to a river system (Fig. 1). The nearest river is the Noyo River, a small coastal river 16 km to the south of the closest part of the upper Noyo Canyon. The canyon and river may have been connected during the last Pleistocene lowstand, but they are currently separated by a wide, mostly flat-lying sedimented shelf with no channel pathway connecting them during the Holocene (Beeson et al., 2017).

The historic era includes at least two extreme storms, the 1964 event and the 1861–1862 events mentioned previously. The general insensitivity of the abyssal stratigraphic record to storm input from shallow coastal waters was discussed extensively in Goldfinger et al. (2012). The specifics of the possible faint appearance of the two historical events suggest the possibility that in the case of very narrow shelves and high sediment loads during storm events, some of these could be represented as thin beds distinguishable from the hemipelagic background. With respect to the northern San Andreas fault doublets, however, such storms would have to have been much larger than the historical maxima, and they would have had to be a good match for the timing and frequency of known great earthquakes in the Cascadia subduction zone, which is clearly implausible. Nevertheless, in one midslope core, TN0909–04TC, a 1079 m site with close links to possible shelf sediment sources, an event bed that is consistent with the 1964 flood event is much more robust than at abyssal sites (Fig. 10B). Hemipelagic intervals in this core contain numerous wisps of silt, suggesting storm input from shallower water. Thus, storm events are most likely present, but they are more robust at shallow sites and minimal at most abyssal sites. Distal tsunamis have the potential to generate slope disturbances in shallow water. Evidence from the Tohoku 2011 Mw 9.0 event shows that even a local tsunami-generated turbidity current settles out primarily on the upper slope (Arai et al., 2013); thus, much smaller distal tsunamis are unlikely sources.

Triggered Earthquakes

Goldfinger et al. (2008) proposed triggering of the northern San Andreas fault by the Cascadia subduction zone (or vice versa) based on the similarity in timing of events in both systems. While the timing was not constrained to values better than the radiocarbon age uncertainties, the sequence of numerous age overlaps seemed a plausible explanation. Now, with improved age models and stratigraphic evidence, we reexamine this hypothesis.

A space-time diagram of Cascadia subduction zone and northern San Andreas fault event beds that includes southern Cascadia subduction zone marine and onshore age data, and the same for the northern San Andreas fault, shows potential relationships between these data (Fig. 21). Comparing the new age and correlation data across the triple junction, many of the events that are correlated northward along the Cascadia subduction zone and southward along the northern San Andreas fault margins have similar radiocarbon overlaps to those noted in earlier work, with some differences (Fig. 22; Goldfinger et al., 2008). The event pairs overlapping in time between both fault systems for the most part also correspond to stratigraphic doublets observed in Noyo Channel, Trinidad plunge pool, or both in some cases. The criteria for the triggering hypothesis are given in Tables 2 and 3.

The comparison shows that with improved age models, the similarity in event sequences is significant (Fig. 22). One key element, however, is that the presence of northern San Andreas fault events such as the 1906 event in the Cascadia subduction zone cores was not previously known. Furthermore, it must be expected that Cascadia subduction zone events should also have generated event beds in Noyo Channel at a similar 90-km range. This alone might explain much of the temporal correspondence between southern Cascadia subduction zone stratigraphy and the northern San Andreas fault sequence at Noyo Channel. In that scenario, many of the ages in Noyo Channel could simply be replicate dates of Cascadia subduction zone earthquakes, and in fact, that is our preferred interpretation. However, this explanation alone is unlikely to explain the doublet stratigraphy. Our ground-truth event is the 1906 event, which is interpreted in both systems and is a simple turbidite on both the Noyo Channel and Cascadia subduction zone sides. This event, one of the few without a Cascadia subduction zone temporal correlative, is much thinner and simpler in structure than the thick beds earlier in time, and it lacks the doublet character. Examining the next significant event, in the 1700 CE time range, a doublet is observed in both systems, and indeed both faults are known to have had an earthquake approximately at that time (exactly 1700 CE for the Cascadia subduction zone; Fig. 21). With the expectation that each fault should be able to trigger turbidity currents in the opposing system, two event beds in that time range would be expected. What is observed, however, is a doublet in both systems, neither of which shows any evidence of time separation. The nearest events in time in Trinidad plunge pool are the overlying event ca. the 1830s CE, and the next significant underlying event at ca. 330 yr B.P. (Fig. 5; there are several minor intervening beds). On the Noyo Channel side, there is also a minor event at ca. 1830 CE, and the nearest underlying bed is ca. 630 yr B.P. Within this ~550–600 yr time span, no other significant events are observed. The ca. 1700 CE bed has no overlap with the lower bounding unit and limited overlap with the upper bounding event bed (Fig. 19).

Potential corroboration has recently been reported in the form of dendrochronologic evidence of the penultimate earthquake on the northern San Andreas fault. Carroll et al. (2025) reported evidence of possible damage related to a penultimate northern San Andreas fault event (8 of 16 trees) in 1698–1700, and another event in 1678–1680 (6 of 15 trees) at sites in northern California

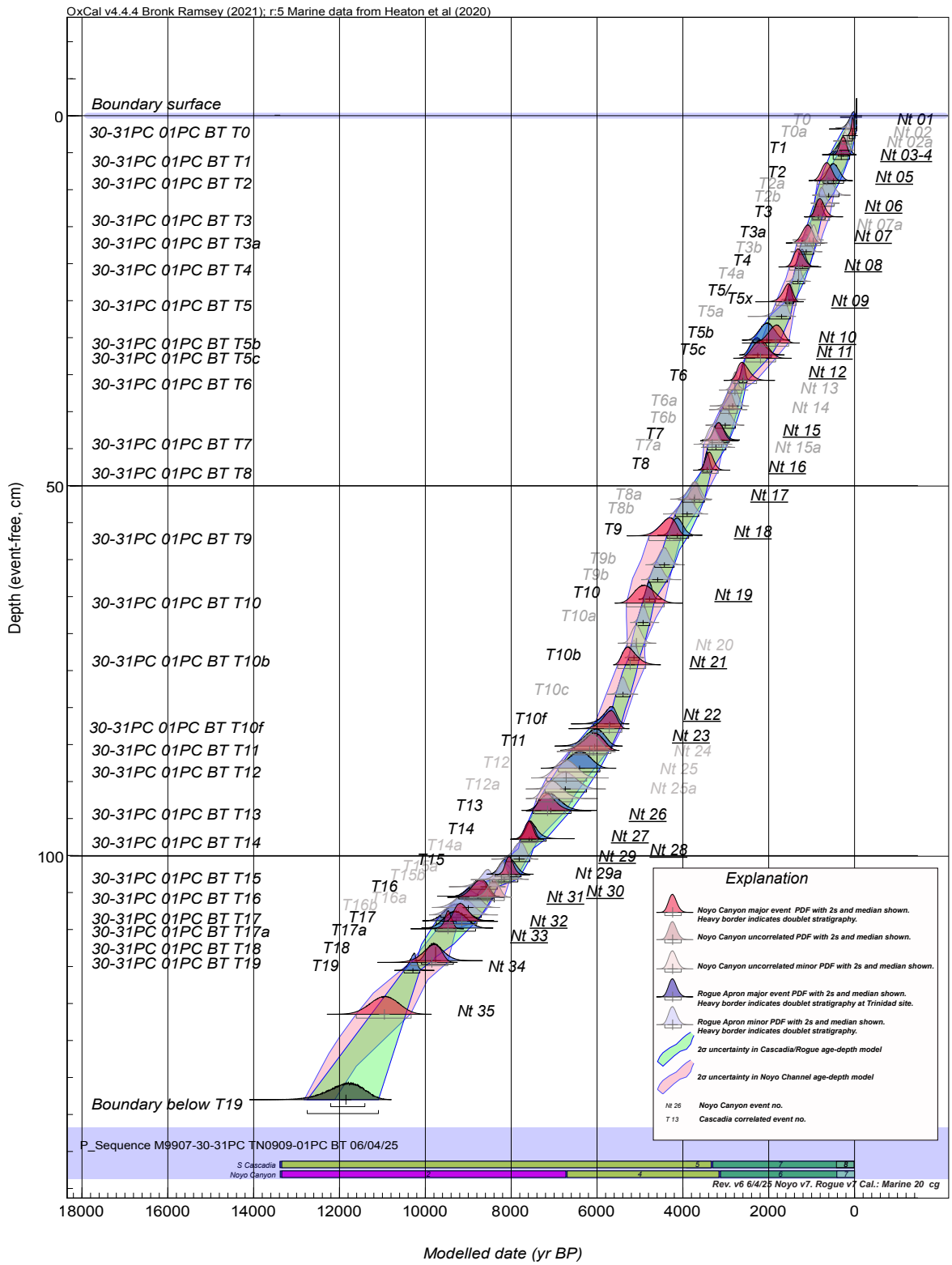

Figure 22. Major event timing through the Holocene for the southern Cascadia subduction zone and the northern San Andreas fault, represented by Noyo Channel. P-sequence model for Rogue Canyon is shown with its event-free depth scale. Noyo Channel events are shifted vertically to compare with Cascadia subduction zone events and are underlined where doublet stratigraphy is apparent. Median values and 2σ ranges are shown below each probability density function (PDF). Major event PDFs are blue, with light gray-blue for minor events. The Noyo P-sequence model is overlain with major event PDFs in red; substantial events with no Cascadia subduction zone correlatives (1906-like) are shown in intermediate red with darker outline; minor events are in very light red-gray. Colored bars at bottom indicate number of cores available to constrain age models for each age range.

TABLE 2. TURBIDITE CHARACTERISTICS FOR CASCADIA VS. NORTH COAST SEGMENT OF THE NORTHERN SAN ANDREAS FAULT (NSAF)

				Noyo doublet	Noyo bed	Cascadia	Casc. doublet	Casc. bed	Along-strike	Cascadia radio-	NSAF onshore	Lake Merced
Noyo event	Doublet?	Inverted?	Thick?	Fades southward?	Thins southward?	Doublet?	Fades northward?	Thins northward?	Extent (NSAF)	Carbon overlap	Overlap?	Overlap?
NT1 (1906)	No	NA	No	NA	No	No	NA	Yes	Full	No	All	Yes, M03
NT3–4	Yes	Yes	Yes	Yes, lower	Yes	yes	Yes	Possible*	Full	Yes, T1	FR-E2, B-2, V-E2, Bo-"H"	M04
NT5–5a	Yes	Yes	Yes	Yes	Yes	Yes	Yes	Yes*	Full	Yes, T2	Yes, FR-E3, B-3, V-E4, B-"S"	M07
NT6	No	NA	No	NA	No	Yes	NA	Yes*	Full	Yes, T3	Yes, B-3, V-E5, -E6, Bo-"S"	Yes, M8
NT7a–7	Yes	No	Yes	Yes, upper	Yes	Yes	Yes	Yes*	Full	Yes, T3a	Yes, FR-E5, V-E7	Yes, M10
NT8	Yes	Yes	Yes	Yes	Yes	?	NA	No	Full	Yes T4	Yes, V-E8, FR-E5	Yes, M11
NT9	Yes	Yes	Yes	Yes, lower	Yes	Yes	No	Yes*	Full	Yes, T5	No	Yes, M12
NT10	Yes	Yes	Yes	Yes, lower	Yes	No	NA	Yes*	Nearly full	Yes, T5b	Yes, V-09	Yes, M14
NT11	Yes	Yes	Yes	Yes, lower	No	No	NA	Yes*	Full	Yes, T5c	Yes, V-E10	Older than LM
NT12	Yes	Yes	Yes	No	Yes	?	?	Yes*	Bodega	Yes, T6	Older than all land sites	Older than LM
NT13	No	NA	No	NA	No	?	?	Yes*	Bodega	Yes, T6a, T6b	Older than all land sites	Older than LM
NT14	No	NA	No	NA	No	?	?	Yes*	Bodega	Yes, T6a, T6b	Older than all land sites	Older than LM
NT15	Yes	Yes	Yes	Yes	Yes	?	?	Yes*	Bodega	Yes, T7	Older than all land sites	Older than LM
NT15a–T16	Yes	Yes	Yes	Yes	Yes	?	?	?	Full	Yes, T8	Older than all land sites	Older than LM
NT17	No	No	No	Noyo only	No	?	?	?	Full	Yes, T8a	Older than all land sites	Older than LM
NT18	Yes	?	Yes	No, terminates at Gualala	No	?	?	?	Gualala	Yes, T8b	Older than all land sites	Older than LM
NT19	Yes	yes	Yes	Yes	Yes	?	?	?	Full	Yes, T9	Older than all land sites	Older than LM

Note: Parameters for triggering model color code: green—best fit; yellow—fair fit; blue—poor or no fit. FR—Fort Ross; B—Bodega; Bo—Bolinas; V—Vedanta; LM—Lake Merced; NA—not applicable.
*Likely due to sediment supply.

(Fig. 1). Other onshore paleoseismic sites do not report a pair of events, with the exception of Lake Merced events 4 and 5 (bed 4: 1730 CE [1580–1950], trimmed by bomb carbon); bed 5: 1670 CE [1510–1830]; Fig. 21). While the 1698–1700 age is a potential match for the penultimate event described in this work, and it carries a timing precision that is invaluable, dendrochronology has significant subjectivity, as do most geologic interpretations (Jacoby, 1997), including our own. The interpretation of tree-ring anomalies, such as abrupt growth suppressions, the formation of traumatic resin ducts, or reaction wood, as evidence of seismic shaking as distinguished from other environmental stressors (e.g., drought, insect infestation, landslides) can be difficult and relies on correlation of anomalies across multiple trees and sites to test for nonseismic causes (Kitzberger et al., 1995; Stoffel and Bollschweiler, 2008). The intensity of ground shaking required to leave detectable evidence likely varies by species and site conditions, so corroboration is generally needed to mitigate these issues (e.g., Van Arsdale et al., 1998).

In addition to radiocarbon overlap, and the presence of the unusual doublets, the Noyo Channel turbidite doublets should fade in thickness with distance from the triple junction. Specifically, either the upper or lower unit should vanish for the Cascadia subduction zone and northern San Andreas fault, respectively, which is consistent with our observations (Figs. 8, S1, and S3). Additionally, the additional bed thickness created at sites proximal to the triple junction should also thin away from the triple junction. Local factors and sedimentation rates, of course, could modify these expected trends. Many, but not all, of the doublet event beds are consistent with these criteria.

In all, in the past 2500 yr, six Cascadia subduction zone–northern San Andreas fault pairs, which includes all significant events for both systems (except the 1906 event), are likely candidates for a stress-triggering relationship, having both inverted doublets in Noyo Channel, good temporal match, and a clear doublet on the Cascadia subduction zone side (Tables 2 and 3). There are two other possible matches, with reduced temporal overlap and/or less well-expressed Noyo Channel inverted doublets, and one pair with temporal overlap but no doublet character. This represents all nine significant Cascadia subduction zone events (six long ruptures and the three largest of the shorter ruptures) having good temporal match and doublet character in one or both fault systems. During the same period on the northern San Andreas fault side, there are also nine significant events with both close overlap and doublet

TABLE 3. DEPOSITIONAL CHARACTER AND STATISTICAL FIT

Casc. bed no.	Noyo bed no.	Fit code	Noyo depositional character	Erosive/nonerosive	Hemipelagic presence	Combine agreement	Combined Chi^2
T0a	0		Weak doublet	Nonerosive	Hemipelagic	NA	
T0f	1		Complex cross-bedded, inverted doublet in some examples	Erosive		NA	
T1	3_4		Strong inverted doublet, cross-bedded upper unit	Erosive	No (n = 12)	94.7	X2-test: df = 1, T = 0.647 (5% 3.841)
T2	5		Strong inverted doublet, cross-bedded upper unit	Erosive	No (n = 4)	121.1	X2-test: df = 1, T = 0.074 (5% 3.841)
T2a	NA		NA	NA		NA	NA
T3	6		Strong inverted doublet, cross-bedded upper unit	Erosive	No (n = 4)	138.8	X2-test: df = 2, T = 0.221 (5% 5.991)
T3a	7		Strong inverted doublet, cross-bedded upper unit	Erosive	No, unexplained T7a UC bed (n = 4)	122.3	X2-test: df = 1, T = 0.034 (5% 3.841)
T4	8		Strong inverted doublet, cross-bedded upper unit	Erosive	No (n = 6)	124.7	X2-test: df = 1, T = 0.006 (5% 3.841)
T4a	NA		NA	NA		NA	NA
T5	9		Strong inverted doublet, cross-bedded upper unit	Erosive	No (n = 6)	121.6	X2-test: df = 1, T = 0.003 (5% 3.841)
T5a	NA		NA	NA		NA	NA
T5b	10		Strong inverted doublet, cross-bedded upper unit	Erosive	No (n = 6) slight possibility, 1 example	119.6	X2-test: df = 1, T = 0.122 (5% 3.841)
T5c	11		Strong inverted doublet, cross-bedded upper unit	Erosive	No (n = 6)	91.3	X2-test: df = 1, T = 1.457 (5% 3.841)
T6	12		Strong inverted doublet, cross-bedded upper unit	Erosive	No (n = 6)	109.5	X2-test: df = 1, T = 0.500 (5% 3.841)
T6a	13		Singlet	Nonerosive	NA		
T6b	14		Singlet	Nonerosive	NA		
T7	15		Strong inverted doublet, cross-bedded upper unit	Erosive	Slight possibility (n = 5)	123.6	X2-test: df = 1, T = 0.049 (5% 3.841)
T7a	NA		NA	NA		NA	NA
T8	15a		Strong inverted doublet, cross-bedded upper unit		No (n = 5)	121.2	X2-test: df = 1, T = 0.069 (5% 3.841)
T8a	16		Doublet in minority of examples	No erosion observed	No (n = 5)		
T8b	17		Faint doublet in some examples	No erosion observed	Possible, 1 example (n = 5)		
T9	18		Doublet in some examples	Erosive	No (n = 5)	103.1	X2-test: df = 1, T = 0.665 (5% 3.841)
T9a	NA		NA	NA		NA	NA
T10	19		Equal doublet strong in one bed	Erosive	No (n = 5)	123.8	X2-test: df = 1, T = 0.002 (5% 3.841)
T10a	20		Singlet	NA	NA		
T10b	21		Equal doublet	Erosive	No (n = 4)	113.6	X2-test: df = 1, T = 0.274 (5% 3.841)
T10c	NA		NA	NA		NA	NA
T10f	22		Equal doublet	Nonerosive	No (n = 4)	126.6	X2-test: df = 1, T = 0.013 (5% 3.841)
	23		Equal doublet, one example inverted	Inverted is erosive, others not	No (n = 4)	63.2	X2-test: df = 1, T = 1.289 (5% 3.841)
T11	24		Unclear if this is a doublet with 23, or a single event	Nonerosive	No (n = 4)	83	X2-test: df = 1, T = 1.289 (5% 3.841)
T12	25		Minor singlet	Nonerosive	NA		
T13	26		Singlet	Nonerosive	NA	78.6	X2-test: df = 1, T = 1.907 (5% 3.841)
T13a	NA		NA	NA		NA	NA
T14	27		Strong inverted doublet	Erosive	No (n = 3)	117	X2-test: df = 1, T = 0.238 (5% 3.841)
T14a	28		Equal doublet in two examples	Erosive	No (n = 3)		
T15	29		Strong inverted doublet in one example	Erosive	No (n = 3)	115.3	X2-test: df = 1, T = 0.116 (5% 3.841)
T15a	30		Doublet weak, complex inverted in one example	Erosive	No (n = 3)		
T16	31		Doublet weak, complex inverted in one example	Erosive	No (n = 3)	122	X2-test: df = 1, T = 0.127 (5% 3.841)
T16a	NA		NA	NA		NA	NA
T17	32		Equal doublet	Erosive	No (n = 2)	74.2	X2-test: df = 1, T = 2.229 (5% 3.841)
T17a	33		Equal doublet	Erosive	No (n = 2)	70.9	X2-test: df = 1, T = 1.865 (5% 3.841)
T18	34		Weak deformed unit	??	No (n = 2)		

Note: Green—good fit; yellow—good age fit, doublet present but not inverted; orange—poor to no fit; blue—Cascadia or northern San Andreas fault only recorded both sites? NA—not applicable; UC—uncorrelated event; df—degree of freedom; n—number; T—temperature.

character of a total of 12 beds. Of those, eight have temporal equivalents at one or more land sites to the south (Tables 2 and 3). For earlier times, from 2500 yr B.P. to the base of the Holocene, many events have similar relationships, including 13 of 21 Noyo events having significant temporal overlap with the Cascadia subduction zone (Fig. 21). The temporal matches include all major Cascadia subduction zone events and the largest of the inferred segmented events T10b and T10f, and could include smaller events T6a, T6b, T8a, T10a, and T12. The events not matched are all minor events, but there could be potential minor event matches to the Cascadia subduction zone. These latter beds could simply be Cascadia subduction zone events recorded in Noyo Channel, our preferred interpretation, as they do not appear to correlate southward along the northern San Andreas fault. Of the 21 Noyo Channel beds, 15 have temporal matches in the Cascadia subduction zone, and of those, 13 have a doublet character, though with weaker evidence and more equal doublets (Tables 2 and 3). Of the six unmatched beds (NT13, NT17, NT20, NT25, NT25a, NT30), five of them are thinner singlet beds; only one bed, NT26, is a thin singlet bed with a significant Cascadia subduction zone temporal correlative (T13). We infer that a model involving a close temporal relationship and potential stress-triggering mechanism is the best-fitting hypothesis to the observations.

Analysis and Implications of a Cascadia Subduction Zone–Northern San Andreas Fault Triggering Model

Head-to-Head Age Comparisons

Direct temporal comparisons between Cascadia subduction zone and northern San Andreas fault sides of the Mendocino triple junction were tested using Bayesian statistical comparisons of the radiocarbon ages. The key comparisons including the Cascadia subduction zone and other north coast section northern San Andreas fault sites for comparison are shown in Table 1. Bayesian age-depth models are powerful tools for comparisons of sequences as shown in the previous sections, but they may be somewhat compromised in comparing single event ages as they can be shifted away from their associated radiocarbon ages in order to arrive at a best-fit for an entire sequence. In comparing head-to-head ages, we give up some of the advantages of the depositional models in order to focus on comparing individual events. If two ages are thought to be coeval (as in this case), but not from the same source, then merging with the OxCal Combine function is appropriate (Ramsey et al., 2010; Ward and Wilson, 1978; Wilson and Ward, 1981). Comparisons of the probability distribution functions with a χ^2 test and the OxCal A_Combine function are discussed in Supplemental Text S1, and graphical outputs are given in Figures S10A–10C.

CSZ T1. To compare the CSZ T1 age with the potentially correlative Noyo event NT3–NT4, the Cascadia subduction zone sample 210 and the Noyo NT3–NT4 sample 50b were assessed (Fig. S10A). Two OxCal Combine functions were done, and each of the Cascadia subduction zone and Noyo ages were compared. The combined data yielded a rejection of the null hypothesis at well above the 95% confidence limit. The combined results were 1700 CE or 250 (380–100) cal yr B.P. (Fig. S10A). See Supplemental Text S1 for further details.

The ca. 1700 CE event is recorded southward at all sites along the northern San Andreas fault, likely including Lake Merced, over a strike length of at least 280 km, and thus, it was a significant event. On the Cascadia subduction zone side, the event is thought to be of Mw ~9.0 with ~1000 km of strike length (Satake et al., 2003; Goldfinger et al., 2012, 2017). The maximum timing separation, exclusive of the stratigraphic evidence, in this case if the northern San Andreas fault followed the Cascadia subduction zone, is likely ~76 yr, established by the full-time occupation of Mission Dolores and the Presidio by Spanish soldiers in mid-1776 (Donkin, 1961).

Comparison of the Noyo age of 1700 (1560–1840) CE to Lake Merced (LM) beds 4 and 5 both shows compatible ages, so either one could be a match for the Noyo Channel and the other land paleoseismic sites (Tables 2 and 3). Bed 3 at Lake Merced is a much more substantial bed, however, and we prefer an interpretation wherein that bed records an earthquake that is a possible correlator along much or all of the north coast of the northern San Andreas fault (Goldfinger, 2021).

CSZ T2. To compare the CSZ T2 age with potentially correlative Noyo event NT5, the T2 model age from the southern Cascadia subduction zone at the Trinidad plunge pool was compared to the Noyo Channel age (Fig. S10A). Model ages were chosen due to high uncertainty for the direct ^{14}C ages in this case. Our interpreted correlation has a median age at the Trinidad plunge pool of ~540 yr, slightly older than the margin average of 490 yr. The median of age of Noyo NT5 is 630 yr B.P., giving a poor temporal fit, but within the uncertainty. Given these discrepancies, this pairing is equivocal at best. In the Noyo Channel examples, the upper unit is cross-bedded with a sharp upper contact. As with the CSZ T1 event pair, the upper part of the Trinidad plunge pool doublet appears to have been deposited either during or immediately following the deposition of the basal unit.

CSZ T3. To compare the CSZ T3 age with potential correlative Noyo event NT6, two T3 ages from the southern Cascadia subduction zone at the Trinidad plunge pool were compared to the available Noyo Channel ages. Figure S10A shows Cascadia subduction zone samples 278 compared to the Noyo age for NT6 sample 59. Another Noyo age, sample 33, is ~100 yr older than sample 59, and it was rejected in this comparison. The combined age yielded a rejection of the null hypothesis at well above the 95% confidence limit and A_{comb} statistic of 139%. NT6 may extend to the latitude of San Francisco (Fig. S3). Interpreted T3 on the Cascadia subduction zone side has a clear doublet structure in all samples that fades northward (Fig. 8). Bed NT6 on the Noyo side has a weak doublet structure in three of the four samples available that fades southward. See Supplemental Text S1 for additional details.

CSZ T3a. The next event pairing was CSZ T3a and Noyo NT7. While the temporal overlap is minimal, the event beds in Noyo Channel are mostly inverted doublets (3 of 4 samples), while the potential Cascadia subduction zone equivalents are difficult to interpret and are weak doublets. We consider

that these beds may be unrelated timing coincidences, or they record a single event by both systems.

CSZ T4. The T4 age from the southern Cascadia subduction zone at the Trinidad plunge pool (sample 83) was compared to the available Noyo Channel NT8 model age (Fig. S10A). The combined age yielded a rejection of the null hypothesis at well above the 95% confidence limit, and an A_{comb} statistic of 125%, with A_{model} agreement at 125%. T4 in the Trinidad plunge pool is a clear doublet, and the upper unit fades northward, becoming the more typical singlet. The doublet character is less clear in the Noyo system, appearing in three of five samples, being somewhat obscured by core deformation in M9907–49PC (Fig. S3). The doublet character in the Noyo system is dissimilar to many of the other doublets, having either a weaker upper unit or two similar units.

CSZ T5. CSZ T5 is a well-correlated major event in the Cascadia subduction zone, and it also has a time equivalent in the form of a major event doublet, NT9, in Noyo Channel. This event is commonly a doublet at most sites in the Cascadia subduction zone, so the doublet character at Trinidad is not particularly diagnostic. The CSZ T5 age, represented by sample Casc. 284, is indistinguishable from onshore ages for this event (Padgett et al., 2021; Nelson et al., 2021) and was compared to the model age of NT9 in Noyo Channel, as it has not been dated directly (Fig. S10A). The combined age yielded a rejection of the null hypothesis at well above the 95% confidence limit, and an A_{comb} statistic of 122% These are among the best examples, with Cascadia subduction zone beds normally stacked and Noyo beds inverted, with a sharp upper contact and cross-bedding of the upper unit in the Noyo location. The Noyo Channel inverted doublet fades southward to complex single unit (Fig. S3). On the Cascadia subduction zone side, T5 in the Trinidad plunge pool is a complex three-pulse unit, overlain closely by another event. The hemipelagic time intervals are ~150 yr above and ~180 yr below on the Cascadia subduction zone side, and 200 yr above and 350 yr below for Noyo, excluding the possibility of misassignment of the matching beds. T5 at many Cascadia subduction zone sites is a doublet with short time separation between the two closely spaced basal units, and this character of the T5 base is observed well to the north, excluding the northern San Andreas fault as a contributor. The potential northern San Andreas fault match may be the second unit above the basal doublet (Fig. 17), though the potential correlative is far less clear than the T1 example.

CSZ T5b. CSZ T5b is a correlated major event in the southern Cascadia subduction zone, and it also has a time equivalent in the form of a major event doublet in Noyo Channel. The CSZ T5b age, represented by sample Casc. 33, was compared to the age of NT10 in Noyo Channel, best represented by the OxCal model age for that event, as it has not been dated directly (Fig. S10A). The combined age yielded a rejection of the null hypothesis at well above the 95% confidence limit, and an A_{comb} statistic of 120%. The Noyo bed examples are strong inverted doublets for all but one sample, with one damaged by core deformation. These examples also have sharp upper contacts, cross-bedding in the uppermost unit, and erosion of the upper unit into the lower unit. On the Cascadia subduction zone side, a weak basal doublet and late secondary event (T5a2) were observed (Fig. 5).

CSZ T5c. CSZ T5c is a correlated major event in the southern Cascadia subduction zone, and it also has a time equivalent in the form of a major event doublet in Noyo Channel. The CSZ T5c age, represented by sample Casc. 285, was compared to the model age of NT11 in Noyo Channel, as it has not been dated directly (Fig. S10A). The combined age yielded a rejection of the null hypothesis at well above the 95% confidence limit, and an A_{comb} statistic of 91%. While these values are statistically acceptable, the fit is far less strong than that shown for other pairings. This is because the CSZ T5c age (sample 285) is younger than expected for this event, and younger than other ages for this correlated event at Rogue Apron and other sites. The age for this event was corrected from benthic foraminifera as discussed in Goldfinger et al. (2012), adding uncertainty, and there always remains the possibility of miscorrelation. The lower unit of NT11 fades southward (Fig. S3), but T5c has no doublet character in the Cascadia subduction zone.

CSZ T6. CSZ T6 is a correlated major event in the southern Cascadia subduction zone, and it also has a time equivalent in the form of a major event doublet in Noyo Channel. The CSZ T6 age, represented by sample Casc. 66, was compared to the age of NT12 in Noyo Channel, best represented by the OxCal model age for that event, as the radiocarbon age for that event is reversed. The combined age yielded a rejection of the null hypothesis at well above the 95% confidence limit, and an A_{comb} statistic of 110% (Fig. S10B). CSZ T6 in the Trinidad plunge pool only has a weak doublet character, while NT12 has no doublet characteristics, and the event bed fades southward. Comparisons for additional temporal pairs are given in Supplemental Text S1 and Figures S10B and S10C.

Timing Considerations and Constraints

It is possible to ascertain even the single year of an earthquake through dendrochronology, Paleomagnetic Secular Variation, or other methods (Atwater et al., 1991; Black et al., 2023; Kanamatsu et al., 2023), a level of precision normally unavailable in radiocarbon-based paleoseismology. As previously noted, time differences between earthquakes in subaqueous paleoseismic investigations with time separation of months, hours, and minutes has been observed. Thus, stratigraphic relationships have the potential to address this relative timing precisely in this study, though with complications. The ability to resolve less than 100 yr separation in time is demonstrated in both faults by the observation of the likely 1906 and 1992 beds on both faults. Similarly, the likely separation of 12 yr between the inferred 1980 and 1992 beds (Fig. 7) is moderately well constrained.

To address subdecadal and possibly annual to subannual timing, the relative timing of the events can be considered, independent of what delivery mechanism(s) is operative. In Noyo Channel, the doublet stratigraphy is in many cases topped by a robust, coarse-grained unit. The typical absence of hemipelagic material between the Noyo doublet units, which might constrain the timing to less than a decade or so, cannot be invoked simply because of the

likely erosive effects of the coarse and dense upper unit on the finer-grained lower unit as noted for CSZ T1 and T2. The observed sharp upper contacts between $T_{A–C}$ and T_E units indicate bypassing of the intermediate grain fractions, a characteristic of a proximal high-velocity flow (Parker et al., 1986; Sequeiros et al., 2018) or autogenic flow fluctuation (Ge et al., 2022), supported by cross-bedding of the upper coarse unit, indicative of a bed-load role for this unit (Bouma, 1962; Stow and Smillie, 2020). On the other hand, the lower parts of the Noyo doublets generally do not have sharp upper contacts, except where visibly eroded by the upper unit, and show no evidence of bypassing. Nonerosive-appearing contacts are inferred in 32% of the doublets (Table 3) but cannot be considered definitive. For these reasons, the timing aspect is better addressed in the Cascadia subduction zone doublet examples, where the fainter proposed northern San Andreas fault event beds may have been deposited into the tails of the underlying Cascadia subduction zone beds as suggested for Cascadia subduction zone beds T1, T3, T4, and T5. There being no evidence of oxidation or erosion between these bed elements, this timing implies minimal separation between them in time, which could be at most a few years, and perhaps as low as hours to a few days. Baas et al. (2000) modeled and tested the depositional timing of turbidity currents and concluded that the Bouma $T_{A–C}$ divisions would be complete in <20 min, potentially setting a very short upper bound on time separation. Transport to the core site likely would have been several hours for both units, so the separation in event time is the element of interest.

In summary, six pairs of events in Noyo Channel and Trinidad plunge pool have a high level of temporal overlap in the past 2500 yr. Of these, all significant events interpreted as full-margin Cascadia subduction zone ruptures may be represented (T1 and T3–T6, with T2 being equivocal), and all have the proposed stratigraphic sequencing, with several more robust than others. Three additional events, T3a, T5b, and T5c, interpreted as partial-margin ruptures (Goldfinger et al., 2012, 2017), have temporal overlaps and well-defined inverted doublets in Noyo Channel but weak to no doublet structure in the Cascadia subduction zone. These three events are the most significant partial rupture beds in the southern Cascadia subduction zone younger than 4000 yr B.P., at least suggestive of greater energy release. Finally, good temporal overlaps exist for five additional pairings (with reduced criteria), CSZ T7, T8, T8a, T8b, and T9 with Noyo events NT15, NT16, NT17, NT18, and NT19, respectively. This result is summarized in Table 3, and other equivocal examples are discussed in Supplemental Text S1.

Event Frequency

During the period of clear doublet occurrence, the major event repeat interval in Noyo Channel was ~210 yr (16 events). In the Cascadia subduction zone, the average repeat time for all events large enough to be included in the segment models of Goldfinger et al. (2012; 15 events) is similar at ~230 yr. In Noyo Channel, at earlier times from ~3100 yr to the base of the Holocene, 14 significant beds are observed (several other thin beds are present as well), with an average repeat time of ~470 yr. In the Cascadia subduction zone, the southernmost record cannot be determined due to limiting core length. However, if Rogue Canyon is representative of these events, then the Cascadia subduction zone during this same 6900 yr period had a major event repeat time of 510–550 yr, for 12 or 13 events (segments A and B, possibly excluding thin T12; Goldfinger et al., 2012, 2017). Doublet stratigraphy for the southernmost Cascadia subduction zone cannot be observed, but in Noyo Channel, 15 of the 20 events in this period are doublets, though sometimes weakly developed and commonly without the strong inverted character (observed in only three of them; Table 2). Two other pairs (NT23-NT24 and NT30-NT31) are likely separate events. The timing of these individual events is generally similar between the southern Cascadia subduction zone and Noyo Channel, permissive but not strongly indicative of a correlation. Nevertheless, the 6900 yr period includes only enough turbidite beds to satisfy recording of major events from one of the two faults, as the number is similar to that of the Cascadia subduction zone alone. Because there are no corroborative onshore records for the northern San Andreas fault for that period, and the along-strike correlation is problematic, we can speculate that: (1) either the northern San Andreas fault had no earthquakes during that period, and only events on the Cascadia subduction zone were recorded; (2) there is a mixed record of Cascadia subduction zone and northern San Andreas fault events that cannot currently be differentiated, and it is coincidentally similar to the Cascadia subduction zone; or (3) the Cascadia subduction zone and the northern San Andreas fault were partially synchronized during this period as well, leaving a record of both faults in amalgamated beds as we propose for the post–2500 yr B.P. period. We prefer the synchronized option as it fits the data well and requires no significant changes in fault behavior or coincidences. If correct, this scenario implies a longer recurrence period on average for both faults in the early Holocene, which has been clearly observed in the Cascadia subduction zone (Goldfinger et al., 2012).

Role of Upper-Plate Faults?

The southern Cascadia subduction zone has several well-known upper-plate faults with relatively high event frequencies and Quaternary slip rates. Notably, these include the Mad River fault zone, Little Salmon fault, and Grogan fault (Kelsey and Carver, 1988; McCrory, 2000). Clarke and Carver (1992) and Witter et al. (2002) observed that the Mad River fault zone and Little Salmon fault may have ruptured in at least four large earthquakes, ca. 260 yr B.P., ca. 800 yr B.P., ca. 1200 yr B.P. (two events?), and ca. 1550 yr B.P., broadly coincident with the age ranges for subsidence events in Humboldt Bay. They presented arguments for these ruptures to have most likely been coincident with subduction zone earthquakes at about those times, and the timings are broadly similar to those found offshore in this and previous work. Further work is needed to establish coincident timing or otherwise for these upper-plate

faults, as the age ranges are so broad as to be speculative. Given existing knowledge, coincident ruptures on these upper-plate faults are unlikely to have been contributors to the offshore record; however, this must remain an open question, and independent rupture remains a possibility. Ladinsky et al. (2020) reported additional work on the Little Salmon fault but were unable to resolve this question. Considering the historical lack of evidence in Noyo Channel for earthquakes from the Mendocino fault or the Gorda plate, those source possibilities seem unlikely for Noyo Channel.

Depositional Model

The deposition of multiple normally graded beds or subunits within single deposits derived from closely spaced earthquakes, multifault earthquakes, or multi-asperity earthquakes has been observed or proposed in a number of settings. The expectation that this should be observed from surging flows with longitudinal heterogeneity was proposed by Lowe (1982). Characteristic stacking that is traceable along strike has been used as a correlation tool and linked to earthquake sourcing and proposed to explain the along-strike correlation of stratigraphy for seismo-turbidites (Nakajima and Kanai, 2000; Goldfinger et al., 2008, 2012; Patton et al., 2015; Howarth et al., 2021). Separation of two distinct turbidites with 3 h of time separation between two earthquakes was reported by Wils et al. (2021). Patton et al. (2015) observed distinct turbidites in Sumatra from the 2004 and 2005 events with 3 months of time separation, and a three-unit 2004 turbidite deposit that closely resembled the seismogram with three rupture patches from the 2004 main shock. Howarth et al. (2021) observed a linkage between ground motions and the resulting turbidite deposits within a complex multifault rupture during the Kaikoura earthquake of 2017. This example is perhaps the worst-case scenario for the "paleoseismogram" hypothesis of recording primary energy-release patterns in turbidite stratigraphy (Goldfinger et al., 2012) with multiple faults rupturing in a complex series. Limited experimental work supports the relationship between surging flows and the depositional sequence (Goldfinger, 2011; Ho et al., 2019), though it is problematic (due to scaling issues) to predict the real-world range at which the surging pulses will eventually merge (Ho et al., 2018, 2019; Ge et al., 2022).

We propose a depositional model for the southern Cascadia subduction zone and northern San Andreas fault turbidites that builds on the observations elsewhere and satisfies the local observations in terms of these elements: (1) the possible close timing between Cascadia subduction zone and northern San Andreas fault events; (2) the doublet stratigraphy observed in the southern Cascadia subduction zone and the northernmost part of the northern San Andreas fault, with strongly inverted doublets being the norm in Noyo Channel; (3) the rapid fading of doublet stratigraphy north and south of the triple junction; (4) the tendency for locally expanded thickness of the beds that have the doublet character and observed thinning away from the triple junction; (5) the lack of a doubling of the turbidite frequency that would result from independent rupture of the two faults, and the observed similar frequency implying paired bed deposition; and (6) the demonstrated ability to trigger turbidity currents at sites along the opposing fault. In the first stage, a Cascadia subduction zone earthquake occurs, triggering a robust turbidity current on systems on the Cascadia subduction zone side and depositing a coarse bed. A weaker turbidity current is triggered simultaneously on the northern San Andreas fault, at 90 km from the southern boundary of the Cascadia subduction zone, depositing a silty bed. In the second stage, a northern San Andreas fault earthquake occurs a short time later, triggering a weak turbidity current in the Cascadia subduction zone, at 90 km range, depositing a silty bed, and a robust sand-bearing turbidity current in Noyo Channel, creating the upper parts of the Noyo doublets. The result is a normally graded doublet on the Cascadia subduction zone side and an inverted doublet on the Noyo side (Fig. 23).

We note that the 1906 event bed is more robust in southern Cascadia subduction zone sites (Fig. 8) than the upper doublets in the Cascadia subduction zone that may have been triggered by northern San Andreas fault events. The likely 1906 bed extends much further to the north than other potential northern San Andreas fault events recorded on the Cascadia subduction zone margin. Morey (2020) and Morey and Goldfinger (2024) observed a likely 1906 bed in Acorn Woman Lake, at a similar range to Rogue Apron, but not other northern San Andreas fault events. Why would this be? One explanation could be that the 1906 event had south to north directivity (Song et al., 2008), which would have strongly influenced the level of ground motion at the northern limit and extended the northern extent of strong shaking. If correct, our triggering model would likely result in north to south directivity for triggered events, reducing ground motion north of the triple junction, and possibly reducing the robustness of the turbidite record for those events in the Cascadia subduction zone.

Fault Synchronization

Earthquake and fault synchronization refers to the tendency of large earthquakes on adjacent faults to repeatedly trigger other segments or other faults. Stress triggering relationships have been observed and reported in a number of settings (Stein, 1999; Parsons et al., 1999; Toda et al., 2011). Longer-term synchronization or cyclic influence over several seismic cycles has also been reported or proposed in a limited number of settings: the Eastern California shear zone (Rockwell et al., 2000; Bell et al., 2004; Scholz, 2010), oceanic transforms (McGuire, 2008), Chile (Cisternas et al., 2005), the Sunda subduction zone (Sieh et al., 2008), and the Cascadia subduction zone–northern San Andreas fault (Goldfinger et al., 2008; this paper).

Scholz (2010) proposed that faults with similar geological slip rates and parallel or conjugate faults, or patches on the same fault, could be prone to synchronization. Scholz (2010) discussed the process in terms of oscillators and used the radio-frequency term "phase locking" as an analog to what might occur in a system of multiple faults (see also Bendick and Bilham, 2017; O'Malley et al., 2018). Scholz (2010) inferred from the spring-slider block work of Gomberg et al. (1998) that static stress transfer would tend to inhibit

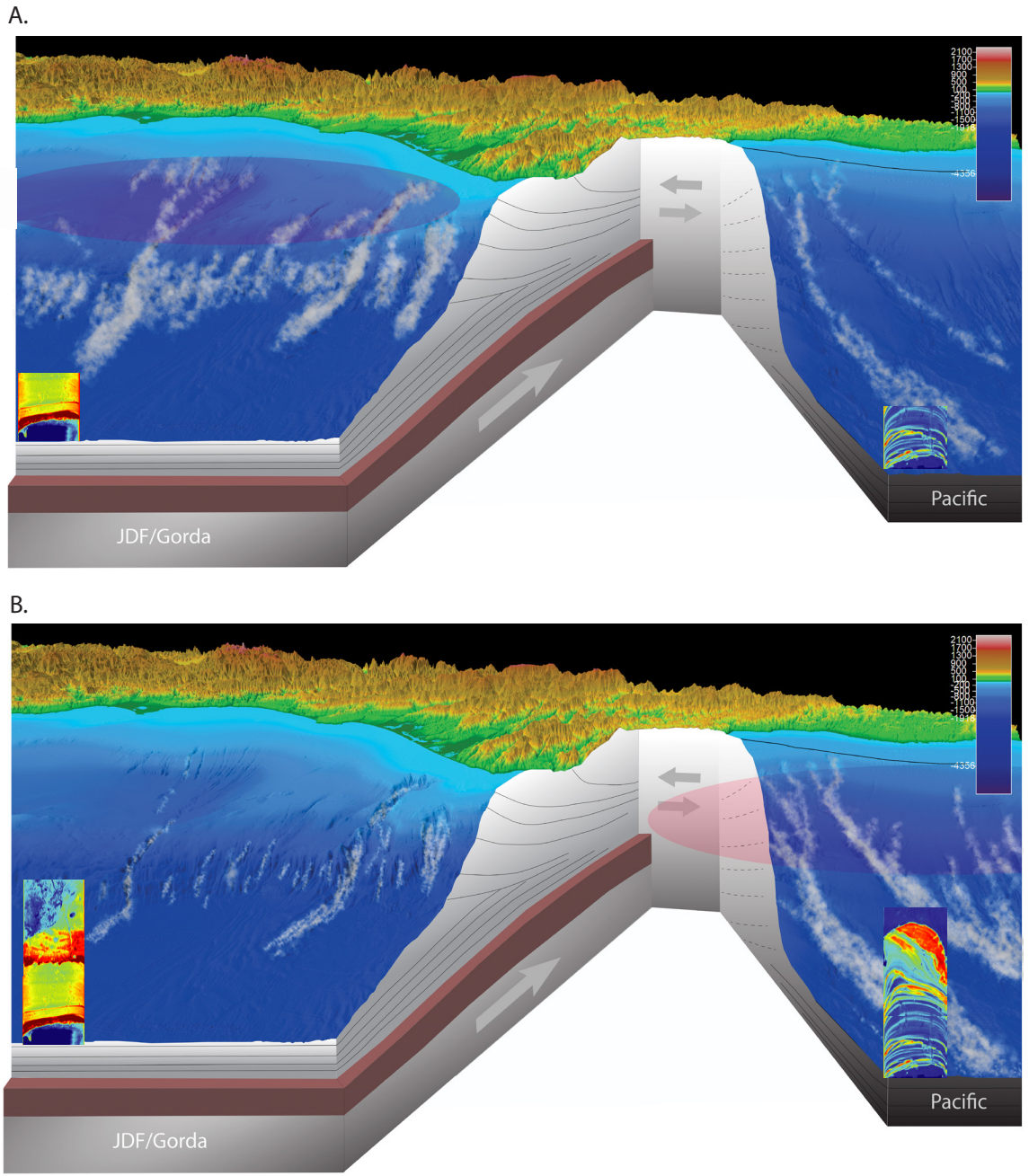

Figure 23. Two-stage depositional sequence proposed for a Cascadia subduction zone–northern San Andreas fault stress interaction. (A) A Cascadia subduction zone earthquake occurs, triggering a robust turbidity current on the Cascadia subduction zone systems and depositing a coarse bed. A weaker turbidity current is triggered simultaneously in Noyo Channel and other sites at 90 km from the southern boundary of the Cascadia subduction zone, depositing a silty bed (computed tomography [CT] example from lower part of 1700 CE shown at bottom). (B) A northern San Andreas fault earthquake occurs a short time later, triggering a weak turbidity current in the Cascadia subduction zone, at 90-km range, depositing a silty bed, and generates a robust sand-bearing turbidity current in Noyo Canyon/Channel, creating the upper part of the doublet. The result is a normally graded doublet on the Cascadia subduction zone side and an inverted doublet on the Noyo side (CT example from complete 1700-CE bed shown at bottom). JDF—Juan de Fuca.

synchronization, while dynamic stress transfer would promote synchronization. Using two-dimensional simulations, Wei and Shi (2021) inferred that both static and dynamic stress transfer can work in a synchronized framework. Goldfinger et al. (2008) proposed and modeled the coseismic, afterslip, and viscoelastic Coulomb Failure Stress cases for the Cascadia subduction zone–northern San Andreas fault interaction. Wei and Shi (2021) in modeling experiments found that synchronization could be maintained for 10–20 cycles, and then the system would devolve into more complex behavior. The evidence presented here suggests that beyond a triggering relationship with a pair of earthquakes, the Cascadia subduction zone and the northern San Andreas fault may have been involved in long-term partial synchronization during much of the Holocene, as described by Scholz (2010). Our data suggest that even very dissimilar faults, such as a subduction thrust and adjacent vertical strike-slip fault, can synchronize, and evidence also suggests that the repeat interval similarity of the involved faults might be important.

CONCLUSIONS

Detailed analysis of cores and subbottom profiles near the northern limit of the northern San Andreas fault at Noyo Channel and in the southern Cascadia subduction zone has yielded improved stratigraphic sequencing, age models, and evidence of both paleo-earthquakes and historic earthquakes. Subbottom data reveal a consistent sequence of event beds along a 240 km stretch between Trinidad plunge pool and ~43.3°N. Several significant event beds overlie the 1700-CE Cascadia subduction zone earthquake bed. High-resolution age models suggest these likely include beds generated by the 1906 northern San Andreas fault, 1980 Eureka, and 1992 Petrolia earthquakes.

A likely northern San Andreas fault 1906 bed in the southern Cascadia subduction zone suggests that other event beds from the northern San Andreas fault could be present as well, and that event beds from Cascadia subduction zone earthquakes should be expected at similar ranges along the northern San Andreas fault. In both Trinidad plunge pool and Noyo Channel cores, unusual doublet event beds are observed. The observed beds in Noyo Channel are unusual, thick doublets with a lower silty unit directly overlain by a robust sandy unit, commonly with an erosional unconformity between the two subunits. On the Cascadia subduction zone side, the observed doublets commonly have a less robust upper unit, and some upper units are embedded in the tails of the lower units. The characteristic doublet stratigraphy in many Noyo Channel beds fades southward along the northern San Andreas fault, while those on the Cascadia subduction zone side fade northward. Similar doublet beds are rarely observed elsewhere in the Cascadia subduction zone or along the northern San Andreas fault. The doublet beds correspond to times when the northern San Andreas fault and the Cascadia subduction zone have both had significant earthquakes. An interpreted 1700 CE earthquake on both faults is corroborated by onshore tree-ring evidence for the Northern San Andreas fault. During the past ~3100 yr, a total of 18 (eight major and 10 minor) turbidite beds interpreted as generated by plate-boundary earthquakes are found in the southern Cascadia subduction zone along with three historic beds from crustal or lower-plate sources. In Noyo Channel and points south, there are 19 likely earthquake-generated beds, 14 significant beds, and five minor beds during the same period. Of the 18 Cascadia subduction zone beds, nine have a close temporal association with the likely earthquake-generated beds in Noyo Channel. This includes all of the major Cascadia subduction zone event beds and the three most significant thinner beds. The radiocarbon age medians for these events in the two systems differ by an average of 63 yr, with a standard deviation of 51 yr, and all exceed statistical tests of coevality. In addition, 8 of 10 of the Noyo beds corresponding to major Cascadia subduction zone events in this period have the distinctive thick inverted doublet stratigraphy, while beds without timing similarities, including the 1906 bed, do not. Many of the Noyo beds younger than 2500 yr B.P. have possible correlatives at other land sites, including some or all of those available where temporal overlap with the land and marine records exists: Point Arena, Fort Ross, Bodega Bay, Bolinas Lagoon, Vedanta marsh, Dogtown, and Lake Merced. For most of the doublet beds, time intervals above and below commonly do not allow enough time for Cascadia subduction zone beds to be present in Noyo Channel but miscorrelated on the basis of radiocarbon.

The recurrence rate of major events near the triple junction (<3100 yr B.P.) where these two great faults intersect is not the additive rate of both faults, but, instead, it is similar to the rate for either fault alone, implying the doublet beds represent pairs of beds from each fault, stacked together as doublets. The doublet character is best explained by earthquakes on both systems spaced closely in time, as opposed to aftershock sequences, hydrodynamic generation, or other causes. The time separation between the Cascadia subduction zone and northern San Andreas fault ruptures is not known. On the Cascadia subduction zone side, several doublet beds appear to have the upper unit embedded in the tail of the initial event, implying a very short time separation where the second event was settling into the still-moving, waning turbidity current from the initial event. This would imply minutes to hours of separation. For other events, temporal relationships are less clear. The earlier Holocene is less well constrained by fewer available cores. Of the 20 Noyo beds during that time, only two beds and event pairings, CSZ T8-NT15a and T14-NT27, meet the same criteria established for the post–3100 yr B.P. time frame. However, 12 of the beds, including eight pairs for all major Cascadia subduction zone events, as well as four minor ones, are temporally close, even though the doublet stratigraphy is not as consistent as that in the later period. Additionally, the apparently excellent recording of Cascadia subduction zone events at Noyo Channel potentially removes much of the uncertainty about the southern extent of Cascadia subduction zone ruptures as noted in Goldfinger et al. (2012, 2017). We consider that Noyo Channel may be treated as another Cascadia subduction zone paleoseismic site for some events.

The hypothesis of a stress-triggering interaction and partial synchronization of the northern San Andreas fault with the Cascadia subduction zone is supported by the new stratigraphic and radiocarbon evidence of occurrence and timing. The stratigraphic stacking suggests that the Cascadia subduction

zone ruptures first, and the northern San Andreas fault ruptures thereafter in most cases. There are several doublets without the inverted character that do not support either of the faults rupturing first over the other. The Holocene sequence of temporal and closely stacked stratigraphic pairs may represent direct evidence of partial synchronization of these two great faults for the latest Holocene, with the possibility of significant interaction at earlier times.

ACKNOWLEDGMENTS

We acknowledge the efforts of the ship's crews of the R/V *Thomas G. Thompson* (2009), R/V *Roger Revelle* (2002, 2022), R/V *Oceanus* (2015, 2020), and R/V *Melville* (1999). We gratefully acknowledge support by National Science Foundation grants OCE-0550843 (reservoir model development), OCE 0850931 (2009 cruise), and OCE 2012801 (2022 cruise). U.S. Geological Survey substantially supported the work through U.S. Geological Survey National Earthquake Hazard Reduction Program grants 02HQGR0019, 03HQGR0037, 06HQGR0149, and 07HQGR0064 to C. Goldfinger and grants 02HQGR0043, 03HQGR0006, and 06HQGR0020 to C.H. Nelson. We thank Michaele Kashgarian (Lawrence Livermore AMS Facility) and John Southon (Keck AMS facility, University of California, Irvine) for assistance with the accelerator mass spectrometry (AMS) radiocarbon dates. We thank the many science party members, Oregon State University Marine Geology Repository staff members Maziet Cheseby, Val Stanley, and Cara Fritz, computed tomography (CT) technician Jason Wiest, and other colleagues that helped at sea and with laboratory work, including Amy Garrett, Danielle Verdugo, Ashley Hatfield, Handoko Wibowo, Morgan Erhardt, Robert Hairston-Porter, Nancy Taylor, Joel Gutiérrez, Rachel Hausmann, and coring technicians Chris Moser, Pete Kalk, Paul Walczak, and David Langner. We thank two anonymous reviewers for thoughtful and detailed comments that improved the manuscript significantly. This work is dedicated to Rheannon Hill.

REFERENCES CITED

Abdeldayem, A.L., Ikehara, K., and Yamazaki, T., 2004, Flow path of the 1993 Hokkaido-Nansei-oki earthquake seismoturbidite, southern margin of the Japan Sea north basin, inferred from anisotropy of magnetic susceptibility: Geophysical Journal International, v. 157, p. 15–24, https://doi.org/10.1111/j.1365-246X.2004.02210.x.

Adams, J., 1990, Paleoseismicity of the Cascadia subduction zone: Evidence from turbidites off the Oregon-Washington margin: Tectonics, v. 9, no. 4, p. 569–583, https://doi.org/10.1029/TC009i004p00569.

Aksu, A.E., Yaşar, D., and Mudie, P.J., 1995, Origin of late glacial–Holocene hemipelagic sediments in the Aegean Sea: Clay mineralogy and carbonate cementation: Marine Geology, v. 123, no. 1–2, p. 33–59, https://doi.org/10.1016/0025-3227(95)80003-T.

Arai, K., Naruse, H., Miura, R., Kawamura, K., Hino, R., Ito, Y., Inazu, D., Yokokawa, M., Izumi, N., Murayama, M., and Kasaya, T., 2013, Tsunami-generated turbidity current of the 2011 Tohoku-Oki earthquake: Geology, v. 41, p. 1195–1198, https://doi.org/10.1130/G34777.1.

Atwater, B.F., 1987, Evidence for great Holocene earthquakes along the outer coast of Washington State: Science, v. 236, p. 942–944, https://doi.org/10.1126/science.236.4804.942.

Atwater, B.F., 1992, Geologic evidence for earthquakes during the past 2000 years along the Copalis River, southern coastal Washington: Journal of Geophysical Research: Solid Earth, v. 97, p. 1901–1919, https://doi.org/10.1029/91JB02346.

Atwater, B.F., Stuiver, M., and Yamaguchi, D.K., 1991, Radiocarbon test of earthquake magnitude at the Cascadia subduction zone: Nature, v. 353, no. 6340, p. 156–158, https://doi.org/10.1038/353156a0.

Baas, J.H., van Dam, R.L., and Storms, J.E.A., 2000, Duration of deposition from decelerating high-density turbidity currents: Sedimentary Geology, v. 136, no. 1–2, p. 71–88, https://doi.org/10.1016/S0037-0738(00)00088-9.

Baldwin, J.N., 1996, Paleoseismic Investigation of the San Andreas Fault on the North Coast Segment, near Manchester, California [M.S. thesis]: San Jose, California, USA, San Jose State University, 127 p.

Baldwin, J.N., Prentice, C., Sundermann, S., Thompson, S., and Wetenkamp, J., 2008, Earthquake Record of the Peninsula Segment of the San Andreas Fault, Portola Valley, California: Collaborative Research with William Lettis & Associates, Inc. and U.S. Geological Survey: U.S. Geological Survey Final Technical Report 05HQGR0073, 41 p.

Beeson, J.W., Johnson, S.Y., and Goldfinger, C., 2017, The transtensional offshore portion of the northern San Andreas fault: Fault zone geometry, late Pleistocene to Holocene sediment deposition, shallow deformation patterns, and asymmetric basin growth: Geosphere, v. 13, p. 1173–1206, https://doi.org/10.1130/GES01367.1.

Bell, J.W., Caskey, S.J., Ramelli, A.R., and Guerrieri, L., 2004, Pattern and rates of faulting in the central Nevada seismic belt, and paleoseismic evidence for prior belt-like behavior: Bulletin of the Seismological Society of America, v. 94, no. 4, p. 1229–1254, https://doi.org/10.1785/012003226.

Bendick, R., and Bilham, R., 2017, Do weak global stresses synchronize earthquakes?: Geophysical Research Letters, v. 44, no. 16, p. 8320–8327, https://doi.org/10.1002/2017GL074934.

Bjornstad, B.N., 2014, Ice-rafted erratics and bergmounds from Pleistocene outburst floods, Rattlesnake Mountain, Washington, USA: Quaternary Science Journal, v. 63, no. 1, p. 44–59, https://doi.org/10.3285/eg.63.1.03.

Black, B., 2014, Stratigraphic Correlation of Seismoturbidites and the Integration of Sediment Cores with 3.5 kHz Chirp Subbottom Data in Southern Cascadia [M.S. thesis]: Corvallis, Oregon, USA, Oregon State University, 211 p.

Black, B.A., Pearl, J.K., Pearson, C.L., Pringle, P.T., Frank, D.C., Page, M.T., Buckley, B.M., Cook, E.R., Harley, G.L., King, K.J., Hughes, J.F., Reynolds, D.J., and Sherrod, B.L., 2023, A multifault earthquake threat for the Seattle metropolitan region revealed by mass tree mortality: Science Advances, v. 9, no. 39, https://doi.org/10.1126/sciadv.adh4973.

Bouma, A.H., 1962, Sedimentology of Some Flysch Deposits: A Graphic Approach to Facies Interpretation: Amsterdam, Netherlands, Elsevier, 168 p.

Brocher, T.M., 2019, Was the 23 November 1873 California-Oregon border earthquake an inslab earthquake?: Seismological Research Letters, v. 90, no. 2B, p. 1060.

Bronk Ramsey, C., 2021, OxCal calibration software v. 4.4, https://c14.arch.ox.ac.uk/oxcal.html (accessed July 2025).

Brothers, D.S., Sherrod, B.L., Singleton, D.M., Padgett, J.S., Hill, J.C., Ritchie, A.C., Kluesner, J.W., and Dartnell, P., 2024, Post-glacial stratigraphy and late Holocene record of great Cascadia earthquakes in Ozette Lake, Washington, USA: Geosphere, v. 20, p. 1315–1346, https://doi.org/10.1130/GES02713.1.

Burger, R.L., Fulthorpe, C.S., Austin, J.A., and Gulick, S.P.S., 2002, Lower Pleistocene to present structural deformation and sequence stratigraphy of the continental shelf, offshore Eel River Basin, northern California: Marine Geology, v. 185, no. 3–4, p. 249–281, https://doi.org/10.1016/S0025-3227(02)00196-2.

Carbotte, S.M., Boston, B., Han, S., Shuck, B., Beeson, J., Canales, J.P., Tobin, H., Miller, N., Nedimovic, M., Tréhu, A., Lee, M., Lucas, M.C., Jian, H., Jiang, D., Moser, L., Anderson, C., Judd, D., Fernandez, J., Campbell, C., Goswami, A., and Gahlawat, R., 2024, Subducting plate structure and megathrust morphology from deep seismic imaging linked to earthquake rupture segmentation at Cascadia: Science Advances, v. 10, no. 23, https://doi.org/10.1126/sciadv.adl3198.

Carroll, A.L., Philibosian, B., Sillett, S.C., Antoine, M.E., and Kozaci, Ö., 2025, Dendroseismological investigation of redwood trees along the north coast section of the San Andreas fault: Quaternary Science Advances, v. 18, https://doi.org/10.1016/j.qsa.2025.100283.

Carver, G.A., 2000, Paleoseismic geology of the southern part of the Cascadia subduction zone, *in* Penrose Conference "Great Cascadia Earthquake Tricentennial" Program Summary and Abstracts: Seaside, Oregon, USA, Oregon Department of Geology and Mineral Industries, p. 38–39.

Carver, G.A., and Plafker, G., 1999, Cascadia subduction zone segmentation in the Mendocino triple junction region: Seismological Research Letters, v. 70, no. 2, p. 245–246.

Chaytor, J.D., Goldfinger, C., Dziak, R.P., and Fox, C.G., 2004, Active deformation of the Gorda plate: Constraining deformation models with new geophysical data: Geology, v. 32, p. 353–356, https://doi.org/10.1130/G20178.2.

Cisternas, M., Atwater, B.F., Torrejon, F., Sawai, Y., Machuca, G., Lagos, M., Eipert, A., Youlton, C., Salgado, I., Kamataki, T., Shishikura, M., Rajendran, C.P., Malik, J., and Husni, M., 2005, Predecessors of the giant 1960 Chile earthquake: Nature, v. 437, p. 404–407, https://doi.org/10.1038/nature03943.

Clarke, S.H., Jr., and Carver, G.A., 1992, Late Holocene tectonics and paleoseismicity, southern Cascadia subduction zone: Science, v. 255, p. 188–192, https://doi.org/10.1126/science.255.5041.188.

DeMets, C., Gordon, R.G., and Argus, D.F., 2010, Geologically current plate motions: Geophysical Journal International, v. 181, p. 1–80, https://doi.org/10.1111/j.1365-246X.2009.04491.x.

Dengler, L., Carver, G., and McPherson, R., 1992, Sources of North coast seismicity: California Geology, v. 45, p. 40–53.

Dickinson, W.R., and Snyder, W.S., 1979, The geometry of the triple junctions related to San Andreas transform: Journal of Geophysical Research: Solid Earth, v. 84, p. 561–572, https://doi.org/10.1029/JB084iB02p00561.

Donkin, R.A., 1961, The contribution of the Franciscan missions to the settlement of Alta California colonization 1769–1823: Revista de Historia de América, v. 52, p. 373–393, http://www.jstor.org/stable/20138450.

Egan, J., Staff, R., and Blackford, J., 2015, A high-precision age estimate of the Holocene Plinian eruption of Mount Mazama, Oregon, USA: The Holocene, v. 25, no. 7, p. 1054–1067, https://doi.org/10.1177/0959683615576230.

Enkin, R.J., Dallimore, A., Baker, J., Southon, J.R., and Ivanochko, T., 2013, A new high-resolution radiocarbon Bayesian age-model of the Holocene and late Pleistocene from core MD02–2494 and others, Effingham Inlet, British Columbia, Canada, with an application to the paleoseismic event chronology of the Cascadia subduction zone: Canadian Journal of Earth Sciences, v. 50, no. 7, p. 746–760, https://doi.org/10.1139/cjes-2012-0150.

Fukuma, K., 1998, Origin and applications of whole-core magnetic susceptibility of sediments and volcanic rocks from Leg 152, *in* Saunders, A.D., Larsen, H.C., and Wise, S.W., Jr., eds., Proceedings of the Ocean Drilling Program Scientific Results Volume 152: College Station, Texas, Ocean Drilling Program, p. 271–280, https://doi.org/10.2973/odp.proc.sr.152.225.1998.

Fumal, T.E., 2012, Timing of large earthquakes during the past 500 years along the Santa Cruz Mountains segment of the San Andreas fault at Mill Canyon, near Watsonville, California: Bulletin of the Seismological Society of America, v. 102, no. 3, p. 1099–1119, https://doi.org/10.1785/0120110161.

Garrison-Laney, C.E., 1998, Diatom Evidence for Tsunami Inundation from Lagoon Creek, A Coastal Freshwater Pond, Del Norte County, California [M.S. thesis]: Arcata, California, USA, Humboldt State University, 106 p.

Ge, Z., Nemec, W., Vellinga, A.J., and Gawthorpe, R.L., 2022, How is a turbidite actually deposited?: Science Advances, v. 8, no. 3, https://doi.org/10.1126/sciadv.abl9124.

Goldfinger, C., 2011, Possible Turbidite Record of Earthquake Source Characteristics: A Small-Scale Test: U.S. Geological Survey, National Earthquake Hazards Reduction Program (NEHRP) Final Technical Report 07HQGR0064, 18 p.

Goldfinger, C., 2017, Cascadia Ground Motions: A Paleoseismic/Ground Motion Transect Across the Cascadia Forearc in the Vicinity of Seattle, WA: U.S. Geological Survey, National Earthquake Hazards Reduction Program (NEHRP) Final Technical Report G13AP00066, 113 p.

Goldfinger, C., 2021, Paleoseismic Record of Peninsula Segment Earthquakes on the San Andreas Fault near San Francisco, CA, and Possible NSAF Linkage to Cascadia: U.S. Geological Survey National Earthquake Hazards Reduction Program (NEHRP) Final Technical Report G18AP00058, 133 p.

Goldfinger, C., Kulm, L.D., Yeats, R.S., Appelgate, B., MacKay, M., and Moore, G.F., 1992, Transverse structural trends along the Oregon convergent margin: Implications for Cascadia earthquake potential: Geology, v. 20, p. 141–144, https://doi.org/10.1130/0091-7613(1992)020<0141:TSTATO>2.3.CO;2.

Goldfinger, C., Kulm, L.D., Yeats, R.S., Appelgate, B., MacKay, M., and Cochrane, G.R., 1996, Active strike-slip faulting and folding of the Cascadia plate boundary and forearc in central and northern Oregon, *in* Rogers, A.M., Walsh, T.J., Kockelman, W.J., and Priest, G., eds., Assessing and Reducing Earthquake Hazards in the Pacific Northwest: U.S. Geological Survey Professional Paper 1560, p. 223–256, https://pubsdata.usgs.gov/pubs/pp/p1560/.

Goldfinger, C., Kulm, L.D., Yeats, R.S., McNeill, L.C., and Hummon, C., 1997, Oblique strike-slip faulting of the central Cascadia submarine forearc: Journal of Geophysical Research: Solid Earth, v. 102, p. 8217–8243, https://doi.org/10.1029/96JB02655.

Goldfinger, C., Nelson, C.H., Johnson, J.E., Erickson, D., Winkler, M., Kalk, P., Pastor, J., Camarero, A., Morri, C., Dunhill, G., Ramos, L., Raab, A., Pisias, N., Pourmanoutscheri, M., van Rooij, D., Amy, L., and Liu, C.-C., 2003, Holocene earthquake records from the Cascadia subduction zone and northern San Andreas fault based on precise dating of offshore turbidites: Annual Review of Earth and Planetary Sciences, v. 31, p. 555–577, https://doi.org/10.1146/annurev.earth.31.100901.141246.

Goldfinger, C., Morey, A.E., Nelson, C.H., Gutiérrez-Pastor, J., Johnson, J.E., Karabanov, E., Chaytor, J., and Ericsson, A., 2007, Rupture lengths and temporal history of significant earthquakes on the offshore and north coast segments of the northern San Andreas fault based on turbidite stratigraphy: Earth and Planetary Science Letters, v. 254, p. 9–27, https://doi.org/10.1016/j.epsl.2006.11.017.

Goldfinger, C., Grijalva, K., Burgmann, R., Morey, A.E., Johnson, J.E., Nelson, C.H., Gutiérrez-Pastor, J., Karabanov, E., Chaytor, J.D., Patton, J., and Gracia, E., 2008, Late Holocene rupture of the northern San Andreas fault and possible stress linkage to the Cascadia subduction zone: Bulletin of the Seismological Society of America, v. 98, p. 861–889, https://doi.org/10.1785/0120060411.

Goldfinger, C., Nelson, C.H., Morey, A., Johnson, J.E., Gutiérrez-Pastor, J., Eriksson, A.T., Karabanov, E., Patton, J., Gracia, E., Enkin, R., Dallimore, A., Dunhill, G., and Vallier, T., 2012, Turbidite Event History: Methods and Implications for Holocene Paleoseismicity of the Cascadia Subduction Zone: U.S. Geological Survey Professional Paper 1661-F, 184 p., http://pubs.usgs.gov/pp/pp1661f/.

Goldfinger, C., Ikeda, Y., Yeats, R.S., and Ren, J., 2013a, Superquakes and supercycles: Seismological Research Letters, v. 84, no. 1, p. 24–32, https://doi.org/10.1785/0220110135.

Goldfinger, C., Morey, A.E., Black, B., Beeson, J., Nelson, C.H., and Patton, J., 2013b, Spatially-limited mud turbidites on the Cascadia margin: Segmented earthquake ruptures?: Natural Hazards and Earth System Sciences, v. 13, no. 8, p. 2109–2146, https://doi.org/10.5194/nhess-13-2109-2013.

Goldfinger, C., Galer, S., Beeson, J., Hamilton, T.S., Black, B., Romsos, C., Patton, J., Nelson, C.H., Hausmann, R., and Morey, A., 2017, The importance of site selection, sediment supply, and hydrodynamics: A case study of submarine paleoseismology on the northern Cascadia margin, Washington USA: Marine Geology, v. 384, p. 4–46, https://doi.org/10.1016/j.margeo.2016.06.008.

Goldfinger, C., Beeson, J.W., Romsos, C., and Patton, J.R., 2023, Neotectonic Map of the Cascadia Margin: Oregon Department of Geology and Mineral Industries Open-File Report O-23–05, 24 p., https://www.oregon.gov/dogami/pubs/pages/ofr/p-o-23-05.aspx.

Gomberg, J., Beeler, N.M., Blanpied, M.L., and Bodin, P., 1998, Earthquake triggering by transient and static deformations: Journal of Geophysical Research: Solid Earth, v. 103, no. B10, p. 24,411–24,426, https://doi.org/10.1029/98JB01125.

Gràcia, E., Vizcaino, A., Escutia, C., Asiolic, A., Garcia-Orellana, J., Pallàse, R., Lebreiro, S., and Goldfinger, C., 2010, Holocene earthquake record offshore Portugal (SW Iberia): Applying turbidite paleoseismology in a slow-convergence margin: Quaternary Science Reviews, v. 29, no. 9–10, p. 1156–1172, https://doi.org/10.1016/j.quascirev.2010.01.010.

Griggs, G.H., and Kulm, L.D., 1970, Sedimentation in the Cascadia deep sea channel: Geological Society of America Bulletin, v. 81, p. 1361–1384, https://doi.org/10.1130/0016-7606(1970)81[1361:SICDC]2.0.CO;2.

Gutiérrez, J., 2020, Exploring Volcano-Tectonic Connections in Cascadia—Temporal Linkages between Tephra Deposition and Megathrust Earthquakes [M.S. thesis]: Corvallis, Oregon, USA, Oregon State University, 188 p.

Gutiérrez-Pastor, J., Nelson, C.H., Goldfinger, C., and Escutia, C., 2013, Sedimentology of seismoturbidites off the Cascadia and northern California active tectonic continental margins, northwest Pacific Ocean: Marine Geology, v. 336, p. 99–119, https://doi.org/10.1016/j.margeo.2012.11.010.

Haak, D., Page, C.-E., and Deserno, T.M., 2016, A survey of DICOM viewer software to integrate clinical research and medical imaging: Journal of Digital Imaging, v. 29, no. 2, p. 206–215, https://doi.org/10.1007/s10278-015-9833-1.

Hall, N.T., and Niemi, T.M., 2008, The 1906 earthquake fault rupture and paleoseismic investigation of the northern San Andreas fault at the Dogtown site, Marin County, California: Bulletin of the Seismological Society of America, v. 98, no. 5, p. 2191–2208, https://doi.org/10.1785/0120060414.

Hamilton, T.S., Enkin, R.J., Riedel, M., Rogers, G.C., Pohlman, J.W., and Benway, H.M., 2015, Slipstream: An early Holocene slump and turbidite record from the frontal ridge of the Cascadia accretionary wedge off western Canada and paleoseismic implications: Canadian Journal of Earth Sciences, v. 52, no. 6, p. 405–430, https://doi.org/10.1139/cjes-2014-0131.

Heaton, T.J., Köhler, P., Butzin, M., Bard, E., Reimer, R.W., Austin, W.E.N., Bronk Ramsey, C., Grootes, P.M., Hughen, K.A., Kromer, B., Reimer, P.J., Adkins, J., Burke, A., Cook, M.S., Olsen, J., and Skinner, L.C., 2020, Marine20—The marine radiocarbon age calibration curve (0–55,000 cal BP): Radiocarbon, v. 62, no. 4, p. 779–820, https://doi.org/10.1017/RDC.2020.68.

Henkart, P., 2003, SIOSEIS Software: La Jolla, California, USA, Scripps Institute of Oceanography, http://sioseis.ucsd.edu (accessed June 2024).

Henry, P., Özeren, S., Yakupoğlu, N., Çakır, Z., de Saint-Léger, E., Desprez de Gésincourt, O., Tengberg, A., Chevalier, C., Papoutsellis, C.E., Postacioglu, N., Doğan, U., Karabulut, H., Uçarkuş, G., and Çağatay, M.N., 2021, Slow build-up of turbidity currents triggered by a moderate earthquake in the Sea of Marmara, *in* 22nd European Geosciences Union General Assembly Programme (held online 4–8 May 2020): European Geosciences Union, abstract 10289, https://doi.org/10.5194/egusphere-egu2020-10289.

Hill, J.C., Watt, J.T., Brothers, D.S., and Kleusner, J.W., 2020, Submarine canyons, slope failures and mass transport processes in southern Cascadia, *in* Georgiopoulou, A., et al., Subaqueous Mass Movements and their Consequences: Advances in Process Understanding, Monitoring and Hazard Assessments: Geological Society, London, Special Publication 500, p. 453–475, https://doi.org/10.1144/SP500-2019-169.

Ho, V.L., Dorrell, R.M., Keevil, G.M., Burns, A.D., and McCaffrey, W.D., 2018, Pulse propagation in turbidity currents: Sedimentology, v. 65, no. 2, p. 620–637, https://doi.org/10.1111/sed.12397.

Ho, V.L., Dorrell, R.M., Keevil, G.M., Thomas, R.E., Burns, A.D., Baas, J.H., and McCaffrey, W.D., 2019, Dynamics and deposition of sediment-bearing multi-pulsed flows and geological implication: Journal of Sedimentary Research, v. 89, no. 11, p. 1127–1139, https://doi.org/10.2110/jsr.2019.62.

Howarth, J.D., et al., 2021, Calibrating the marine turbidite palaeoseismometer using the 2016 Kaikōura earthquake: Nature Geoscience, v. 14, p. 161–167, https://doi.org/10.1038/s41561-021-00692-6.

Hua, Q., Barbetti, M., and Rakowski, A.Z., 2013, Atmospheric Radiocarbon for the Period 1950–2010: Radiocarbon, v. 55, no. 4, p. 2059-2072, https://doi.org/10.2458/azu_js_rc.v55i2.16177.

Ikehara, K., Usami, K., and Kanamatsu, T., 2023, How large peak ground acceleration by large earthquakes could generate turbidity currents along the slope of northern Japan Trench: Progress in Earth and Planetary Science, v. 10, no. 1, p. 8, https://doi.org/10.1186/s40645-023-00540-8.

Jacoby, G.C., 1997, Application of tree-ring analysis to paleoseismology: Reviews of Geophysics, v. 35, no. 2, p. 109–124, https://doi.org/10.1029/96RG03526.

Kanamatsu, T., Ikehara, K., and Hsiung, K.-H., 2023, Submarine paleoseismology in the Japan Trench of northeastern Japan: Turbidite stratigraphy and sedimentology using paleomagnetic and rock magnetic analyses: Progress in Earth and Planetary Science, v. 10, no. 1, p. 16, https://doi.org/10.1186/s40645-023-00545-3.

Karlin, R.E., Holmes, M., Abella, S.E.B., and Sylwester, R., 2004, Holocene landslides and a 3500-year record of Pacific Northwest earthquakes from sediments in Lake Washington: Geological Society of America Bulletin, v. 116, p. 94–108, https://doi.org/10.1130/B25158.1.

Kelsey, H.M., and Carver, G.A., 1988, Late Neogene and Quaternary tectonics associated with northward growth of the San Andreas transform fault, northern California: Journal of Geophysical Research: Solid Earth, v. 93, p. 4797–4819, https://doi.org/10.1029/JB093iB05p04797.

Kelsey, H.M., Nelson, A.R., Hemphill-Haley, E., and Witter, R.C., 2005, Tsunami history of an Oregon coastal lake reveals a 4600 yr record of great earthquakes on the Cascadia subduction zone: Geological Society of America Bulletin, v. 117, p. 1009–1032, https://doi.org/10.1130/B25452.1.

Kelson, K., Strieg, A., Koehler, R., and Kang, K.H., 2006, Timing of late Holocene paleoearthquakes on the northern San Andreas fault at the Fort Ross Orchard site, Sonoma County, California: Seismological Research Letters, v. 96, no. 3, p. 1012–1028, https://doi.org/10.1785/0120050123.

Kemnitz, N., Berelson, W.M., Hammond, D.E., Morine, L., Figueroa, M., Lyons, T.W., Scharf, S., Rollins, N., Petsios, E., Lemieux, S., and Treude, T., 2020, Evidence of changes in sedimentation rate and sediment fabric in a low-oxygen setting: Santa Monica Basin, CA: Biogeosciences, v. 17, no. 8, p. 2381–2396, https://doi.org/10.5194/bg-17-2381-2020.

Kioka, A., Schwestermann, T., Moernaut, J., Ikehara, K., Kanamatsu, T., McHugh, C.M., dos Santos Ferreira, C., Wiemer, G., Haghipour, N., Kopf, A.J., Eglinton, T.I., and Strasser, M., 2019, Megathrust earthquake drives drastic organic carbon supply to the Hadal Trench: Scientific Reports, v. 9, no. 1, https://doi.org/10.1038/s41598-019-38834-x.

Kitzberger, T., Veblen, T.T., and Villalba, R., 1995, Climatic and human influences on fire regimes in temperate forests of western North America, *in* Clark, J.S., Cachier, H., Goldammer, J.G., and Stocks, B., eds., Sediment Records of Biomass Burning and Global Change: Berlin, Springer, p. 95–119, https://doi.org/10.1007/978-3-662-05238-9_5.

Kneller, B.C., and McCaffrey, W.D., 2003, The interpretation of vertical sequences in turbidite beds: The influence of longitudinal flow structure: Journal of Sedimentary Research, v. 73, no. 5, p. 706–713, https://doi.org/10.1306/031103730706.

Knudsen, K.L., Witter, R.C., Garrison-Laney, C.E., Baldwin, J.N., Carver, G.A., Grant, L.B., and Lettis, W.R., 2002, Past earthquake-induced rapid subsidence along the northern San Andreas fault: A paleoseismological method for investigating strike-slip faults: Bulletin of the Seismological Society of America, v. 92, p. 2612–2636, https://doi.org/10.1785/0120000613.

Komar, P.D., 1985, The hydraulic interpretation of turbidites from their grain sizes and sedimentary structures: Sedimentology, v. 32, no. 3, p. 395–407, https://doi.org/10.1111/j.1365-3091.1985.tb00519.x.

Ladinsky, T., Kelsey, H., Michalak, M., Witter, R., Sherrod, B., Bold, S., Cashman, S., and Buck, J., 2020, In Southern Cascadia, Do Upper Plate Faults Rupture in Concert with Subduction Zone Earthquakes: A Paleoseismic Investigation of the Little Salmon Fault Zone: U.S. Geological Survey National Earthquake Hazards Reduction Program (NEHRP) Final Technical Report G19AP00046, 39 p.

Lay, T., Given, J.W., and Kanamori, H., 1982, Long-period mechanism of the 8 November 1980 Eureka, California, earthquake: Bulletin of the Seismological Society of America, v. 72, p. 439–456, https://doi.org/10.1785/BSSA0720020439.

Lee, S.E., Talling, P.J., Ernst, G.C.J., and Hogg, A.J., 2002, Occurrence and origin of submarine plunge pools at the base of the US continental slope: Marine Geology, v. 185, p. 363–377, https://doi.org/10.1016/S0025-3227(01)00298-5.

Leithold, E.L., Wegmann, K.W., Bohnenstiehl, D.R., Joyner, C.N., and Pollen, A.F., 2019, Repeated megaturbidite deposition in Lake Crescent, Washington, USA, triggered by Holocene ruptures of the Lake Creek–Boundary Creek fault system: Geological Society of America Bulletin, v. 131, p. 2039–2055, https://doi.org/10.1130/B35076.1.

Lock, J., Kelsey, H., Furlong, K., and Woolace, A., 2006, Late Neogene and Quaternary landscape evolution of the northern California Coast Ranges: Evidence for Mendocino triple junction tectonics: Geological Society of America Bulletin, v. 118, p. 1232–1246, https://doi.org/10.1130/B25885.1.

Løvlie, R., and van Veen, P., 1995, Magnetic susceptibility of a 180 m sediment core: Reliability of incremental sampling and evidence for a relationship between susceptibility and gamma activity, *in* Turner, P., and Turner, A., eds., Palaeomagnetic Applications in Hydrocarbon Exploration and Production: Geological Society, London, Special Publication 98, p. 259–266, https://doi.org/10.1144/GSL.SP.1995.098.01.16.

Lowe, D., 1982, Sediment gravity flows: II. Depositional models with special reference to the deposits of high-density turbidity currents: Journal of Sedimentary Research, v. 52, no. 1, p. 279–297, https://doi.org/10.1306/212F7F31-2B24-11D7-8648000102C1865D.

Mari, J.L., and Coppens, F., 2003, La sismique de puits (Seismic Well Surveying): Paris, Editions Technip, 256 p.

Materna, K., Murray, J.R., Pollitz, F., and Patton, J.R., 2023, Slip deficit rates on southern Cascadia faults resolved with viscoelastic earthquake cycle modeling of geodetic deformation: Bulletin of the Seismological Society of America, v. 113, no. 6, p. 2505–2518, https://doi.org/10.1785/0120230007.

McCaffrey, R., and Goldfinger, C., 1995, Forearc deformation and great subduction earthquakes: Implications for Cascadia offshore earthquake potential: Science, v. 267, no. 5199, p. 856–859, https://doi.org/10.1126/science.267.5199.856.

McCloskey, J., Nalbant, S.S., and Steacy, S., 2005, Earthquake risk from co-seismic stress: Nature, v. 434, no. 7031, https://doi.org/10.1038/434291a.

McCrory, P.A., 2000, Upper plate contraction north of the migrating Mendocino triple junction, northern California: Implications for partitioning of strain: Tectonics, v. 19, no. 6, p. 1144–1160, https://doi.org/10.1029/1999TC001177.

McCubbin, D.G., 1982, Barrier-island and strand-plain facies, *in* Scholle, P.A., and Spearing, D., eds., Sandstone Depositional Environments: American Association of Petroleum Geologists Memoir 31, p. 247–258, https://doi.org/10.1306/M31424C10.

McGuire, J.J., 2008, Seismic cycles and earthquake predictability on East Pacific Rise transform faults: Bulletin of the Seismological Society of America, v. 98, no. 3, p. 1067–1084, https://doi.org/10.1785/0120070154.

McHugh, C.M., Seeber, L., Gulick, S.P.S., Magnani, M.B., Hornbach, M., Steckler, M.S., Wright, V., Leroy, S., Cabiativa-Pico, V., Dasent, J., Kersh, J., Kilburn, R., and James-Williamson, S., 2024, Sedimentary signatures of large earthquakes along the submerged Enriquillo–Plantain Garden transpressional plate boundary, northern Caribbean: Geology, v. 52, p. 769–773, https://doi.org/10.1130/G52258.1.

McKay, C.P., Long, A., and Friedmann, E.I., 1986, Radiocarbon dating of open systems with bomb effect: Journal of Geophysical Research: Solid Earth, v. 91, no. B3, p. 3836–3840, https://doi.org/10.1029/JB091iB03p03836.

Melgar, D., 2021, Was the January 26th, 1700, Cascadia earthquake part of a rupture sequence?: Journal of Geophysical Research: Solid Earth, v. 126, no. 10, https://doi.org/10.1029/2021JB021822.

Meltzner, A.J., Sieh, K., Chiang, H.-W., Shen, C.-C., Suwargadi, B.W., Natawidjaja, D.H., Philibosian, B.E., Briggs, R.W., and Galetzka, J., 2010, Coral evidence for earthquake recurrence and an A.D. 1390–1455 cluster at the south end of the 2004 Aceh–Andaman rupture: Journal of Geophysical Research: Solid Earth, v. 115, no. B10, https://doi.org/10.1029/2010JB007499.

Mitchum, R.M., and Wagoner, J.C., 1991, High-frequency sequences and their stacking patterns: Sequence stratigraphic evidence of high-frequency eustatic cycles: Sedimentary Geology, v. 70, p. 131–160, https://doi.org/10.1016/0037-0738(91)90139-5.

Moernaut, J., Van Daele, M., Strasser, M., Clare, M.A., Heirman, K., Viel, M., Cardenas, J., Kilian, R., de Guevara, B.L., Pino, M., Urrutia, R., and De Batist, M., 2017, Lacustrine turbidites produced by surficial slope sediment remobilization: A mechanism for continuous and sensitive turbidite paleoseismic records: Marine Geology, v. 384, p. 159–176, https://doi.org/10.1016/j.margeo.2015.10.009.

Mofjeld, H.O., Foreman, M.G.G., and Ruffman, A., 1997, West Coast tides during Cascadia subduction zone tsunamis: Geophysical Research Letters, v. 24, no. 17, p. 2215–2218, https://doi.org/10.1029/97GL02060.

Morey, A.E., 2020, Cascadia Earthquakes Disturb Sediment in Small Oregon and California Lakes [Ph.D. dissertation]: Corvallis, Oregon, USA, Oregon State University, 232 p.

Morey, A.E., and Goldfinger, C., 2024, A 2700-year record of Cascadia megathrust and crustal/slab earthquakes from Acorn Woman Lakes, Oregon: Natural Hazards and Earth System Sciences, v. 24, no. 12, p. 4563–4584, https://doi.org/10.5194/nhess-24-4563-2024.

Morey, A.E., Goldfinger, C., Briles, C.E., Gavin, D.G., Colombaroli, D., and Kusler, J.E., 2013, Are great Cascadia earthquakes recorded in the sedimentary records from small forearc lakes?: Natural Hazards and Earth System Sciences, v. 13, no. 10, p. 2441–2463, https://doi.org/10.5194/nhess-13-2441-2013.

Morey, A.E., Shapley, M.D., Gavin, D.G., Nelson, A.R., and Goldfinger, C., 2024, Sedimentary record of historical seismicity in a small, southern Oregon lake: Natural Hazards and Earth System Sciences, v. 24, no. 12, p. 4523–4561, https://doi.org/10.5194/nhess-24-4523-2024.

Mountjoy, J.J., Howarth, J.D., Orpin, A.R., Barnes, P.M., Bowden, D.A., Rowden, A.A., and Kane, T., 2018, Earthquakes drive large-scale submarine canyon development and sediment supply to deep-ocean basins: Science Advances, v. 4, no. 3, https://doi.org/10.1126/sciadv.aar3748.

Mulder, T., Migeon, S., Savoye, B., and Jouanneau, J.M., 2001, Twentieth century floods recorded in the deep Mediterranean sediments: Geology, v. 29, p. 1011–1014, https://doi.org/10.1130/0091-7613(2001)029<1011:TCFRIT>2.0.CO;2.

Nakajima, T., and Kanai, Y., 2000, Sedimentary features of seismoturbidites triggered by the 1983 and older historical earthquakes in the eastern margin of the Japan Sea: Sedimentary Geology, v. 135, p. 1–19, https://doi.org/10.1016/S0037-0738(00)00059-2.

Nelson, A.R., Christopher, B., DuRoss, C.B., Robert, C., Witter, R.C., Harvey, M., Kelsey, H.M., Simon, E., Engelhart, S.E., Shannon, A., Mahan, S.A., Harrison, J., Gray, H.J., Andrea, D., Hawkes, A.D., Benjamin, P., Horton, B.P., Jason, S., and Padgett, J.S., 2021, A maximum rupture model for the central and southern Cascadia subduction zone—Reassessing ages for coastal evidence of megathrust earthquakes and tsunamis: Quaternary Science Reviews, v. 261, https://doi.org/10.1016/j.quascirev.2021.106922.

Nelson, C.H., 1976, Late Pleistocene and Holocene depositional trends, processes and history of Astoria deep-sea fan, northeast Pacific: Marine Geology, v. 20, p. 129–173, https://doi.org/10.1016/0025-3227(76)90083-9.

Noda, A., Tuzino, T., Kanai, Y., Furukawa, R., and Uchida, J., 2008, Paleoseismicity along the southern Kuril Trench deduced from submarine-fan turbidites: Marine Geology, v. 254, no. 1–2, p. 73–90, https://doi.org/10.1016/j.margeo.2008.05.015.

Null, J., and Hulbert, J., 2007, California washed away: The Great Flood of 1862: Weatherwise, v. 60, no. 1, p. 26–30, https://doi.org/10.3200/WEWI.60.1.26-30.

Oguri, K., Kawamura, K., Sakaguchi, A., Toyofuku, T., Kasaya, T., Murayama, M., Fujikura, K., Glud, R.N., and Kitazato, H., 2013, Hadal disturbance in the Japan Trench induced by the 2011 Tohoku-Oki earthquake: Scientific Reports, v. 3, no. 1, https://doi.org/10.1038/srep01915.

Okutsu, N., Ashi, J., Yamaguchi, A., Irino, T., Ikehara, K., Kanamatsu, T., Suganuma, Y., and Murayama, M., 2019, Evidence for surface sediment remobilization by earthquakes in the Nankai forearc region from sedimentary records, *in* Lintern, D.G., et al., eds., Subaqueous Mass Movements and their Consequences: Assessing Geohazards, Environmental Implications and Economic Significance of Subaqueous Landslides: Geological Society, London, Special Publication 477, p. 37–45, https://doi.org/10.1144/SP477.22.

O'Malley, R.T., Mondal, D., Goldfinger, C., and Behrenfeld, M.J., 2018, Evidence of systematic triggering at teleseismic distances following large earthquakes: Scientific Reports, v. 8, no. 1, 11611, https://doi.org/10.1038/s41598-018-30019-2.

Oppenheimer, D., et al., 1993, The Cape Mendocino, California, earthquakes of April 1992: Subduction at the triple junction: Science, v. 261, p. 433–438, https://doi.org/10.1126/science.261.5120.433.

Padgett, J.S., Engelhart, S.E., Kelsey, H.M., Witter, R.C., Cahill, N., and Hemphill-Haley, E., 2021, Timing and amount of southern Cascadia earthquake subsidence over the past 1,700 years at Northern Humboldt Bay, California: Geological Society of America Bulletin, v. 133, p. 2137–2156, https://doi.org/10.1130/B35701.1.

Parker, G., Fukushima, Y., and Pantin, H.M., 1986, Self-accelerating turbidity currents: Journal of Fluid Mechanics, v. 171, p. 145–181, https://doi.org/10.1017/S0022112086001404.

Parsons, T., Stein, R.S., Simpson, R.W., and Reasenberg, P.A., 1999, Stress sensitivity of fault seismicity: A comparison between limited-offset oblique and major strike-slip faults: Journal of Geophysical Research: Solid Earth, v. 104, no. B9, p. 20,183–20,202, https://doi.org/10.1029/1999JB900056.

Patton, J.R., et al., 2015, A 6600-year earthquake history in the region of the 2004 Sumatra-Andaman subduction zone earthquake: Geosphere, v. 11, p. 2067–2129, https://doi.org/10.1130/GES01066.1.

Paull, C.K., McGann, M., Sumner, E.J., Barnes, P.M., Lundsten, E.M., Anderson, K., Gwiazda, R., Edwards, B., and Caress, D.W., 2014, Sub-decadal turbidite frequency during the early Holocene: Eel Fan, offshore northern California: Geology, v. 42, p. 855–858, https://doi.org/10.1130/G35768.1.

Philibosian, B., Sieh, K., Avouac, J.-P., Natawidjaja, D.H., Chiang, H.-W., Wu, C.-C., Shen, C.-C., Daryono, M.R., Perfettini, H., Suwargadi, B.W., Lu, Y., and Wang, X., 2017, Earthquake supercycles on the Mentawai segment of the Sunda megathrust in the seventeenth century and earlier: Journal of Geophysical Research: Solid Earth, v. 122, no. 1, p. 642–676, https://doi.org/10.1002/2016JB013560.

Pickering, K., and Hiscott, R., 2016, Deep Marine Systems: Processes, Deposits, Environments, Tectonics and Sedimentation: Washington, D.C., Wiley & American Geophysical Union, 688 p.

Piper, D.J.W., Shor, A.N., and Hughes Clarke, J.E., 1988, The 1929 "Grand Banks" earthquake, slump, and turbidity current, *in* Clifton, H.E., ed., Sedimentologic Consequences of Convulsive Geologic Events: Geological Society of America Special Paper 229, p. 77–92, https://doi.org/10.1130/SPE229-p77.

Prentice, C.S., 1989, Earthquake Geology of the Northern San Andreas Fault near Point Arena, California [Ph.D. dissertation]: Pasadena, California, USA, California Institute of Technology, 252 p.

Prentice, C.S., Merritts, D.J., Beutner, E.C., Bodin, P., Schill, A., and Muller, J.R., 1999, Northern San Andreas fault near Shelter Cove, California: Geological Society of America Bulletin, v. 111, p. 512–523, https://doi.org/10.1130/0016-7606(1999)111<0512:NSAFNS>2.3.CO;2.

Prentice, C.S., Zachariasen, J.A., Kozaci, O., Clahan, K., Sickler, R.R., Rosa, C.M., Hassett, W., Feigelson, L., Haproff, P.J., DeLong, S., Perkins, A., Brooks, B.A., Delano, J., and Baldwin, J.N., 2013, Paleoseismic studies of the peninsula San Andreas fault near Crystal Springs Reservoir, Woodside, California: San Francisco, California, USA, American Geophysical Union, Fall Meeting, abstract T43A–2620.

Prentice, C.S., Sickler, R.R., Clahan, K., Pickering, A., and DeLong, S., 2016, Preliminary results from paleoseismic excavations across the San Andreas fault at the Scarp Creek site on the San Francisco Peninsula, California: San Francisco, California, USA, American Geophysical Union, Fall Meeting, abstract T41B–2922.

Priest, G.R., Zhang, Y., Witter, R.C., Wang, K., Goldfinger, C., and Stimely, L., 2014, Tsunami impact to Washington and northern Oregon from segment ruptures on the southern Cascadia subduction zone: Natural Hazards, v. 72, p. 849–870, https://doi.org/10.1007/s11069-014-1041-7.

Puig, P., Ogston, A.S., Mullenbach, B.L., Nittrouer, C.A., and Sternberg, R.W., 2003, Shelf-to-canyon sediment-transport processes on the Eel continental margin (northern California): Marine Geology, v. 193, p. 129–149, https://doi.org/10.1016/S0025-3227(02)00641-2.

Ralph, F.M., and Dettinger, M.D., 2011, Storms, floods, and the science of atmospheric rivers: Eos (Washington, D.C.), v. 92, no. 32, p. 265–266, https://doi.org/10.1029/2011EO320001.

Ramsey, C.B., 2001, Development of the radiocarbon program OxCal: Radiocarbon, v. 43, p. 355–363, https://doi.org/10.1017/S0033822200038212.

Ramsey, C.B., 2008, Deposition models for chronological records: Quaternary Science Reviews, v. 27, no. 1–2, p. 42–60, https://doi.org/10.1016/j.quascirev.2007.01.019.

Ramsey, C.B., 2009, Bayesian analysis of radiocarbon dates: Radiocarbon, v. 51, no. 1, p. 337–360, https://doi.org/10.1017/S0033822200033865.

Ramsey, C.B., Dee, M., Lee, S., Nakagawa, T., and Staff, R., 2010, Developments in the calibration and modelling of radiocarbon dates: Radiocarbon, v. 52, no. 3, p. 953–961, https://doi.org/10.1017/S0033822200046063.

Rao, P.S., Ramaswamy, V., and Thwin, S., 2005, Sediment texture, distribution and transport on the Ayeyarwady continental shelf, Andaman Sea: Marine Geology, v. 216, no. 4, p. 239–247, https://doi.org/10.1016/j.margeo.2005.02.016.

Reimer, P.J., Brown, T.J., and Reimer, R.W., 2004, Reporting and calibration of post-bomb ^{14}C data: Radiocarbon, v. 46, p. 1299–1304, https://doi.org/10.1017/S0033822200033154.

Reimer, P.J., et al., 2020, The IntCal20 Northern Hemisphere Radiocarbon Age Calibration Curve (0–55 cal kBP): Radiocarbon, v. 62, no. 4, p. 725-757, https://doi.org/10.1017/RDC.2020.41.

Riedel, M., and Conway, K.W., 2015, Paleoseismicity derived from piston-coring methods, Explorer and Juan de Fuca plate systems, British Columbia, *in* Current Research (Online), 2015-10: Geological Survey of Canada, Natural Resources Canada, 15 p., https://doi.org/10.4095/297317.

Rockwell, T.K., Lindvall, S., Herzberg, M., Murbach, D., Dawson, T., and Berger, G., 2000, Paleoseismology of the Johnson Valley, Kickapoo, and Homestead Valley faults: Clustering of earthquakes in the Eastern California shear zone: Bulletin of the Seismological Society of America, v. 90, no. 5, p. 1200–1236, https://doi.org/10.1785/0119990023.

Rong, Y., Jackson, D.D., Magistrale, H., and Goldfinger, C., 2014, Magnitude limits of subduction zone earthquakes: Bulletin of the Seismological Society of America, v. 104, no. 5, p. 2359–2377, https://doi.org/10.1785/0120130287.

Rosset, A., Spadola, L., and Ratib, O., 2004, OsiriX: An open-source software for navigating in multidimensional DICOM images: Journal of Digital Imaging, v. 17, no. 3, p. 205–216, https://doi.org/10.1007/s10278-004-1014-6.

Satake, K., Wang, K., and Atwater, B.F., 2003, Fault slip and seismic moment of the 1700 Cascadia earthquake inferred from Japanese tsunami descriptions: Journal of Geophysical Research: Solid Earth, v. 108, no. 11, https://doi.org/10.1029/2003JB002521.

Scholz, C.H., 2010, Large earthquake triggering, clustering, and the synchronization of faults: Bulletin of the Seismological Society of America, v. 100, no. 3, p. 901–909, https://doi.org/10.1785/0120090309.

Schwartz, D.P., Lienkaemper, J.J., Hecker, S., Kelson, K.I., Fumal, T.E., Baldwin, J.N., Seitz, G.G., and Niemi, T.M., 2014, The earthquake cycle in the San Francisco Bay region: A.D. 1600–2012: Bulletin of the Seismological Society of America, v. 104, no. 3, p. 1299–1328, https://doi.org/10.1785/0120120322.

Seibert, C., Feuillet, N., Ratzov, G., Beck, C., Morena, P., Johannes, L., Ducassou, E., Cattaneo, A., Goldfinger, C., Moreno, E., and Bieber, A., 2024, Sedimentary records in the Lesser Antilles fore-arc basins provide evidence of large late Quaternary megathrust earthquakes: Geochemistry, Geophysics, Geosystems, v. 25, no. 2, https://doi.org/10.1029/2023GC011152.

Seitz, G.G., 2018, Filling a Paleoseismic Data Gap on the San Andreas Fault: Northern Santa Cruz Mountains–San Francisco Peninsula: U.S. Geological Survey Final Technical Report G11AP20130, 36 p., https://earthquake.usgs.gov/cfusion/external_grants/reports/G11AP20130.pdf.

Sequeiros, O.E., Mosquera, R., and Pedocchi, F., 2018, Internal structure of a self-accelerating turbidity current: Journal of Geophysical Research: Oceans, v. 123, no. 9, p. 6260–6276, https://doi.org/10.1029/2018JC014061.

Sieh, K., Natawidjaja, D.H., Meltzner, A.J., Shen, C.-C., Cheng, H., Li, K.-S., Suwargadi, B.W., Galetzka, J., Philibosian, B., and Edwards, R.L., 2008, Earthquake supercycles inferred from sea-level changes recorded in the corals of West Sumatra: Science, v. 322, no. 5908, p. 1674–1678, https://doi.org/10.1126/science.1163589.

Silver, E.A., 1971, Tectonics of the Mendocino triple junction: Geological Society of America Bulletin, v. 82, p. 2965–2978, https://doi.org/10.1130/0016-7606(1971)82[2965:TOTMTJ]2.0.CO;2.

Small, D.T., Melgar, D., La Selle, S., and Meigs, A., 2025, Combining multisite tsunami and deformation modeling to constrain slip distributions for the 1700 C.E. Cascadia earthquake: Bulletin of the Seismological Society of America, v. 115, no. 2, p. 431–451, https://doi.org/10.1785/0120240218.

Song, S.G., Beroza, G.C., and Segall, P., 2008, A unified source model for the 1906 San Francisco earthquake: Bulletin of the Seismological Society of America, v. 98, no. 2, p. 823–831, https://doi.org/10.1785/0120060402.

Staisch, L.M., et al., 2024, Compiled Onshore and Offshore Paleoseismic Data along the Cascadia Subduction Zone: U.S. Geological Survey data release, https://doi.org/10.5066/P13OJQYW.

Stein, R.S., 1999, The role of stress transfer in earthquake occurrence: Nature, v. 402, no. 6762, p. 605–609, https://doi.org/10.1038/45144.

Sternberg, R.W., 1986, Transport and accumulation of river-derived sediment on the Washington continental shelf: Journal of the Geological Society, v. 143, p. 945–956, https://doi.org/10.1144/gsjgs.143.6.0945.

Stoffel, M., and Bollschweiler, M., 2008, Tree-ring analysis in natural hazards research—An overview: Natural Hazards and Earth System Sciences, v. 8, no. 2, p. 187–202, https://doi.org/10.5194/nhess-8-187-2008.

St-Onge, G., Mulder, T., Piper, D.J.W., Hillaire-Marcel, C., and Stoner, J.S., 2004, Earthquake and flood-induced turbidites in the Saguenay Fjord (Québec): A Holocene paleoseismicity record: Quaternary Science Reviews, v. 23, p. 283–294, https://doi.org/10.1016/j.quascirev.2003.03.001.

Stover, C.W., and Coffman, J.L., 1993, Seismicity of the United States, 1568–1989 (Revised): U.S. Geological Survey Professional Paper 1527, 417 p., https://doi.org/10.3133/pp1527.

Stow, D., and Smillie, Z., 2020, Distinguishing between deep-water sediment facies: Turbidites, contourites and hemipelagites: Geosciences, v. 10, no. 2, 68, https://doi.org/10.3390/geosciences10020068.

Stow, D.A.V., and Tabrez, A.R., 1998, Hemipelagites: Processes, facies and model, *in* Stoker, M.S., Evans, D., and Cramp, A., eds., Geological Processes on Continental Margins: Sedimentation, Mass-Wasting and Stability: Geological Society, London, Special Publication 129, p. 317–337, https://doi.org/10.1144/GSL.SP.1998.129.01.19.

Streig, A., Weldon, R.J., Biasi, G., Dawson, T.E., Gavin, D.G., and Guilderson, T.P., 2020, New insights into paleoseismic age models on the northern San Andreas fault: Charcoal inbuilt ages and updated earthquake correlations: Bulletin of the Seismological Society of America, v. 110, no. 3, p. 1077–1089, https://doi.org/10.1785/0120190307.

Toda, S., Lin, J., and Stein, R.S., 2011, Using the 2011 Mw 9.0 off the Pacific coast of Tohoku earthquake to test the Coulomb stress triggering hypothesis and to calculate faults brought closer to failure: Earth, Planets, and Space, v. 63, no. 7, p. 725–730, https://doi.org/10.5047/eps.2011.05.010.

Underwood, M.B., and Hoke, K.D., 2000, Composition and provenance of turbidite sand and hemipelagic mud in northwestern Cascadia Basin, *in* Fisher, A.T., Davis, E.E., and Escutia, C., eds., Proceedings of the Ocean Drilling Program Scientific Results Volume 168: College Station, Texas, Ocean Drilling Program, p. 51–65, https://doi.org/10.2973/odp.proc.sr.168.012.2000.

Valentine, D.W., Keller, E.A., Carver, G., Li, W.H., Manhart, C., and Simms, A.R., 2012, Paleoseismicity of the southern end of the Cascadia subduction zone, northwestern California: Bulletin of the Seismological Society of America, v. 102, no. 3, p. 1059–1078, https://doi.org/10.1785/0120110103.

Van Arsdale, R.B., Stahle, D.W., Cleaveland, M.K., and Guccione, M.J., 1998, Earthquake signals in tree-ring data from the New Madrid seismic zone and implications for paleoseismicity: Geology, v. 26, p. 819–822, https://doi.org/10.1130/0091-7613(1998)026<0515:ESITRD>2.3.CO;2.

Van Daele, M., Meyer, I., Moernaut, J., De Decker, S., Verschuren, D., and De Batist, M., 2017, A revised classification and terminology for stacked and amalgamated turbidites in environments dominated by (hemi)pelagic sedimentation: Sedimentary Geology, v. 357, p. 72–82, https://doi.org/10.1016/j.sedgeo.2017.06.007.

Waananen, A.O., Harris, D.D., and Williams, R.C., 1970, Floods of December 1964 and January 1965 in the Far Western States: U.S. Geological Survey Water Supply Paper 1866-A, 265 p., https://doi.org/10.3133/wsp1866A.

Walker, R.G., 1965, The origin and significance of the internal sedimentary structures of turbidites: Proceedings of the Yorkshire Geological Society, v. 35, no. 1, p. 1–32, https://doi.org/10.1144/pygs.35.1.1.

Ward, G.K., and Wilson, S.R., 1978, Procedures for comparing and combining radiocarbon age determinations: A critique: Archaeometry, v. 20, p. 19–31, https://doi.org/10.1111/j.1475-4754.1978.tb00208.x.

Wei, M., and Shi, P., 2021, Synchronization of earthquake cycles of adjacent segments on oceanic transform faults revealed by numerical simulation in the framework of rate-and-state friction: Journal of Geophysical Research: Solid Earth, v. 126, no. 1, https://doi.org/10.1029/2020JB020231.

Weldon, R.J., Dawson, T.E., Biasi, G., Madden, C., and Streig, A.R., 2013, Appendix G, Paleoseismic Sites Recurrence Database, *in* Uniform California Earthquake Rupture Forecast, Version 3 (UCERF3)—The Time-Independent Model: U.S. Geological Survey Open-File Report 2013–1165, 97 p., California Geological Survey Special Report 228, and Southern California Earthquake Center Publication 1792, http://pubs.usgs.gov/of/2013/1165/ (last accessed April 2021).

Wells, M.G., 2007, Influence of Coriolis forces on turbidity currents and sediment deposition, *in* Geurts, B.J., Clercx, H., and Uijttewaal, W., eds., Particle-Laden Flow: From Geophysical to Kolmogorov Scales: Dordrecht, Netherlands, Springer, European Research Community on Flow, Turbulence and Combustion (ERCOFTAC) Series 11, p. 331–343, https://doi.org/10.1007/978-1-4020-6218-6_26.

Wetzel, A., and Balson, P., 1992, Sedimentology of fine-grained turbidites inferred from continuously recorded physical properties data: Marine Geology, v. 104, p. 165–178, https://doi.org/10.1016/0025-3227(92)90091-U.

Wheatcroft, R.A., Sommerfield, C.K., Drake, D.E., Borgeld, J., and Nittrouer, C.A., 1997, Rapid and widespread dispersal of flood sediment on the northern California margin: Geology, v. 25, p. 163–166, https://doi.org/10.1130/0091-7613(1997)025<0163:RAWDOF>2.3.CO;2.

Wils, K., Deprez, M., Kissel, C., Vervoort, M., Van Daele, M., Daryono, M.R., Cnudde, V., Natawidjaja, D.H., and De Batist, M., 2021, Earthquake doublet revealed by multiple pulses in lacustrine seismo-turbidites: Geology, v. 49, p. 1301–1306, https://doi.org/10.1130/G48940.1.

Wilson, S.R., and Ward, G.K., 1981, Evaluation and clustering of radiocarbon age determinations: Procedures and paradigms: Archaeometry, v. 23, no. 1, p. 19–39, https://doi.org/10.1111/j.1475-4754.1981.tb00952.x.

Witter, R.C., Patton, J.R., Carver, G.A., Kelsey, H.M., Garrison-Laney, C.E., Koehler, R.D., and Hemphill-Haley, E., 2002, Upper-Plate Earthquakes on the Western Little Salmon Fault and Contemporaneous Subsidence of Southern Humboldt Bay over the Past 3,600 Years, Northwestern California: U.S. Geological Survey National Earthquake Hazards Reduction Program (NEHRP) Final Technical Report, 44 p.

Witter, R.C., Zhang, Y., Wang, K., Priest, G.R., Goldfinger, C., Stimeley, L., English, J.T., and Ferro, P.A., 2013, Simulated tsunami inundation for a range of Cascadia megathrust earthquake scenarios at Bandon, Oregon, USA: Geosphere, v. 9, p. 1783–1803, https://doi.org/10.1130/GES00899.1.

Zhang, H., 2005, Paleoseismic Studies of the Northern San Andreas Fault at Vedanta Marsh Site, Olema, California [Ph.D. dissertation]: Columbia, Missouri, USA, University of Missouri, 343 p.

Zhang, H., Niemi, T., and Fumal, T., 2006, A 3000-year record of earthquakes on the northern San Andreas fault at the Vedanta Marsh site, Olema, California: Seismological Research Letters, v. 77, no. 2, p. 248, https://doi.org/10.1785/gssrl.77.2.160.